Understanding coastal dynamics at an ebb-tidal delta in the Wadden Sea

A case study of Schiermonnikoog NW with Delft3D Flexible Mesh

S. C. (Stendert) Laan

TU Delft
Deltares
Enabling Delta Life
Rijkswaterstaat
Ministry of Infrastructure and Water Management

Understanding coastal dynamics at an ebb-tidal delta in the Wadden Sea

A case study of Schiermonnikoog NW with Delft3D Flexible Mesh

by

S. C. (Stendert) Laan

to obtain the degree of Master of Science
at the Delft University of Technology,
to be defended publicly on Monday July 1, 2019 at 4:00 PM
in Pulse (TU Delft, Building 33a), Hall 4.

Student number:	4206339	
Project duration:	September 19, 2018 – July 1, 2019	
Thesis committee:	Prof. dr. ir. Z. B. Wang,	TU Delft and Deltares
	Dr. ir. B. C. van Prooijen,	TU Delft
	Ir. A. P. Luijendijk,	TU Delft and Deltares
	Ir. C. M. Nederhoff,	Deltares
	Ir. R. Zijlstra,	Rijkswaterstaat Noord-Nederland

An electronic version of this thesis is available at `http://repository.tudelft.nl/`.

Cover: aerial photograph of Schiermonnikoog, taken from the Zoutkamperlaag inlet `https://beeldbank.rws.nl`, © Rijkswaterstaat / Joop van Houdt

TU Delft

Deltares
Enabling Delta Life

Rijkswaterstaat
Ministry of Infrastructure and Water Management

Preface

In this MSc-thesis the outcome of my graduation project is presented. This is the last step in obtaining my master's degree in Civil Engineering at the Delft University of Technology. In this study program I have chosen the track of Hydraulic Engineering with a specialization in Coastal Engineering, a field I grew particularly fond of.

End of September 2018, I got the opportunity to start my graduation project at Rijkswaterstaat and Deltares. This collaboration has enabled me to get to know two different sides of coastal engineering projects. I am grateful to Rijkswaterstaat for introducing me to the policy making part of the job and for letting me see the ins and outs of the organization. Deltares, and especially the employees at the department of Applied Morphodynamics, I would like to thank for welcoming me into their community during the course of my project, for pointing out state-of-the-art research related to my thesis, and, of course, for providing me with an excellent workplace.

I want to acknowledge everyone who was involved in my graduation project and especially the members of my graduation committee for their support and guidance. First of all, I want to express my gratitude to professor Wang for presiding over the committee and for his suggestions during the progress meetings. Bram van Prooijen and Arjen Luijendijk have helped me by sharing their knowledge and insights over the last months. Their critical questions helped me to reach the level and results I present in this thesis. I am very grateful to Robert Zijlstra, my supervisor at Rijkswaterstaat, for providing me with hands-on knowledge for my project, and with insight into recent developments at Schiermonnikoog and other Wadden Islands. Finally, I thank Kees Nederhoff, my daily supervisor at Deltares, very much for his indispensable support in setting up a reliable numerical model, and for his day-to-day guidance to make this thesis a success.

Furthermore, I would like to thank my fellow graduate students at Deltares for the re-energizing coffee breaks and lunches, the good discussions and the time together. Also, I want to say thanks to my friends in Delft for being around during my graduation project. Special thanks goes to my mother for giving me the chance to make the best out of my study life in the last years and thank you, Katharina, for your enthusiasm and support during the busy last months.

S. C. (Stendert) Laan
Delft, June 2019

Summary

Introduction
The barrier island Schiermonnikoog is located in the eastern part of the Dutch Wadden Sea. With highly dynamic tidal inlets on both sides of the island, the island head and tail are in constant morphological development. In the last decades, the island has shown accretionary behavior and no major human interventions have been required to maintain a safe coastline position, contrary to other Wadden Islands. Since the closure of the Lauwerszee embayment, a large surplus of sediment was present at the island head in the northwest (NW) due to a reduction of the tidal prism and the ebb-tidal delta volume. However, in recent years a strong erosion has been observed, bringing the coastline back to its pre-closure position. This erosion can be attributed to the landward migration of a sand shoal from the adjacent ebb-tidal delta. This migration forces a channel toward the coast. Within a couple of years, the legally defined basal coastline (*BKL*) is about to be transgressed. This requires action from the coastal zone manager Rijkswaterstaat. Therefore, the placement of a beach nourishment before 2022 is discussed.

For future coastal management, a more detailed understanding of this site and its surrounding area is necessary. A tidal inlet and its adjacent ebb-tidal delta experience a combination of many different physical processes. Mainly tides, waves, winds, and the resulting surge impact the occurring sediment transport pathways at the island head and contribute to the morphological development of the area. Insight into the contribution of individual physical processes helps to better understand the behavior of an approaching sand shoal and of the ebb-tidal delta as a whole. With this improved knowledge, an optimal management strategy can be made that is efficient and effective.

The main objective of this thesis is to assess which factors determine the future development of Schiermonnikoog NW. This is based on a combination of available literature, an extrapolation of bathymetric measurement data and a numerical model study. The latter helps to distinguish between the influence of different physical processes and its relation to the bathymetry.

Observed development
The ebb-tidal delta off Schiermonnikoog shows a cyclic behavior. In a period of about 26 years accretion and erosion at the island head are observed (Ridderinkhof et al., 2016). Shoals and channels rotate clockwise from the west to the east, which is in line with the ebb-tidal delta breaching conceptual model by FitzGerald (1988). From west to east, the flow bypassing and bar welding scheme can be observed in the morphological patterns over the tidal inlet. This is expected for cases with tide-dominance (Bruun and Gerritsen, 1959) and with fine to medium sediment grain sizes (Herrling and Winter, 2018).

In recent years, the main flood channel at Schiermonnikoog NW has reached an eastward direction. The observed cyclic behavior shows that the flood channel elongates, as a migrating shoal forces it toward the coast. As more material gets deposited in the flood channel, the channel will become hydraulically inefficient and tidal currents will follow a different path. Locally, this results in a decrease of tidal action and therefore the channel start to fill in, until it is fully abandoned and the shoal attaches with the coast.

Based on yearly cross-shore transect measurements (*JarKus*) and three-yearly ebb-tidal delta bathymetry scans (*Vaklodingen*) these described coastal changes are quantified. From these datasets, the shoal migration speed is estimated to be 200 m/y. In the last years this has reduced to around 100 m/y. The coastline retraction is slower with around 40 m/y. Extrapolating these values, an attachment of the approaching shoal can be expected within 10 years. However, this has to be interpreted carefully, because the migration speeds show large fluctuations over time and the migration process cannot be considered to be linear.

Numerical model
A model is developed with the coupled D-Flow FM (Kernkamp et al., 2011) and D-Waves modules (SWAN, Booij et al., 1999). The hydrodynamic part has a spatially varying resolution of the unstructured grid. At Schiermonnikoog NW and the adjacent ebb-tidal delta the resolution is about 50 m. This decreases step-wise for the deeper and more remote parts of the model. Water level data on the

boundaries is taken from the model DCSMv6-ZuNov4 by Zijl et al. (2013). The wave model includes three nested structured grids increasing in resolution from the southern North Sea to the Dutch Wadden Sea and finally to 150 m at the investigated tidal inlet. Wave conditions on the boundary of the largest grid are taken from the larger ERA5 atmospheric reanalysis (Hersbach, 2016). Spatially varying wind speeds and atmospheric pressures in both models originate from the same reanalysis.

A comparison of the model results to measurement data shows an adequate hindcast of water levels and waves in the investigated area. The resulting bias and accuracy is in line with other recent model studies. A further improvement of these processes does not show an equally significant improvement of the calculated sediment transport magnitudes. This thesis focuses mainly on transport pathways and gradients. The patterns of these are stable and not related to the exact sediment transport magnitudes.

Relevant processes

The model study shows a large spatial variation in the influence of different physical processes on the occurring sediment transport. In line with the theory, tidal action is the main contributor to transports in the ebb channel Westgat. However, no significant contribution of tides can be detected in the Plaatgat in front of the island head coast. In this channel and on the shallower parts of the ebb-tidal delta wave action is the main driver of sediment transport. Without the contribution of waves, no longshore transport component is present and significant transport can only be observed in and around the Westgat. Winds enhance transport to the east and dampen transport to the west, corresponding to its main direction. Furthermore, wind-related water level set-ups allow for larger waves to reach over shallower parts of the ebb-tidal delta, causing an increase in sediment transport. Water discharges into the Wadden Sea from sluices in the Lauwersmeerdam are large compared to residual discharges through the inlet, but have no significant effect on sediment transport over the ebb-tidal delta.

A significant impact of storm events is observed. The annual sediment transport over the approaching shoal and in the Plaatgat is strongly determined by these specific events. This is related to the above-described increased wave action impact due to wind-driven water level set-ups. Therefore, the migration of the shoal and the development of the Plaatgat are mainly determined by single events. The stochastic occurrence of storms makes the forecast of exact future morphological development in this area very complex.

Conclusion

The attachment of the approaching shoal can be expected within 10 years. Erosion mainly takes place to the west of the attachment point. The sediment transport in recent years, which keeps this channel open, is caused by a gradient in the wave height along the Plaatgat of about 7% on average over a year. Thus, a gradient in the longshore sediment transport is present. At the location of the largest wave height in the Plaatgat, a divergence point is present. Sediment transport to the southwest of this point is directed toward the southwest, into the inlet, and transport to the east of this point is directed toward the east.

Relatively large waves can reach the Plaatgat and coastline at the divergence point due to a deep cut through the shoal, where once the previous ebb channel was located. Therefore, it is concluded that the development of the shape of the shoal is key to sedimentation and erosion patterns at the coast. A more structural solution to the erosion problem can be the placement of a sand nourishment in this deep cut to smoothen the shoal's bathymetry. This will prevent significant wave height gradients from occurring and stop the present sediment transport gradient and subsequent erosion. Tactically placed sand nourishments may allow for a more structural solution for erosion, instead of only delaying its effect by means of a beach nourishment.

Contents

Preface ii

Summary iii

List of Figures viii

List of Tables ix

List of Symbols x

1 Introduction 1
- 1.1 Background . . . 1
- 1.2 Problem description . . . 2
- 1.3 Objectives and research questions . . . 3
- 1.4 Methodology and structure of the thesis . . . 4

2 Literature review 5
- 2.1 Area description . . . 5
  - 2.1.1 Historical background . . . 5
  - 2.1.2 Large-scale developments . . . 6
  - 2.1.3 Relevant processes . . . 9
- 2.2 Similar tidal inlet systems . . . 10
  - 2.2.1 Borndiep . . . 10
  - 2.2.2 Otzumer Balje . . . 11
- 2.3 Morphological models . . . 11
  - 2.3.1 Empirical models . . . 11
  - 2.3.2 Process-based models . . . 11
- 2.4 Chapter conclusion . . . 12

3 Data analysis 13
- 3.1 JarKus dataset . . . 13
  - 3.1.1 Basal and momentary coastlines . . . 13
  - 3.1.2 Observed recent developments . . . 14
- 3.2 Vaklodingen dataset . . . 16
  - 3.2.1 Hypsometric curve . . . 16
  - 3.2.2 Migration speed of the shoal . . . 17
  - 3.2.3 Sediment volumes in the ebb-tidal delta . . . 17
- 3.3 Description of the ebb-tidal delta development . . . 19
- 3.4 Chapter conclusion . . . 19

4 Model set-up, calibration and validation 21
- 4.1 Motivation of the choice for Delft3D-FM . . . 21
- 4.2 Model set-up . . . 21
  - 4.2.1 Grid . . . 21
  - 4.2.2 Bathymetry . . . 23
  - 4.2.3 Input data . . . 23
  - 4.2.4 Further settings . . . 25
- 4.3 Model calibration . . . 26
  - 4.3.1 Grid size and bathymetry . . . 26
  - 4.3.2 Bottom friction . . . 26

4.4 Model validation . . . 27
4.4.1 Hydrodynamics . . . 27
4.4.2 Waves . . . 29
4.4.3 Sediment transport . . . 30
4.5 Chapter conclusion . . . 31

5 Model results **36**
5.1 Overview of model runs . . . 36
5.2 Model-derived characterization of processes . . . 36
5.2.1 Hydrodynamics . . . 36
5.2.2 Waves . . . 37
5.2.3 Sediment transport . . . 40
5.3 Unraveling dominant processes . . . 42
5.3.1 Spatial variation in influence . . . 42
5.3.2 Sediment transport over cross-sections . . . 44
5.3.3 Resulting erosion and sedimentation . . . 45
5.4 Interpretation of processes in the Plaatgat . . . 47
5.4.1 Processes and sediment transport . . . 48
5.4.2 Comparison to observed erosion . . . 48
5.5 Impact of different bathymetric configurations . . . 48
5.5.1 Bathymetry of 2009 . . . 48
5.5.2 Sand nourishments . . . 50
5.6 Storms . . . 52
5.7 Chapter conclusion . . . 53

6 Conceptual model **54**
6.1 Three case studies . . . 54
6.1.1 Texel . . . 54
6.1.2 Ameland . . . 55
6.1.3 Schiermonnikoog . . . 56
6.2 General case . . . 56

7 Discussion **58**
7.1 Software and model set-up . . . 58
7.1.1 Software . . . 58
7.1.2 Representation of processes . . . 59
7.1.3 Sedimentation and erosion on the ebb-tidal delta . . . 59
7.2 Model results . . . 59
7.2.1 Hydrodynamics . . . 59
7.2.2 Waves . . . 60
7.2.3 Sediment transport . . . 60

8 Conclusions **62**
8.1 Conclusions . . . 62
8.1.1 Development at Schiermonnikoog NW . . . 62
8.1.2 Applicability of Delft3D-FM . . . 65
8.2 Recommendations . . . 65
8.2.1 Further research . . . 65
8.2.2 Possible sand nourishments . . . 66

Bibliography **68**

A DCSMv6-ZuNov4 **74**

B Model set-up and calibration **75**
B.1 WadSea 2009 grid optimization . . . 75
B.2 Manning friction coefficient . . . 75

C Wave modeling **77**
C.1 Calibration . . . 77
C.2 Comparison of the model results with other studies . . . 77
C.3 Effect of the accuracy on sediment transport . . . 78
C.4 Effect of the communication time step on sediment transport . . . 78

D Formulas for statistical analysis **80**
D.1 Bias . . . 80
D.2 Accuracy . . . 80

E Additional model results **81**
E.1 Discharge and sediment transport per cross-section . . . 81
E.2 Wave height and sediment transport at the Plaatgat . . . 83
E.3 Sediment transport pathways . . . 85
E.4 Sediment transport at the Plaatgat on a grid . . . 86

Glossary **87**

List of Figures

1.1 Overview map of Friesche Zeegat . . . 1
1.2 Morphological development at Schiermonnikoog NW . . . 2

2.1 Conceptual model of a typical Wadden Island . . . 6
2.2 Morphological cycle of the Zoutkamperlaag inlet . . . 6
2.3 Conceptual model for ebb-tidal delta breaching . . . 7
2.4 Typical flow patterns in an ebb-tidal delta . . . 7
2.5 Sediment bypassing schemes over tidal inlets . . . 10

3.1 Displacement of the *MKL* . . . 14
3.2 Calculation method for the *MKL* . . . 14
3.3 Development of *JarKus* transect 500 . . . 15
3.4 Development of current-carrying area of the Plaatgat . . . 16
3.5 Shoal migration and coastline retreat speeds . . . 16
3.6 Hypsometric curve for the Zoutkamperlaag . . . 17
3.7 Migration of the center of mass of the approaching shoal . . . 17
3.8 Sediment volumes in the ebb-tidal delta . . . 18
3.9 Sediment volumes in the main sand shoal . . . 18

4.1 Grid by De Graaff (2009) and its adaption in this thesis . . . 22
4.2 Overview of used grids and grid cell sizes . . . 22
4.3 Seniority map of the used bathymetry . . . 23
4.4 Wind and wave roses for the Friesche Zeegat . . . 24
4.5 Root-mean-square errors for water levels at measurement stations . . . 27
4.6 Tidal prisms, residual discharges and sediment transports . . . 29
4.7 Sediment transport through the Zoutkamperlaag inlet throat . . . 31
4.8 Water levels at three measurement stations at the Friesche Zeegat . . . 33
4.9 Tidal amplitudes in and phase lags in at measurement stations . . . 35

5.1 Flow patterns at the Zoutkamperlaag ebb-tidal delta . . . 38
5.2 Flow patterns at the Plaatgat . . . 39
5.3 Wave height and wave energy dissipation at the Zoutkamperlaag . . . 40
5.4 Annual average total sediment transport for 2017 at the Zoutkamperlaag . . . 41
5.5 Spatial variation of the relative importance of different physical processes . . . 43
5.6 Cumulative total sediment transports for 2017 through 4 characteristic cross-sections . . . 44
5.7 Observed and modeled bed level change . . . 46
5.8 Annual cumulative total sediment transport at Plaatgat on a structured grid . . . 47
5.9 Development of processes along the Plaatgat for different runs . . . 49
5.10 Development of the *JarKus* transects at Schiermonnikoog NW . . . 49
5.11 Flow patterns in the Plaatgat for 2009 and 2017 . . . 50
5.12 Development of processes along the Plaatgat for different nourishments . . . 51
5.13 Wave height and wave energy dissipation with a smooth shoal . . . 52

6.1 Conceptual model for Texel SW . . . 54
6.2 Conceptual model for Ameland NW . . . 55
6.3 Conceptual model for Schiermonnikoog NW . . . 56
6.4 Conceptual model for a general case . . . 57

7.1 Cumulative total sediment transports for 2017 through the Friesche Zeegat . . . 60

8.1 Conceptual model for present-day behavior of Plaatgat 64

A.1 Root-mean-square errors in DCSMv6-ZuNov4 for water levels at measurement stations 74

B.1 Root-mean-square errors for water levels during calibration with grid resolution 75
B.2 Root-mean-square errors for water levels during calibration with bottom friction 76

C.1 Fit of observed and modeled wave heights 77
C.2 Difference in total sediment transport for different communication time steps 79

E.1 Current and sediment transport through the inlet 81
E.2 Current and sediment transport along *JarKus* transect 220 82
E.3 Current and sediment transport along *JarKus* transect 303 82
E.4 Current and sediment transport along *JarKus* transect 420 82
E.5 Current and sediment transport along *JarKus* transect 540 83
E.6 Wave height and sediment transport at the Plaatgat 84
E.7 Annual average total sediment transport for 2017 at the Zoutkamperlaag 85
E.8 Annual average total sediment transport at Plaatgat on a structured grid 86

List of Tables

4.1 Wind stress formulation values by Vatvani et al. (2012) 26
4.2 Tidal prisms and residual discharges through inlets 28
4.3 Root-mean-square errors, biases and scatter indices for the significant wave heights . . 29
4.4 Modeled and measured sediment import and export through the tidal inlets 30
4.5 Root-mean-square errors for water levels, tidal amplitude ratios and phase differences . 34

5.1 Overview of conducted model runs 37
5.2 Annual average discharges and currents in the Zoutkamperlaag for 2017 37
5.3 Annual average discharges and currents in the Zoutkamperlaag for 2009 50

C.1 Overview of performance of developed model compared to other studies 78

List of Symbols

a	the amplitude (of a tidal component) [m].
α	the Charnock-value, used in wind stress formulations [-].
C_d	the drag coefficient to quantify the resistance of an object [-].
d_{50}	the median diameter of sediment particles [μm].
d_{90}	the 90_{th} percentile diameter of sediment particles [μm].
ϵ_{wave}	the wave energy dissipation [$N/m/s$].
ϕ	the Greenwich phase lag [$\circ$].
H_{m0}	the significant wave height [m].
$\overline{H}_{m0}$	the average significant wave height [m].
H_{rms}	the root-mean-square wave height [m].
n	the Manning friction coefficient [$s/m^{1/3}$].
P	the tidal prism of a basin [m^3].
Q	the instantaneous discharge through a cross-section [m^3/s].
$\overline{Q}$	the average discharge through a cross-section during a tidal cycle [m^3/s].
$\overline{Q}_{ebb}$	the average discharge through a cross-section during the ebb phase [m^3/s].
$\overline{Q}_{flood}$	the average discharge through a cross-section during the flood phase [m^3/s].
Q_{res}	the residual discharge [$m^3/tidalcycle$].
ρ_b	the initial dry bed density [$1600 kg/m^3$].
ρ_s	the specific density of sand [$2650 kg/m^3$].
ρ_w	the specific density of sea water [$1025 kg/m^3$].
S_{bed}	the bed load sediment transport as defined in the formulation by Van Rijn (1993) [m^3/s]; the volume flux is directly taken from the modeled mass and therefore excludes pores.
$S_{susp.}$	the suspended sediment transport as defined in the formulation by Van Rijn (1993) [m^3/s]; the volume flux is directly taken from the modeled mass and therefore excludes pores.

S_{total}	the total sediment transport, forming the summation of the bed load transport and the suspended transport as defined in the formulation by Van Rijn (1993) [m^3/s]; the volume flux is directly taken from the modeled mass and therefore excludes pores.
θ	the wave direction [$\circ$].
u	the instantaneous velocity through a cross-section [m^3/s].
$\overline{u}$	the average water velocity through a cross-section during a tidal cycle [m^3/s].
$\overline{u}_{ebb}$	the average water velocity through a cross-section during the ebb phase [m^3/s].
$\overline{u}_{flood}$	the average water velocity through a cross-section during the flood phase [m^3/s].
z_b	the bed level measured from NAP [m].
z_{s0}	the tidal water level measured from MSL [m].
z_{s1}	the water level including surge measured from MSL [m].

1

Introduction

1.1. Background

In the Dutch Wadden Sea, Schiermonnikoog is the most easterly inhabited island, separated by the Friesche Zeegat tidal inlet system from the island Ameland in the west and by the Lauwers tidal inlet system from the island Rottumerplaat in the east. The parts of these inlets adjacent to the coast are the Zoutkamperlaag and the Eilanderbalg respectively. An overview of the area around the island and its geographic location is given in Figure 1.1.

The Wadden Sea was formed roughly 7,000 years ago due to sea level rise after the last Ice Age (Van der Spek, 1994). The islands in the system moved southward in the first 2,000 years, creating the tidal flats and consequently the present-day Wadden Sea. Afterwards, due to avulsion and accretion of land, the islands slowly migrated from west to east (Oost and Dijkema, 1993).

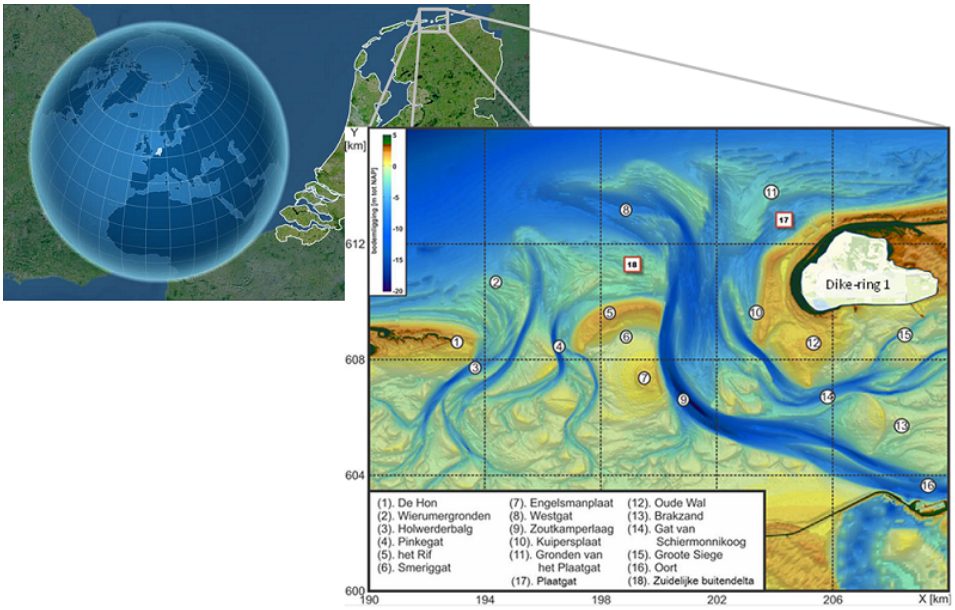

Figure 1.1: System overview of Friesche Zeegat after Oost et al. (2015) with its geographic location

The main focus for this master thesis is the island head, which is the western end of Schiermonnikoog. The area of interest includes the adjacent ebb-tidal delta of the Zoutkamperlaag with its channels and shoals. Historical data shows that approximately every 26 years a new sand shoal reaches the island and merges with the beach (Ridderinkhof et al., 2016). The closure of the Lauwerszee embayment in 1969 resulted in an exceptionally large amount of sand to reach the coast, due to erosion of the ebb-tidal delta (Oost and De Haas, 1992). Therefore, the beach at the island head is locally more

than 1 km wide and includes a part near the dunes, which has become higher and shows considerable vegetation.

1.2. Problem description

During the last several decades the island of Schiermonnikoog has, on average, accreted. However, over the last ten years, the northwestern part has suffered from strong erosion due to the landward migration of a channel from the ebb-tidal delta. If the erosion of the relatively wide beach continues, it might threaten the dune system. Data from the past has shown that the morphological development of the island is cyclic (Figure 1.2, Oost, 1995). On time scales of decades, periods of accretion, associated with the landing of sand shoals from the ebb-tidal delta, alternate with periods of erosion, associated with nearby channels from the tidal inlet system. Nevertheless, this is no perfect cycle and, moreover, the cycle is influenced by man-made effects, such as the construction of dikes and the closure of the Lauwerszee embayment.

The exact relation between the tidal inlet system development and the adjacent coastal development is poorly understood (Wang et al., 2012). A relatively good representation of the system on larger time scales can be made by use of a (semi-)empirical model, when fixed morphological and hydraulic boundaries are assumed. The results on these time scales are, however, not accurate enough, nor reliable enough to be used on an engineering time scale of several years to a decade. In this case process-based models (e.g. Delft3D simulations) can be more helpful.

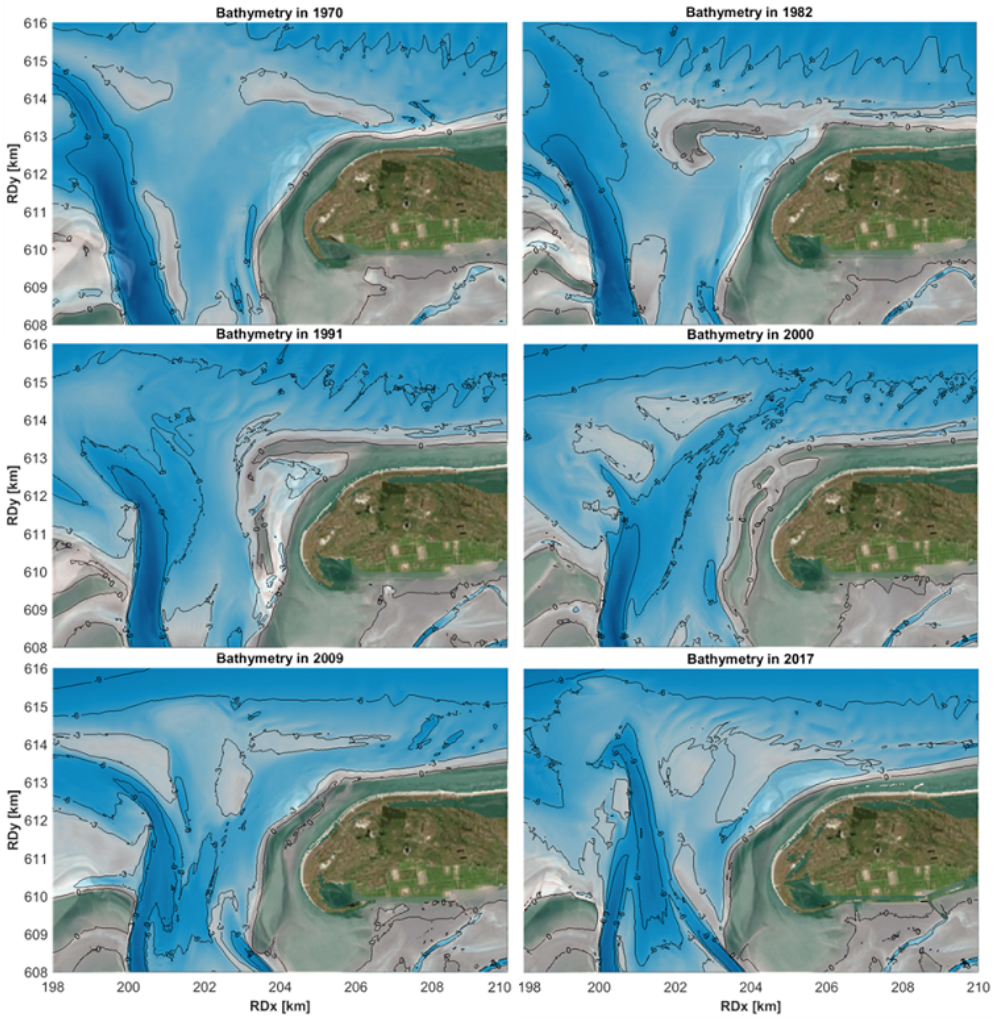

Figure 1.2: Changing bathymetry at Schiermonnikoog NW since the closure of the Lauwerszee embayment (Vaklodingen by Rijkswaterstaat)

Schiermonnikoog has 940 permanent inhabitants and is visited by 300 000 people per year. The local population has shown concerns about the safety of their coastal defense system. This is caused by the significant erosion of the beach on the northwestern part of the island in recent years. Informing them about the functioning of this part of the system and providing an overview of possible future scenarios can contribute to and reassure their perception of safety. The main concern is whether the extent of the erosion will be acceptable until a new sand shoal lands.

In landward direction of the shoreline, an extensive coastal defense system is present in the form of a dune landscape with multiple dune rows. This primary coastal defense has been transferred from Rijkswaterstaat to Wetterskip Fryslân in 2009 according to the Governance Agreement on Water, *Bestuursakkoord Water* (Ministerie van Infrastructuur en Milieu, 2011). The position of the dike-ring is made visible in Figure 1.1. There is no reason to assume that this does not live up to its required safety level, because the dunes are sufficiently high, wide and vegetated (Wetterskip Fryslân, 2011). However, it is important to understand the possible future development of the beach and shoreface seaward of the dunes in the dike-ring. Ongoing coastal erosion may threaten the stability of the most seaward dune row within a couple of years if this is not mitigated.

The beach and dunes are part of the Schiermonnikoog National Park and have a high ecological value. In this 54 km^2 nature reserve, the connected dune system of the dune arch is part of the Natura 2000 network of the European Union. A significant reduction of the beach and dune area may threaten the current ecology. On the other hand, a more dynamic dune system may benefit the ecology by ensuring diversity.

1.3. Objectives and research questions

For Rijkswaterstaat to properly manage this part of the Dutch coastline, more insight is required into the future development of the northwestern part of Schiermonnikoog. The main objective of this thesis is to analyze the system in such a way, that the driving mechanisms behind the development in the upcoming years up to two decades can be unraveled. For this purpose, the dominant processes contributing to the erosion at the island head are determined by means of a data analysis and a numerical model study. More in general, the relation between the coastal development at the island head and the tidal inlet system development is described in a clear and structured manner.

Rijkswaterstaat is looking into the placement of a beach nourishment at the island head before 2022 to mitigate the erosion. This thesis helps to assess the importance of this nourishment. It is of interest whether in time natural developments may result in accretion, and how the placement of a sand nourishment can be most effective, based on the behavior of the present shoal and channel.

In this thesis, the answers to the following research question and subquestions are provided:

- What determines the possible future development of the northwestern part of the island head of Schiermonnikoog and the adjacent ebb-tidal delta in the upcoming years up to two decades?
  - Which changes in the morphology of the coast and ebb-tidal delta occurred at the island head of Schiermonnikoog?
  - How can the recent morphological changes be explained from literature, focusing on dominant processes and the relation with the development of the tidal inlet system?
  - Which processes at northwestern Schiermonnikoog contribute most to the development of the current situation?
  - What is the relation between the influence of the driving processes and the bathymetry?
  - What is a correct conceptual model for the system behavior at northwestern Schiermonnikoog and how does this relate to similar locations?

A secondary objective of this thesis is to investigate the applicability of the Delft3D Flexible Mesh Suite by Deltares (2018) to analyze a subsystem in a larger scale system. This mainly focuses on the benefits of using a local refinement in a crude overall model. It will be assessed whether this can be an easy-to-use approach to zoom in on elements in a larger system. In this thesis, this relates to the subsystem of the Friesche Zeegat in the larger Dutch Wadden Sea.

1.4. Methodology and structure of the thesis

The first two subquestions are partially answered by means of a literature review. For a more detailed answer to the first subquestion a data analysis is required. To answer the third and fourth subquestions a model study has been conducted. These results provide the basis for the answer to the last subquestion. With answers to all subquestions, a solution for the main research question can be found. All steps for this methodology and the structure of the thesis are further elaborated below.

The literature review in Chapter 2 focuses on a system analysis at the island head of Schiermonnikoog and the adjacent part of the Friesche Zeegat tidal inlet system. This includes a general understanding of the development of an ebb-tidal delta and its main drivers, an overview on the results of previously conducted investigations regarding the area of interest, a comparison with similar tidal inlet systems in the Wadden Sea, and a review of different modeling approaches.

After the literature review, an analysis of the available bathymetric measurements is given in Chapter 3. This helps to answer the first subquestion and to quantify the observed erosion. Concluding, an extrapolation into the upcoming years is made.

Subsequently, a model study is presented in Chapter 4. Here the set-up, calibration and validation of the model are given. The latter consists of a comparison of model results to available literature and measurement data on water levels, waves and sediment transport.

The results of the calibrated and validated model are given in Chapter 5. This includes a description of the occurring processes in the area of interest is given, an assessment of the influence of the dominant processes on the sediment transport, the behavior of the channel Plaatgat in front of the island coast, the changes of the before-mentioned aspects under different bathymetric configurations, and a closer look at storm events.

The model results are used to develop a conceptual model for Schiermonnikoog NW. This model is compared to recent model studies of similar areas. Combining these, a conceptual model for the final stage of a flood channel before its abandonment is presented in Chapter 6.

A discussion of this thesis is given in Chapter 7. This includes a section on the possibility of improving the developed model and the modeling software, and a section on the model results and how to interpret these.

In Chapter 8, a clear answer to the two objectives and to the research questions is stated. Additionally, further research topics are suggested to better understand and explore the findings in this thesis. For Rijkswaterstaat a recommendation for a possible sand nourishment in the near future is given.

2

Literature review

In this chapter an overview of relevant literature is given, commencing with an area description in Section 2.1. This section starts with the paleogeographic description of the Wadden Sea and Schiermonnikoog, which continues with the more recent developments in that area. Subsequently, the large-scale developments are explained. This results in an overview of the behavior of the Zoutkamperlaag inlet system, near the island head. Finally, in this first section, an overview of further relevant processes is presented. Section 2.2 focuses on a comparison with similar tidal inlet systems to broaden the understanding of the Friesche Zeegat. Section 2.3 is on morphological models and the difference between the empirical and process-based modeling approaches. A chapter conclusion is given in Section 2.4.

2.1. Area description

2.1.1. Historical background

Paleogeography of the Wadden Sea

There is paleogeographic evidence for the existence of the Wadden Sea up to 7.000 years ago (Elias et al., 2012). Due to the rising sea level the Wadden Islands initially migrated landward till the beginning of the Subboreal, around 3000 BCE (Van der Spek, 1994). From around this moment onward, the Wadden Islands no longer migrated mainly toward the land. Instead, due to the direction of the tidal propagation and the dominant wave direction, a migration toward the east became more predominant (Oost and Dijkema, 1993). Human activity led to a strong reduction of the storage capacity for silt due to the construction of dikes. The reduced distance between the mainland and the islands resulted in an increase in wave energy in the system and the reduced storage capacity resulted in an increased turbidity in the system (Oost et al., 2018). Recently, movement of the islands to the south and to the east has largely halted due to human interventions, in particular since the Coastal Preservation act went in effect in 1990. Numerous sand nourishments have prevented farther coastal retreat and barrier island migration.

Along the coast of the mainland, over the centuries several embayments opened up. In the eastern Wadden Sea, this can mainly be attributed to land subsidence due to peat excavation and drainage (Oost and Dijkema, 1993). During the Middle Ages, south of Schiermonnikoog, the Lauwerszee embayment developed out of a local river mouth. This embayment was initially connected to the North Sea through the inlet to the east of the island and eventually through the current Friesche Zeegat inlet to the west (Oost, 1995).

Historical development of Schiermonnikoog

Conceptually, Löffler et al. (2008) divide a Wadden Island into different elements, as given in Figure 2.1. Each element of the island has a its own morphological behavior. For the Dutch islands, the individual elements of such a model island are best preserved at Schiermonnikoog (Oost et al., 2018).

The eastern end of the island, the island tail (4c in Figure 2.1), elongates with a wide empty sand spit, until this is breached by a channel, the Eilanderbalg in this case, and the cut-off sand flat ends up in the adjacent ebb-tidal delta. At the tail the cycle starts again, generating a new sand spit. The island

tail is difficult to incorporate in a process-based model, due to the frequently occurring overwash over the sand spit during stormy weather conditions.

The western end of the island, the island head (1b and 1c in Figure 2.1), undergoes a cyclic development with landing of channels and sand shoals from the ebb-tidal delta. For Schiermonnikoog this is the Zoutkamperlaag in the Friesche Zeegat. The landing of a sand shoal occurs approximately every two to four decades (Doornenbal et al., 2011). This process is, however, highly stochastic and related to extreme events, such as storm events.

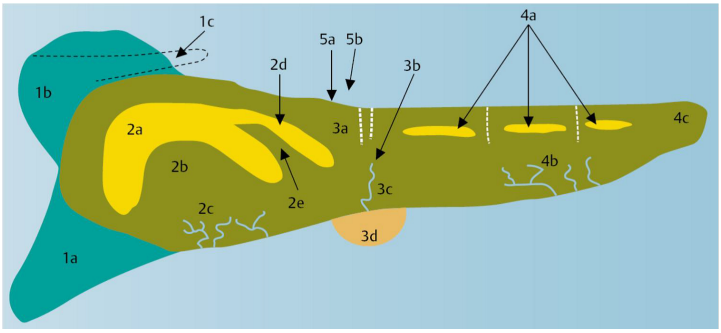

Figure 2.1: Conceptual Wadden Island with different elements according to Löffler et al. (2008),
with the **1: *island head***, 1a: *flood-tidal delta flat*, 1b: *ebb-tidal delta swash bar*, 1c: *ebb-tidal delta flood channel*, **2: *dune arch complex***, 2a: *dune arch*, 2b: *enclosed beach area*, 2c: *salt marshes*, 2d: *parallel dune ridge*, 2e: *enclosed dune valley*, **3: *wash-over complex***, 3a: *wash-over channel*, 3b: *wash-over flats*, 3c: *salt marsh*, 3d: *wash-over fan*, **4: *island tail***, 4a: *foredunes*, 4b: *salt marshes*, 4c: *empty beach area*, **5: *shoreline***, 5a: *beach*, and 5b: *foreshore*

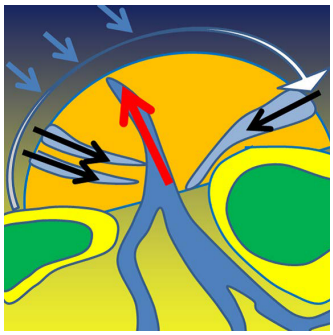

Figure 2.2: Simplified cycle of the Zoutkamperlaag tidal inlet (Oost et al., 2015);
explanation of colored arrows: black: flood channels, red: ebb channel, blue: wave action, white: clockwise rotation of channels and shoals

At a typical Wadden Island, the eastern end accretes and the western end erodes (Oost and Dijkema, 1993). Schiermonnikoog shows atypical behavior with recent overall accretion of the North Sea coast and island head. Therefore, besides the construction of some sand-drift dikes in the past, so far no major mitigation measures have been implemented (Oost et al., 2018).

This phenomenon of accretion is related to the closure of the Lauwerszee embayment in 1969. This closure reduced the tidal prism of the Friesche Zeegat system from 306×10^6 m^3 to 200×10^6 m^3 (Van Sijp, 1989). As a consequence the ebb-tidal delta eroded and the original channels silted up to reach a new equilibrium. Part of the excess sediments in the ebb-tidal delta ended up on the coast of Schiermonnikoog (Oost and De Haas, 1992), in the shape of a large sand hook at the island head (see 1982 and 1991 in Figure 1.2). Based on historical sedimentation rates (Elias et al., 2012), it is expected that the entire inlet system, including the northwestern island head of Schiermonnikoog, is - almost - in morphological equilibrium again. Since 1985 the sedimentation rates in the basin are comparable to the rates recorded before the closure. This is more or less in agreement with the 18.1 year adaptation time, as calculated by Steijn (1991).

Furthermore, the closure of the Lauwerszee embayment resulted in a relatively increased importance of waves in the system. Due to the reduced tidal prism, the tidal currents reduced. This may have influenced the natural behavior of the inlet.

2.1.2. Large-scale developments

Shoal attachments

FitzGerald (1988) categorized three different types of tidal inlets. These are inlet migration with spit breaching, stable inlet processes with a fixed position of the main ebb channel, and ebb-tidal delta breaching, where the main ebb channel is constantly migrating downdrift[1] due to accumulation of sediments on the updrift side, until it is abandoned and replaced by a new channel (see Figure 2.3). The latter is the category to which the Zoutkamperlaag inlet belongs.

Above NAP -5 m, shoals build up. Waves have a large influence on the dynamics of these shoals. Shoals mainly build up on the updrift side of channels, but also on the downdrift side. These shoals are

[1] In this thesis, several times the terms up- and downdrift are mentioned. These relate to the tidal wave propagation direction. Therefore, in the Dutch Wadden Sea, updrift is directed to the west and downdrift is directed to the east.

mainly linear bars along the channel, formed by the interaction of ebb and flood currents together with wave action and currents generated by waves (Hayes, 1975; Sha, 1989a). The updrift shoals force the channel downdrift, which continues till the channel has migrated so far that it becomes hydraulically inefficient and is abandoned. The abandoned channel experiences a reduced flow and starts to gradually fill in with sediments (FitzGerald, 1988). After that, the shoal becomes a bar in front of the downdrift island till it finally merges with the beach. In between of these larger breaching events with large shoals moving onshore, smaller shoals may form. These will also migrate shoreward (FitzGerald, 1988).

Ridderinkhof et al. (2016) show that in the Wadden Sea a negative relation between the tidal prism and the velocity of sand shoal migration through ebb-tidal delta systems may be valid for inlets with a single ebb channel. The Zoutkamperlaag is such a tidal inlet. Also, a positive relation between the migration velocity and the frequency of sand shoal attachments to the downdrift barrier island is found. Since the landing of sand shoals at Schiermonnikoog occurred more or less every 26 years (Ridderinkhof et al., 2016) before the closure of the Lauwerszee embayment, it can be expected that this will happen more frequently with the new reduced tidal prism. Since the closure, only two (upcoming) attachments can be observed; one in the years after 1972 and probably one in the upcoming 15 years (Oost et al., 2015). This is not in agreement with the expected attachment frequency, but can be related to the large disturbance in the system by the closure. It can also be the case that smaller, more recent attachment could not be detected due to the presence of the exceptionally large sand hook (A.P. Oost, pers. comm.). It is expected that the future attachments will consist of a lower sediment volume than the average before the closure (Elias et al., 2012). Based on measurements, this seems to be the case, as is explained in Section 3.2.3.

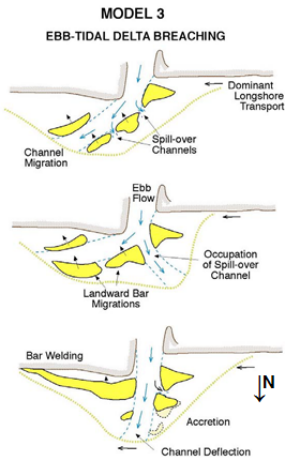

Figure 2.3: Conceptual model for ebb-tidal delta breaching (Fitzgerald et al., 2000)

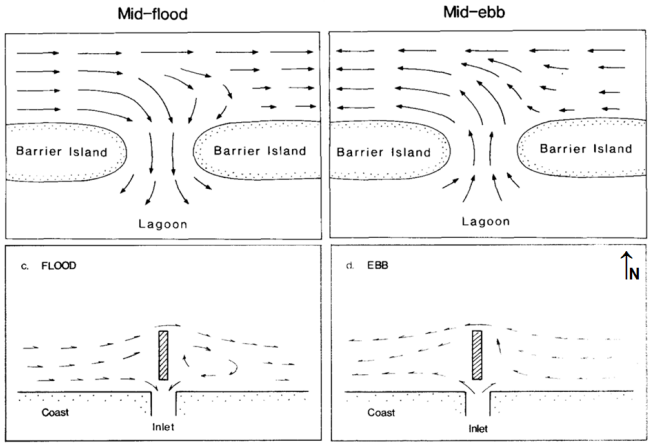

Figure 2.4: Typical flow patterns in an ebb-tidal delta (Sha, 1989a,b)

Ebb-tidal delta asymmetry and barrier island offset

The larger the tidal prism of an inlet, the more tide-dominated the inlet is. This results in a more updrift directed asymmetry of the ebb-tidal delta. More wave-dominated tidal inlet systems show a more downdrift directed asymmetry (Sha, 1989a). The asymmetry is related to the interaction between the shore-parallel tidal currents and the tidal currents through the inlet.

Shore-parallel tidal currents are disturbed by perpendicular tidal currents through the inlet. Updrift, this enhances the shore-parallel currents, but downdrift, refraction and deflection occur during both ebb and flood (see Figure 2.4). In the Dutch Wadden Sea, this disturbance is maximal with a north-northwest- or north-oriented ebb channel, because the ebb-tidal delta acts as a groyne in this situation. This results in weak rotational currents on the downdrift side (Sha, 1989a), leading to more sedimentation. In combination with wave action, the influence on sedimentation increases (Steijn and Hartsuiker, 1992; Steijn and Louters, 1992). This phenomenon results in an increase in activity of shoal development and channel migration on the downdrift side of the ebb channel. Flood channels on this side will no longer be required, since the ebb channel can also be used by the flood flow. The ebb-tidal

delta near Schiermonnikoog is currently in this state and strong sedimentation on the downdrift side is occurring (see Figure 1.2).

Lenstra et al. (2019) state that the position of the ebb channel also influences the sediment bypassing volumes over a tidal inlet. Consequently, this will influence the amount of sedimentation on the downdrift side. With an orientation more to the north or north-northeast these volumes are smaller than with an orientation to the northwest (NW). The fluctuations are related to the tidal changes due to the rotation of the ebb channel.

The above described current pattern also explains the observed downdrift offset in seaward direction of the barrier islands in the Wadden Sea. This offset is a result of wave refraction and the interaction between the currents, as mentioned above. The refraction leads to a local reversal of the longshore sediment transport, which makes the ebb-tidal delta a sediment trap. The offset is of importance for the location of sand shoal attachments from the ebb-tidal delta, because the location of sand shoal attachments is farther from the inlet, when the ebb-tidal delta is downdrift asymmetric (Fitzgerald et al., 1984). The same goes for when the inlet is larger. Elias et al. (2012) expected future attachments of sand shoals at Schiermonnikoog to be located closer to the inlet, due to the reduced ebb-tidal delta volume. However, the attachments of the NAP −3 m contour are recently observed at a location around transect[2] 480 in 1972 and 540 in 2017 (Van der Lugt et al., 2018), indicating a location slightly farther from the inlet instead. The eventual attachment of the NAP 0 m contour will show whether this theory holds for Schiermonnikoog.

18.6 year lunar nodal cycle

With a period of 18.6 years a significant variation of 5°9′ in the angle between the lunar orbit and the equator occurs. This variation is called the lunar standstill. It results in a tidal amplitude change of 2.8 to 5.2% near Delfzijl (Oost et al., 1993). The change in tidal currents is in the same range, but because the sediment transport is related to this to the third (Van Rijn, 1984) to fifth (Engelund and Hansen, 1967) power, the resulting change in sediment transport capacity would be 15 to 20%, which is quite significant.

During the maximum tidal amplitude in this cycle, the strength of the tidal currents through the inlet and in shore-parallel direction will increase. This results in a shift of the main ebb channel toward the updrift island with respect to the residual current (Sha and De Boer, 1991). In the case of the Zoutkamperlaag, this is the intertidal flat-complex Engelsmanplaat and Het Rif. With the channel closer to the eastern part of this flat this will result in erosion there. At the same time the ebb channel is relatively far from the downdrift island, the island head of Schiermonnikoog, so accretion will occur at that location. This phenomenon will shift during the 18.6 year lunar nodal cycle. At the minimum tidal amplitude, the situation will be exactly opposite with erosion at the island head of Schiermonnikoog and accretion at the eastern side of the Engelsmanplaat (Oost et al., 1993). Furthermore, since it is known that the ebb-tidal delta immediately reacts to a change in tidal prism and does so fastest at first (Steijn, 1991), the differences in tidal amplitude will result in a dynamic equilibrium of the volume of sediment in the ebb-tidal delta.

In June 2006 the lunar standstill was at its maximum, where in October 2015 it was at its minimum. Bathymetric measurements confirm a more eastern position of the inlet throat in 2015, which corresponds with the maximum coastal erosion related to this phenomenon. It can be expected that the upcoming westward shift of the inlet throat will lower the erosion at the island head. However, it is uncertain to say how this cyclic behavior exactly affects the erosion near the channel Plaatgat at Schiermonnikoog NW, located farther away from the inlet.

Cycle of Zoutkamperlaag

In Figure 2.2 and below, an overview is given of the cyclic behavior of the Zoutkamperlaag due to the factors mentioned by Oost (1995). The resulting cycle and main driving factors are given below.

New (flood) channels in the ebb-tidal delta of the Zoutkamperlaag develop mostly in the west with a west-northwest-to-east-southeast orientation. This is related to the maximal 'motoric capacity', which is based on the gradient between lines of equal tidal phase. Where this gradient is largest, the current velocities will be largest (Van Veen, 1936) and thereby the formation of channels is enhanced.

[2]The transects refer to the cross-shore profiles in the *JarKus* measurements, as is further explained in Section 3.1.

The main ebb channel tends to be directed to the north, due to the inertia of the ebb current, leaving the main south-to-north-oriented back barrier channel. This brings about a clockwise rotation of channels toward the north. Wave action rotates the channel farther toward the east.

When a channel has a mostly south-to-north orientation it becomes an ebb channel to later function as a flood channel again, when approaching Schiermonnikoog in the east. Eventually, the flood channel off the coast of Schiermonnikoog will be abandoned.

When the position of the ebb channel is to the NNE, it may also be used as a flood channel, which makes a separate flood channel in this quadrant redundant. From time to time a flood channel is formed in the northeast, near the island head. This is suspected to be related to a combination of an eastward orientation of the Pinkegat channels and the presence of all other channels in the western part of the Zoutkamperlaag. Under the present-day bathymetry this is unlikely to occur (Oost et al., 2015).

Extrapolation of the cycle For a study on sills hindering navigation in the current ebb channel, Oost et al. (2015) forecast the upcoming developments of the Zoutkamperlaag ebb-tidal delta, based on measurements and literature. It has to be noted, that this extrapolation has a high order of uncertainty, since the development of a single element in the system is always influenced by all other developments in both the ebb-tidal delta and the back barrier basin.

Relevant outcomes for this thesis are the expected north-northeast orientation of the ebb channel in 10 to 20 years from now. This orientation will enable the use of this channel by both ebb and flood. Therefore, the channel, between the ebb channel and the flood channel near the coast of Schiermonnikoog, will become redundant and be abandoned due to its hydraulic inefficiency. The start of this process is already visible in the *Vaklodingen* (see Figure 1.2) with the development of a sill at the eastern end of the channel, the attachment point of the approaching shoal. For this scenario, the next flood channel to approach the coast of Schiermonnikoog is the present-day ebb channel in the period 2050-2060. This means that, when the recent erosion stops due to the attachment of the shoal, Schiermonnikoog will again experience a relatively long period of accretion. It can, however, be expected that the scale of this accretion is lower than the previous one, due to the decreased ebb-tidal delta volume and the more stable situation, compared to that just after the closure of the Lauwerszee embayment.

Alternatively, if the eastern Pinkegat channels will hinder the development of flood channels in the west of the Zoutkamperlaag, a more dominant flood channel near the coast of Schiermonnikoog may remain. Nevertheless, this scenario is deemed unlikely, because currently the ebb channel and other major channels in the Pinkegat are not direct toward the east.

2.1.3. Relevant processes

Sediment bypassing

In literature three common forms of sediment bypassing at tidal inlets are mentioned (Herrling and Winter, 2018). For a visualization, see Figure 2.5.

- *Flow bypassing and bar welding* occurs due to the seaward directed ebb-tidal current in the main ebb channel of the ebb-tidal delta and subsequent shoreward bar migration and its attachment to the barrier island head.
- *Semicircular sediment recirculation* is the circular movement of sediments seaward through the main ebb channel and back into the inlet through the marginal flood channels.
- *Ebb-tidal delta periphery bypassing* is the seaward zig-zag movement of sediments through the system of smaller channels and shoals, and the movement of sediments by shoreward bar migration, both along the periphery of the ebb-tidal delta.

These forms are, however, still ambiguous, especially when it comes to their relation to different grain sizes (Wang et al., 2012). Herrling and Winter (2018) suggest that very fine to fine sands (of 125 µm) mainly follow the third, but also the first form, fine to medium sands (of 250 µm) follow the first form, but also the second form, and medium sands (of 275 µm) follow the second form. Bruun and Gerritsen (1959) state that the relative importance of the tide over the waves is governing. Tide-dominated systems are mainly of the first form and wave-dominated systems are of the third form.

The Zoutkamperlaag tidal inlet system seems to be in the first category of seaward sediment transport through the main ebb channel and shoreward transport by bar migration (Oost, 1995). This is in line with its tide-dominance and its observed grain size distribution.

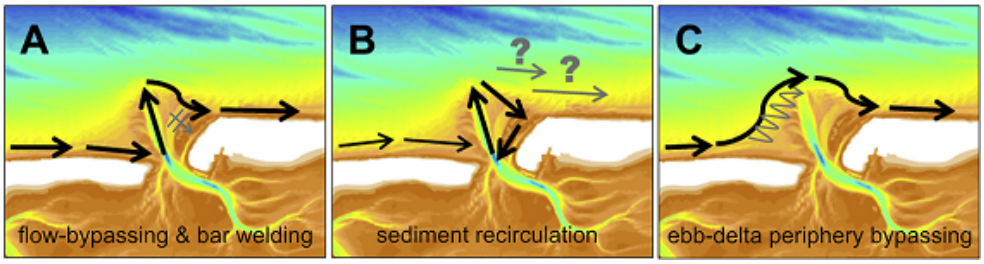

Figure 2.5: Sediment bypassing schemes over tidal inlets (Herrling and Winter, 2018)

Wave sheltering by ebb-tidal delta
The shallow parts of the Zoutkamperlaag ebb-tidal delta will reduce the impact of waves on the (down-drift) island head of Schiermonnikoog. In general this sheltering effect is largest for mixed energy coasts, such as the Dutch Wadden Sea. The main contributions are by the occurrence of wave breaking on the ebb-tidal delta shoals and the resulting dissipation of wave energy (FitzGerald, 1988) - mainly during low water, but also during high water - and by the reduction in wave energy due to oppositely directed ebb-tidal currents (Herbich and Hales, 1972). According to Olabarrieta et al. (2014), the latter is of lesser importance.

Besides the influence of currents on waves, also the waves influence the currents. The shoaling and breaking of waves on the ebb-tidal delta shoals reduces the ebb current, but augments the flood currents (Fitzgerald et al., 2000). Also, the interaction between the two is of importance. In general, waves stir up the (fine) sediments and currents transport them. At the ebb-tidal delta this leads to transport over the swash bars and along the periphery of the delta (the first and third bypassing schemes in Figure 2.5).

2.2. Similar tidal inlet systems

In the Wadden Sea many tidal inlet systems are present. Oost et al. (2017) compared most systems in the Dutch, German and Danish Wadden Sea. From this study it can be concluded that two other inlets are similar to the Friesche Zeegat. These are the Borndiep, one inlet to the west of the Friesche Zeegat, and the Otzumer Balje, between the German islands of Langeoog and Spiekeroog.

All three inlets:

- have an ebb-tidal delta against the tidal wave propagation direction,
- are in the higher mesotidal range,
- are mixed energy systems, where the Friesche Zeegat and Borndiep are more tide-dominated and the Otzumer Balje is more wave-dominated.

Furthermore the Friesche Zeegat and the Otzumer Balje have a similar tidal prism, littoral drift and, hence, ratio of tidal prism over littoral drift. For the Borndiep this ratio is larger, due to its significantly larger tidal prism.

2.2.1. Borndiep

The Borndiep tidal inlet is located between the Dutch Wadden Islands of Terschelling and Ameland. This system has a largely stable back barrier area and an ebb-tidal delta development with cycles of channel and sand shoal migration. On average a cycle takes 59 years (Ridderinkhof et al., 2016). Different from the Friesche Zeegat system, this ebb-tidal delta has had a relatively stable sediment volume over the past decades (Elias et al., 2012).

Regular attachments of the Bornrif sand shoal cause the alteration of large coastal accretion and erosion periods. The attachment point is located in the NW, where a wide seaward extension of the beach forms. Sediment from the shoal is mostly transported to the east after attachment, which causes structural erosion of the coastal section closer to the inlet. At that location no significant sediment volumes from the ebb-tidal delta reach the coast. A recent study by Nederhoff et al. (2016) found that wave action has an important role in delaying the present-day shoal attachment at the western half of the island head. This causes erosion due to the persistence of the flood channel Oostgat, even when tidal action no longer plays an important role. In this situation, the orientation of the ebb channel

in combination with the shape of the shoal causes a wave height gradient that in its turn causes a sediment transport gradient along the Oostgat. This phenomenon is further addressed and compared to Schiermonnikoog in Chapter 6.

2.2.2. Otzumer Balje

The Otzumer Balje is a tidal inlet in the German Wadden Sea. Due to shifting tidal watersheds (Ladage et al., 2006), the back barrier area has slightly decreased. However, the tidal prism of this system has recently increased, caused by a decreasing back barrier bathymetry and an increasing tidal range. As a consequence, the ebb-tidal delta has reached a larger sediment volume. Also, this system shows a clockwise rotation of channels and shoals (Ladage et al., 2006), where one cycle takes about 10 years (Ridderinkhof et al., 2016).

An eastward shift of the main inlet channel and the caused coastal erosion led to the construction of groynes along the western coast of Spiekeroog. The development of the island head coast is strongly influenced by the cyclic behavior of the inlet. Regular attachments of the Robbenplate sand shoal are observed. These contribute to a positive sediment budget and a stable coastline in the NW. When a shoal attaches an elongating sand hook is formed that gradually spreads out over the coast in both directions. Sediment transport through the flood channel between the shoal and coast is mainly directed inward. Measurements indicate full sediment recirculation in the system and no evidence for alongshore sediment bypassing is found (Son et al., 2011). This is caused by the presence of mainly medium sands on the shoals in the system.

2.3. Morphological models

In the field of morphological modeling a distinction between two main approaches can be made. One category of models follows a (semi-)empirical approach and another category follows a process-based approach. A third approach, the idealized models, is, very simplistically said, a toned down physical and mathematical representation of a system. This last approach is ignored in the following. This overview and the comparison are mainly based on the paper by Wang et al. (2012).

2.3.1. Empirical models

Empirical or semi-empirical models are also known as behavior-oriented models. This is because the main assumption made for this modeling approach is that all morphological systems will, after being disturbed, return to a certain equilibrium. This equilibrium is included in the model by use of empirical relations. An example of such a model is the ASMITA model (Stive and Wang, 2003; Stive et al., 1998), which makes use of empirical equilibrium relations between different system elements.

This modeling approach is very suitable to analyze the effects of long-term developments (Van Goor et al., 2003) and large-scale human interference (Kragtwijk et al., 2004). It is, nonetheless, a black-box approach, which does not provide any insight into the importance of relevant processes. Moreover, it is not suitable for use on engineering time scales of several years and for use on a more detailed level, zoomed-in on a smaller scale than that of system elements.

2.3.2. Process-based models

A process-based model is also known as a complex or quasi-realistic model, because it aims at an as accurate as possible description of all relevant processes. In the Delft3D system by Deltares (Lesser et al., 2004), mathematical equations represent the physical processes of water movement and sediment transport. Subsequently, through the mass balance, this results in a change in morphology on a detailed scale.

The process-based approach is very suitable for short-term and detailed studies and is often used for engineering purposes. It has also been used for long-term studies (Hibma et al., 2003a,b, 2004; Marciano et al., 2005; Wang et al., 1995; Van der Wegen and Roelvink, 2008), but, besides the required computing power, these studies face problems related to the lack of convergence to a certain equilibrium. Furthermore, there are concerns regarding the correctness and accuracy of the predicted morphological changes. These concerns may be reassured by use of large sets of historical data to calibrate and validate models.

Morphostatic modeling

For this thesis, it is relevant to elaborate a specific shortcoming of process-based models. In highly dynamic systems with many non-linear processes, such as ebb-tidal deltas, the detailed morphodynamic results are often unreliable (Elias et al., 2015; Wang et al., 2016). Coastlines at island heads do not show the same behavior as regular uninterrupted coastlines. Therefore, the resulting movement of sand shoals, sand bars, gullies and general erosion of the foreshore from these models will often be incorrect. Wang et al. (2012) state that the large-scale morphological equilibrium is crucial for smaller-scale developments, which may explain the poor results of process-based models in these complex systems. After all, no equilibrium is forced in these models. Furthermore, the present-day sediment transport formulas are not accurate enough to represent transport patterns and magnitudes in highly dynamic environments.

Another difficulty is the highly stochastic behavior of sand shoal migration. This can be seen in the fact that westerly storms cause considerable sediment transport to the east and result in sudden morphological changes in the ebb-tidal delta of the Friesche Zeegat. In the vicinity of Schiermonnikoog this is observed by Winkelmolen and Veenstra (1980).

To reach a more realistic outcome, the main focus of the model analysis is on the morphostatics. This means that no bottom updating has been used and mainly the sediment transport volumes are analyzed.

2.4. Chapter conclusion

The Zoutkamperlaag ebb-tidal delta undergoes a cyclic clockwise migration of channels and shoals. New (flood) channels are formed in the west, function as ebb channels when oriented more to the north and are eventually abandoned in front of the island head of Schiermonnikoog after fulfilling the role of flood channels with an orientation to the east. This abandonment goes hand-in-hand with the attachment of a sand shoal to the island coast. The wave-driven migration of sand shoals is seen as the main cause of the ebb-tidal delta dynamics.

Schiermonnikoog has mainly accreted over the last decades, since the closure of the Lauwerszee embayment. This behavior is atypical for Dutch Wadden Islands, where cycles of erosion and accretion are expected. Only recently strong erosion has been observed. The same closure has reduced the tidal action in the system, increasing the relative importance of wave action and consequently speeding up the cyclic behavior. Therefore, the effect of wave sheltering by the ebb-tidal delta is of larger importance for the development of the island head.

By combining different studies, the recent strong sedimentation at and increase of the sand shoal in front of the island coast can be explained. The orientation of the ebb channel Westgat and the formation of a new channel in the west of the ebb-tidal delta reduce the tidal action in front of the island head by deviating the flood currents. Furthermore, the northward orientation of the Westgat causes increased sedimentation due to the resulting weak rotational currents at Schiermonnikoog NW. In addition the north-northwestward orientation of this channel allows for a relatively larger volume of sediment bypassing the inlet. The expected bypassing scheme for the Zoutkamperlaag inlet is flow bypassing and bar welding, based on the tide-dominance and present grain sizes.

An evaluation of different modeling approaches has shown that a process-based model is the best option for this thesis. In the highly dynamic ebb-tidal delta, morphodynamic results will not be correct. It is decided to use a morphostatic approach with mainly an analysis of sediment transports.

3

Data analysis

In this chapter the data analysis to answer the first research question of this thesis is presented. This results in an overview of the observed morphological changes in the area of interest and an extrapolation of these. Section 3.1 and 3.2 focus on the available datasets by Rijkswaterstaat. An analysis of the cross-shore profiles and bathymetric data is conducted. The analysis of historical data focuses on the coastline retreat, the migration of the approaching shoal, the development of the channel Plaatgat and the development of the ebb-tidal delta morphology. A full description of the latter since the closure of the Lauwerszee embayment is given in Section 3.3. Concluding, an extrapolation of the migration is presented in Section 3.4. The starting point of the analysis in this chapter is the recent QuickScan by Deltares for Rijkswaterstaat (Van der Lugt et al., 2018).

3.1. JarKus dataset

The *JarKus* program by Rijkswaterstaat entails yearly measurements of the height and depth along fixed cross-shore profiles (*raaien*). These transects are placed 200 m apart and start at the respective beach poles, placed along the entire Dutch coast. Along 1 km, all transects are positioned parallel to each other, after which the angle of these cross-shore profiles is redefined. At this point, every one-hundredth transect, several cross-sections are measured to complete the rotation. For these yearly transect measurements, underwater single beam scans and coastal LiDAR measurements are conducted. These transects cover at least the NAP $+5$ m till the NAP -10 m lines.

The northwestern part of Schiermonnikoog is covered in the transects 2000200 till 2000900. In this notation the first digit stands for the area of Schiermonnikoog, 2, the fifth digit stands for the main beach poles every 1 km, the sixth digit stands for the transects every 200 m and the last digit is an indication for the rotated profiles from the main beach poles. In the rest of this thesis the area code is omitted, using only 3-digit codes. An overview of the beach poles and corresponding transects is given in Figure 3.1.

3.1.1. Basal and momentary coastlines

Since the commencement of the Coastal Preservation act in 1990, a basal coastline (*BKL*) has been defined. This line indicates the furthest point up to which beaches in The Netherlands are allowed to erode. If a threat to this position is perceived, Rijkswaterstaat will take action to prevent further erosion. A common measure in such a situation is the use of sand nourishments. However, there are cases where a minor transgression of the basal coastline is accepted. This decision is taken when erosion is not deemed structural, but part of the dynamic behavior of the coast.

In combination with the basal coastline, the momentary coastline (*MKL*) is important. Based on the yearly measured *JarKus* profiles the position of this line is calculated. An illustration of the method for this calculation is given in Figure 3.2. The area *o*, that is taken into account, may have interruptions when it includes breaker bars, that are not directly connected to the beach. Sand shoals separated from the beach by a deeper gully (NAP -3 m or below) are, however, not included in the calculation for the momentary coastline.

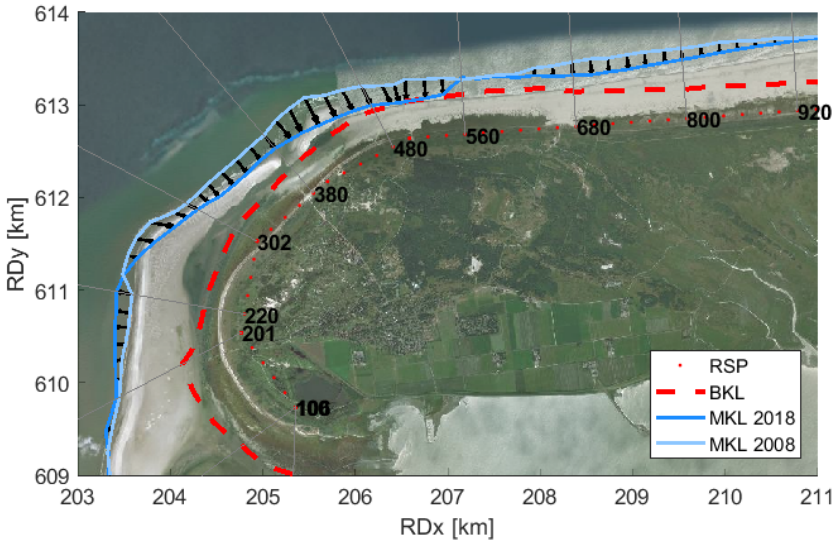

Figure 3.1: Displacement of the momentary coastline (*MKL*) between 2008 and 2018, including the position of the *BKL*, the main beach poles (*RSP*) and some transects

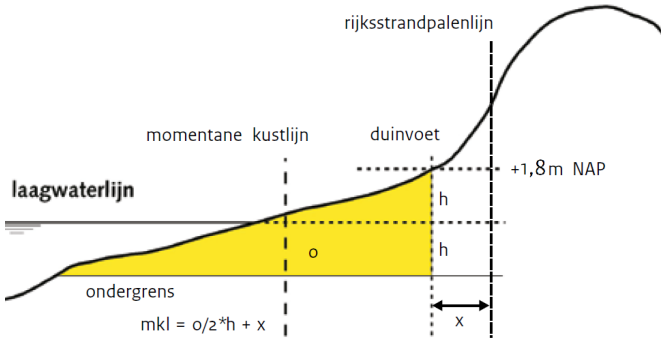

Figure 3.2: Calculation of momentary coastline (*momentane kustlijn*) after Ministerie van Infrastructuur en Milieu (2012),
where: *o* is the calculation area of the yellow part, *h* is the distance between the dune foot (*duinvoet*) and the MLW (*laagwaterlijn*), and *x* is the distance between the dune foot and the location of the respective beach pole (*rijksstrandpalenlijn*)

3.1.2. Observed recent developments

Coastline

The use of a non-constant seaward boundary, excluding the approaching sand shoal, causes 'jumps' in the development of the momentary coastline. This approach causes a sudden decrease of the calculation area, when it is cut off by a newly defined seaward boundary. This makes the comparison of the momentary coastline between different years difficult. Additionally, the presence of a large sand shoal will to a certain degree contribute to coastal protection by dissipating waves.

Another remark is the relatively low dune foot of NAP +1.8 m at Schiermonnikoog, excluding some of the embryo dunes. This choice seems justified by the sharp change in the slope between the beach and dunes at this height at most transects. Around transect 500, however, this seems a bit low, since the dune foot in the profile is present around NAP +2.2 m.

As can be seen in Figure 3.1 a significant transgression of the momentary coastline occurred in the period between 2008 and 2018. Especially at transect 500, the distance to the basal coastline has decreased significantly, to only 22.4 m, but this is mainly a result of a landward displacement of the seaward boundary over the years. With a constant seaward boundary position, the distance is 153.8 m. Also the position of the dune foot at NAP +1.8 m shows a significant transgression due to steepening

of the foreshore profile in the last 10 years. However, it can also be observed that a sand shoal is approaching the beach and that the flood channel Plaatgat is already silting up (see Figure 3.3). This channel has not yet been fully abandoned (see Section 3.1.2: Flood channel), and thereby slows down the attachment of the shoal to the beach. This raises the question whether the approaching shoal can counteract the recent erosion and whether this will happen before the basal coastline is transgressed.

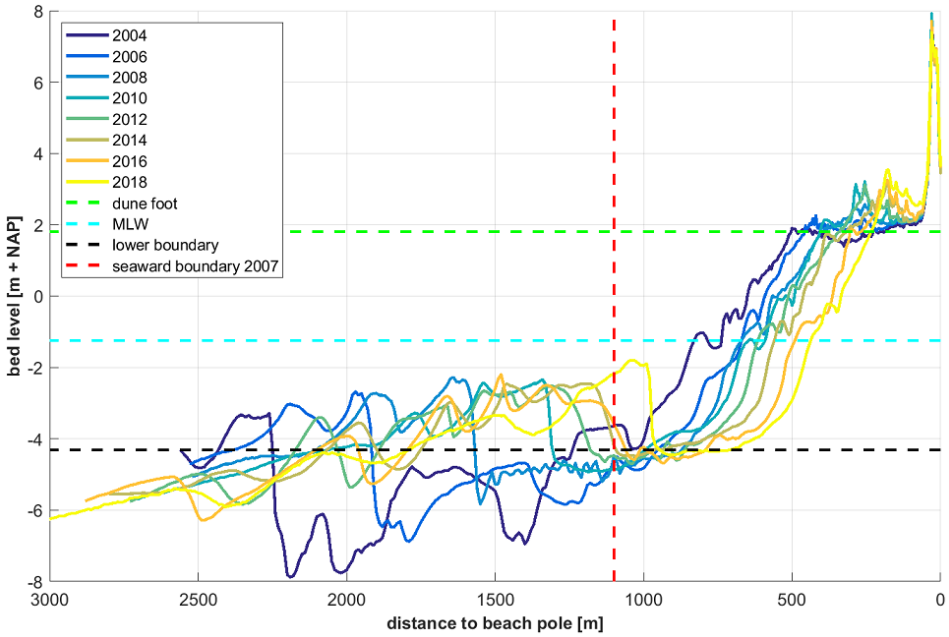

Figure 3.3: Development of *JarKus* transect 500 between 2004 and 2018 with the main calculation components as dashed lines

Flood channel

The development of the flood channel Plaatgat is of importance for the attachment of the approaching shoal. As long as the Plaatgat is kept open, this attachment will not occur and the coastal erosion is likely to continue.

Here, the channel is quantified by computing the current-carrying area by integrating all area below NAP −3 m per transect. In this manner the development of the cross-sectional area over the years can be visualized. Figure 3.4 shows this area over time (x-axis) and for different transects (colors). After a decline in the years 2005 to 2011, the area has been fairly stable. This could indicate that the size and importance of the Plaatgat, between the beach and the approaching sand shoal, has not yet decreased. In combination with the observed steepening of the foreshore profile, as is visible in Figure 3.3, this may indicate the occurrence of erosion by tidal currents through the channel, as was suggested by Van der Lugt et al. (2018).

This erosion would be caused by the landward 'pushed' Plaatgat forced by the landward migrating sand shoal. Also, it could mean that sediment from the approaching shoal is being transported by the flood current into the inlet without depositing in the Plaatgat, following the second bypassing mechanism from Figure 2.5. The model results in 5 further explain the current- and sediment-carrying capacity of the Plaatgat and show that another process is governing, namely wave action.

Migration speed of the shoal and coastline

By calculating the position over the years of the NAP −3 m depth contour of the approaching sand shoal, the migration speed of the landward edge of the shoal is determined per transect. This speed is extrapolated for the upcoming years to estimate the future development of the upcoming attachment. The same is done for the mean low waterline of the beach at NAP −1.25 m (*MLW*), which results in an estimate for the coastline retreat. The results are displayed in Figure 3.5.

It is visible that the coastline retreat is relatively stable at the most eroded transects 500, 501 and 502, with values of about 20 m/y. Nevertheless, the channel is still moving landward. This seems to

Figure 3.4: Development over time of current-carrying area of the Plaatgat below NAP −3 m till 2 000 m from the main beach pole (*RSP*)

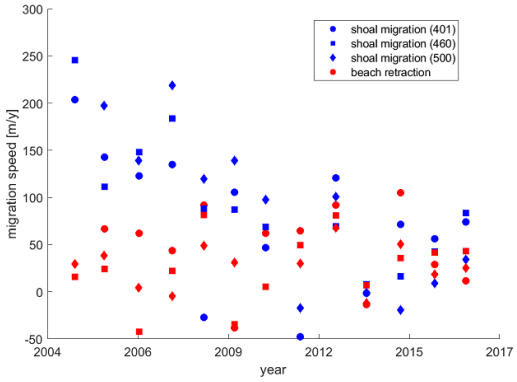

Figure 3.5: Shoal migration speed and speed of coastline retreat over time, where positive values are landward

be mainly the case at transects west of transect 500. Here the coastline retreat is accelerating from 20 m/y in 2004 to 40 m/y in 2018. The speed of the approaching shoal is less easy to forecast. Overall, it seems to have decreased, but recently a slight increase in speed can be observed. On average, a current speed of about 50 m/y to 100 m/y is found, but this shows a large uncertainty.

The most important aspects to note are the faster approach of the shoal than coastline retreat, which indicates a narrowing of the Plaatgat, and the stabilization of coastline retreat at the transects where the basal coastline is almost exceeded. Also, an increase in coastline retreat is visible to the west of this location, indicating a shift in the erosion hotspot.

The recent shoal migration is slower than the 170 m/y to 460 m/y found by Ridderinkhof et al. (2016). Before 2007, the migration speed was more in line with this range from literature. There is no general rule for the development of the migration speed over time, but intuitively the decrease as shoals are closer to the downdrift coast is credible.

3.2. Vaklodingen dataset

In the Dutch Wadden Sea bathymetric measurement campaigns are conducted on a regular basis. Since 1987, the so called *Vaklodingen* have been realized every 3 years for the coastal area, including the ebb-tidal deltas and every 6 years for the basins. The datasets consist of bathymetric information on a resolution of 20 m, built up from a combination of underwater single and multibeam measurements till the NAP −20 m line, LiDAR measurements of intertidal and land areas and *JarKus* measurements of the shore profiles above the NAP −10 m line. Before 1987, bathymetric measurements are available on a 90 m resolution and without a constant measurement frequency.

For the land area of the Netherlands a digital elevation model (*AHN*) is available. LiDAR measurements have been conducted for several years, resulting in a resolution of 0.5 m for the entire European part of the Netherlands above water.

3.2.1. Hypsometric curve

A hypsometric curve for the area of the Zoutkamperlaag below the Dutch reference level, *NAP*, is given in Figure 3.6. This curve gives the percentage of the area above a certain depth. In this manner it is visualized how the bathymetry of the Zoutkamperlaag tidal inlet and ebb-tidal delta has developed over time between RDx = 197 and 207 km, and RDy = 610 and 616 km.

It can be concluded that since the closure of the Lauwerszee embayment in 1969 the average depth has increased, where it was decreasing before the closure. This is in line with the expected reduction in size of the ebb-tidal delta, due to the reduced tidal prism. Hence, the shrunken ebb-tidal delta volume will result in future attachments of a smaller scale, as was explained in Section 2.1.2.

Furthermore, the attachment of sand shoals is visible in the temporary increase in the area of shallower parts (above NAP −3 m). For the most recent data an initiation of a similar increase in shallower parts in the system is visible. This can be perceived between the depths of NAP −6 m and NAP −3 m.

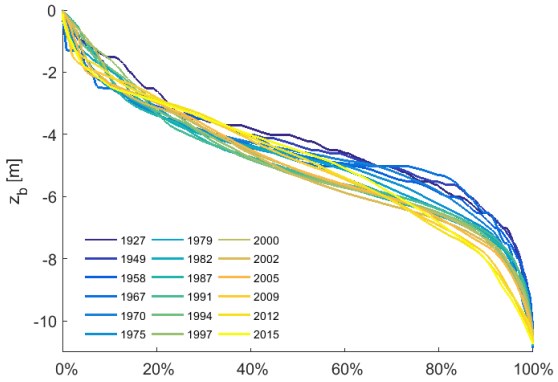

Figure 3.6: Development of the hypsometric curve for all historic *Vaklodingen*

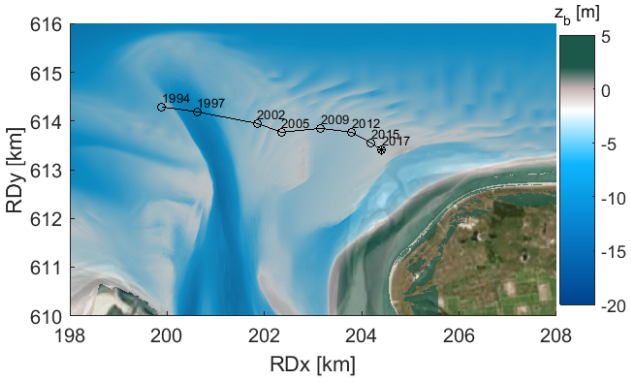

Figure 3.7: Path of center of mass of approaching sand shoal on the 2017 bathymetry

3.2.2. Migration speed of the shoal

In Section 3.1.2, the migration speed of the edge of the approaching shoal is determined. As comparison, this section presents the migration speed of the entire shoal. This is done by following the center of mass of the present-day eastern half of the shoal, because the western half has merged with the current shoal only recently. The path of the center of mass on top of the bathymetry of 2017 is given in Figure 3.7.

The average speed of the approaching shoal is 196 m/y. This is within the range of 170 m/y to 460 m/y as found by Ridderinkhof et al. (2016). As the shoal migrates closer to the shore, a decrease in speed is visible. From the last measurements a lower speed of 130 m/y is observed, which is similar to the found speeds from the *JarKus* dataset.

3.2.3. Sediment volumes in the ebb-tidal delta

In addition to the hypsometric curves, another evaluation of the available sediment in the ebb-tidal delta is conducted. For this purpose a comparison of the sediment volumes of today with the volumes of 1970 is made. The situation in 1970 shows the ebb-tidal delta with still only limited effects of the closure of the Lauwerszee embayment at approximately the same stage in the cycle of sand shoal attachment to the island head of Schiermonnikoog. The eventual attachment at that time occurred in 1972.

Polygons are defined between the waterline and the NAP -5 m depth contour of 1970, and the waterline and the NAP -3 m depth contour of 2017. Subsequently, the sediment volume in this area, above the threshold, is calculated based on data from the bathymetric information (*Vaklodingen*) by Rijkswaterstaat. From Figure 3.8 and Figure 3.9 it can be concluded that the same volume of sediment is available within the 2017 ebb-tidal delta contour. This volume is rather stable around 40×10^6 m^3, besides the peak between 1975 and 1990, which is probably related to the large attachment after the closure of the Lauwerszee embayment. Noordstra (1989) estimates the volume of sediment above NAP -3 m in the large sand hook after the closure to be 11×10^6 m^3. However, a similar peak volume can be found in the bathymetric data from 1927.

The fact that the shoals are located at a larger depth and that additional sediment in the surrounding parts of the ebb-tidal delta is limited may hint at a smaller sediment volume for the upcoming shoal attachment than in 1972. Nevertheless, the 2017 contour of the approaching shoal seems to contain more sediment above the NAP -3 m profile than back then. This volume is comparable to the volume in 1975, after the shoal attachment.

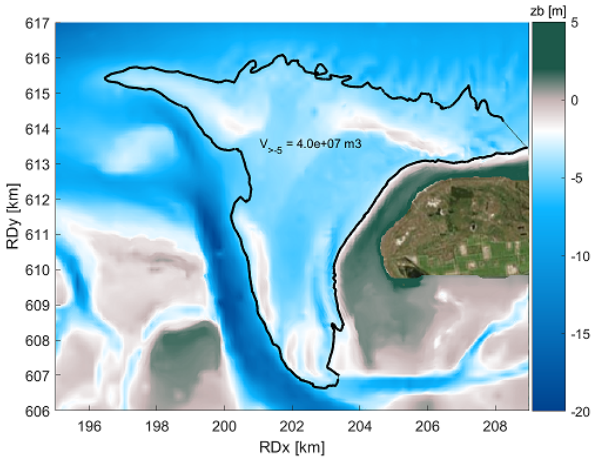

(a) In 1970

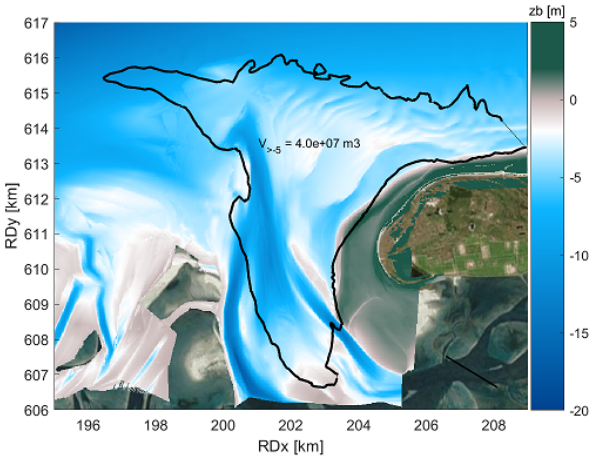

(b) In 2017

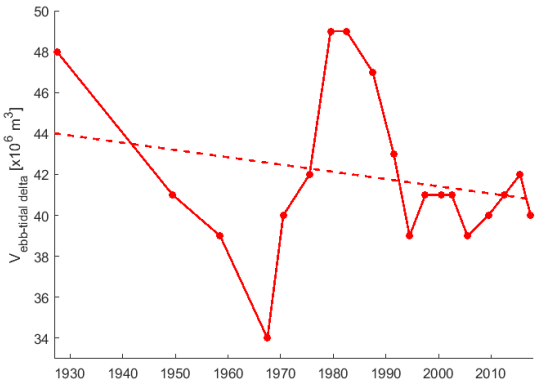

(c) Development over time of the volume in the ebb-tidal delta above NAP −5 m

Figure 3.8: Sediment volumes in the ebb-tidal delta

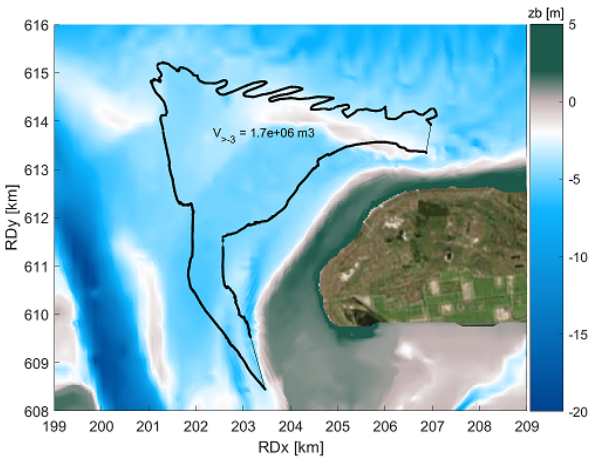

(a) In 1970

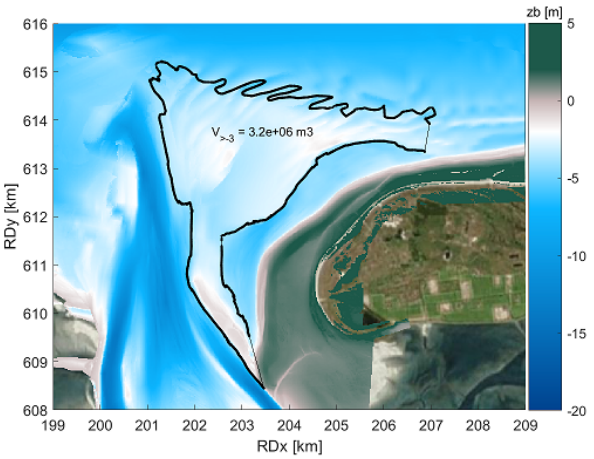

(b) In 2017

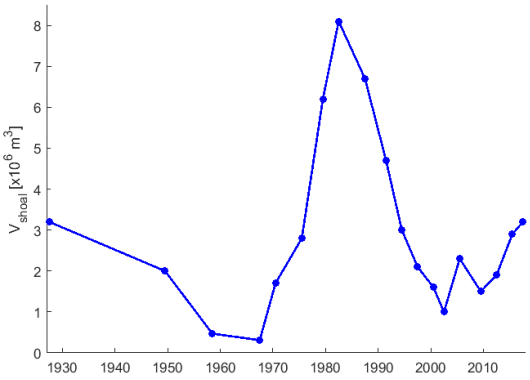

(c) Development over time of the volume in the approaching shoal

Figure 3.9: Sediment volumes in the main sand shoal above NAP −3 m

3.3. Description of the ebb-tidal delta development

From the combination of the *JarKus* and *Vaklodingen* datasets, the historical development of the ebb-tidal delta can be described from the time of the closure of the Lauwerszee embayment till now. An area description and this development were given before in Figure 1.1 and 1.2 in Chapter 1. The development shows an ongoing migration of shoals in a clock-wise direction from west to east. Channels form in the west and migrate along the same path till they are filled in and abandoned during the attachment of a shoal to the island coast of Schiermonnikoog.

The last shoal attachment to Schiermonnikoog occurred in 1972. A large, straight shoal attached near the present-day attachment point. After an initial orientation to the west-northwest, a large sand hook developed following the main coastline orientation. This sand hook slowly migrated toward the island until it merged with the rest of the island head in the northwest, forming a wide beach. Since 2000, with the landward migration of the present-day sand shoal and the Plaatgat this beach has started to erode.

The present-day (flood channel) Plaatgat used to be the (ebb channel) Westgat until a new Westgat took over in 2001. This Westgat of 2001 was soon of minor importance when the present-day Westgat formed in 2005 out of a then recently opened flood channel in the west. The remains of the Westgat of 2001 are now known as the Oude Westgat, a cut through the approaching sand shoal. The present-day Westgat itself is rotating toward the north.

With the closure of the Lauwerszee embayment, the Westgat and the inlet throat have started to fill in. Furthermore the channel and throat have become narrower and the Westgat has translated toward the east. In recent years, the inlet throat consists of two channels with the northern part of a typical flood flat formation between them. In the east, around the island head, the Gat van Schiermonnikoog has elongated farther to the north. Since 2005, a bar out of deposits of this channel has started to develop from the southwestern end of the island toward the northwest. Since 2011, the channel connects to the Westgat and this bar starts to increase in length and seals off the southern end of the Plaatgat. In 2017 the eastern end of the Plaatgat is also sealed off due to the attachment of the NAP -3 m contour of the approaching shoal.

The most recent *JarKus* data from 2018 shows the opening of a new channel in the west of the system. This could indicate the formation of a new flood channel.

3.4. Chapter conclusion

The data from the sections described above, is used to forecast the future development of the Plaatgat, the coastline and the approaching shoal. The development of the Plaatgat and the migration speeds of the shoal and the coastline retraction are combined. Nevertheless, the large uncertainty in the observed trends has to be taken into account when interpreting this extrapolation.

Future development of the Plaatgat

The stabilization of the current-carrying area of the Plaatgat indicates that this channel may not yet be abandoned in the upcoming years. It is likely that a extreme event, reshaping or moving the approaching shoal, will cause a final closure of the channel. However, the formation of bars on both ends of the channel may have decreased its hydraulic efficiency and have had an effect on the currents through the channel. The numerical model results in Chapter 5 give a better understanding of the behavior of the channel.

Basal coastline transgression

The critical part of the coastline near transect 500, where the basal coastline is almost surpassed, shows a retraction of about 20 m/y. This value is of the same magnitude as the available width between the momentary and basal coastlines. Therefore, a transgression will probably occur within a couple of years or less. More to the west of this location, the retraction is increasing to about 40 m/y. In this area the beach is wider, but a future transgression of the basal coastline before the upcoming attachment is likely to occur between transects 400 and 500. According to Rijkswaterstaat's policy it is in principle required to intervene in the upcoming years.

Upcoming shoal attachment

Based on the calculated migration speeds and because the Plaatgat is only 100 m to 500 m wide between transects 500 and 540 respectively, a full attachment of the shoal can be expected in 5 to 10

years. This is a rough linear extrapolation based on the difference between the two migration speeds around the attachment point, assuming no major changes in the current dynamics will occur.

The reduced volume of the ebb-tidal delta, the reduced area of the shallow part in front of the island head and the deeper position of the approaching shoal indicate a smaller volume of the upcoming attachment. Less sediment is available in the system and close to the coast to form a sand hook. This does not come as a surprise, because the sand hook formed after 1972 was exceptionally large and moreover attachments for the new equilibrium situation are expected to be of a smaller volume than the usual.

Observed ebb-tidal delta development

The development of the ebb-tidal delta follows the description given in literature (Oost, 1995; Oost et al., 2015). A new observation in the data of 2018 is the opening of a new channel in the west of the system, north of Het Rif. This channel can be a new flood channel, which would speed up the abandonment of the Plaatgat by relocating a portion of the flood currents through this new opening. The same effect is expected due to the northward rotation of the Westgat, which will allow for the use of this channel by flood currents from the east.

4

Model set-up, calibration and validation

After a short motivation of the choice for the Delft3D Flexible Mesh Suite (Deltares, 2018; Kernkamp et al., 2011) as modeling software in Section 4.1, Section 4.2 gives a description of the set-up of the model developed for this thesis. This includes all made assumptions and settings. Furthermore, it is explained how the model presented in this thesis has been calibrated in Section 4.3. After that, the model validation is presented in Section 4.4. This is done to show the skill of this model and its applicability to be used to assess the occurring sediment transports at Schiermonnikoog NW.

4.1. Motivation of the choice for Delft3D-FM

The main advantage of using the Delft3D Flexible Mesh Suite for this thesis, compared to the more widely used Delft3D 4 Suite, is the ability to locally refine the used grid in the area of interest. In Delft3D 4 this is usually solved by nesting different grids and taking the model results of the coarser grid as input for the boundaries of the finer, nested grid. By nesting, not all information is passed on to the higher resolution grid and the information flow works in one direction only. In the Flexible Mesh approach no information loss occurs. The higher resolution area is an integral part of the rest of the model and receives all information, such as velocities, water levels and waves.

Another significant advantage of the Flexible Mesh Suite over the previous Delft3D 4 software is the ability to run a model as parallel computations. This results in a large reduction in computing time and thereby allows for a more detailed model study. For this thesis, parallel computing has been applied for calculations of both the hydrodynamics and the waves (SWAN). The model is split into 16 partitions.

Furthermore, from the perspective of the programmer, a large advantage is the implementation of a coordinate system. Grid features in the Flexible Mesh Suite are coordinate-based, instead of grid administration based. This allows for quick adaptations of the grid without the time consuming task of updating all definitions of boundaries, cross-sections and observation points. These are defined by their position in the used coordinate system and not linked to specific grid points.

4.2. Model set-up

This section presents the developed model for this thesis. This includes an explanation of the developed grid and the sources of the used bathymetry. Subsequently, the used input data is presented, including water levels, wind, waves and surface water discharges. This is followed by further hydrodynamic and sediment-related settings.

4.2.1. Grid

The starting point of the set-up model is the original Wadden Sea model by Deltares Appendix B.1, De Graaff, 2009), with grid sizes in the inlets of roughly 200 m (see Figure 4.1). The structured grid has been transformed into an unstructured Delft3D Flexible Mesh grid, without any initial alterations. Subsequently, for computational efficiency and a higher resolution at areas of interest, the grid has been coarsened for the deeper parts of the North Sea and refined near the Friesche Zeegat inlet and basin. Figure 4.1 gives the original structured grid by De Graaff (2009) and the adaptation of this grid for

this thesis. The removal of the radiation of finer grid cells to the offshore parts and the grid refinement around Schiermonnikoog and the Friesche Zeegat stand out.

The transition between different resolutions is made out of triangular cells for sufficient smoothness and orthogonality. A choice for a mainly curvilinear grid - similar to the original structured grid - is made based on the high computational efficiency compared to differently shaped grids. A more thorough analysis of different grid types and resolutions is provided in Appendix B.1.

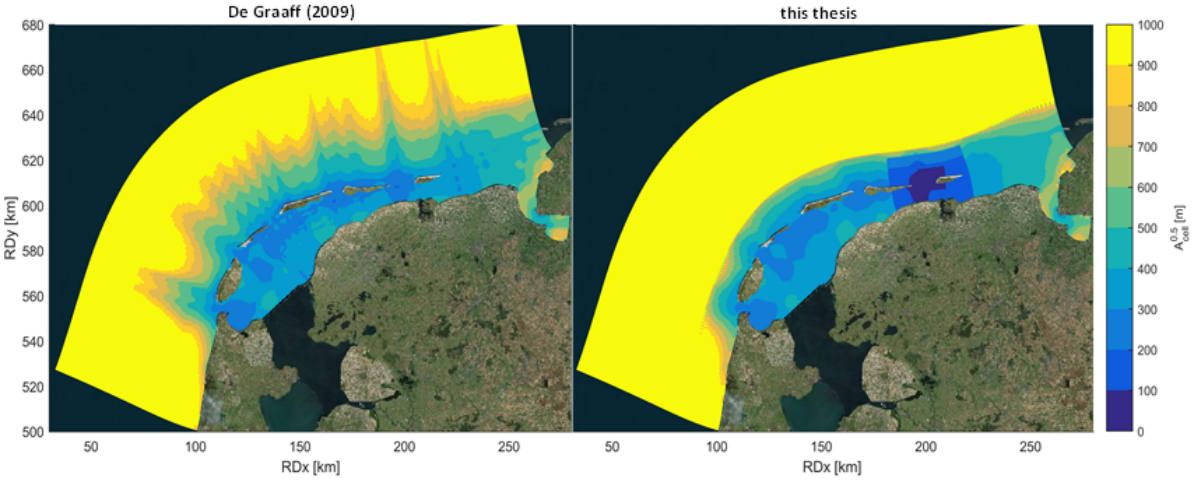

Figure 4.1: Comparison of the grid cell sizes between the model by De Graaff (2009) and its adaptation in this thesis

Three structured (Delft3D 4 Suite) grids have been constructed for the wave modeling with SWAN. These grids have been nested into each other. A large coarse grid with cell dimensions of 10 km is used to cover the northern half of the Dutch North Sea. An intermediate grid is made a factor 2 coarser than the original Wadden Sea model to reduce the required computational time for the model in its entirety. This results in a resolution of 600 m in the tidal inlets. Furthermore, this grid spans a slightly (1 cell) larger area to avoid problems at the boundary with the hydrodynamic computations. To locally obtain more detailed wave information, a finer grid is used for the Friesche Zeegat with a resolution of 150 m.

All resulting wave and hydrodynamic grids are presented in Figure 4.2a. The resolution of the unstructured grid varies over the domain. At the height of the Friesche Zeegat the resolution is about 1 000 m offshore, 200 m offshore of the ebb-tidal delta and in most of the rest of the Wadden Sea, 100 m around the investigated tidal inlet and its back barrier basin, and 50 m on the Zoutkamperlaag ebb-tidal delta.

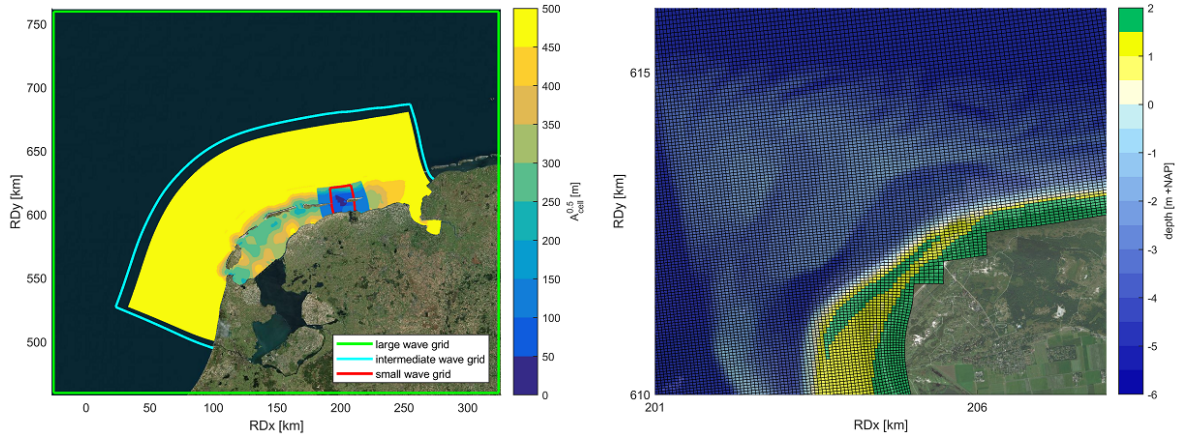

(a) Edge length of hydrodynamic grid cells in [m] and wave grid boundaries

(b) Hydrodynamic grid cells and bathymetry at Schiermonnikoog NW

Figure 4.2: Overview of used grids and grid cell sizes

4.2.2. Bathymetry

Subsequently, bathymetric data is added to every individual grid point. To do so, bed level information is obtained from the *Vaklodingen* by Rijkswaterstaat, the Digital Elevation Model of the Netherlands (*AHN*) by the Waterschapshuis, the bathymetry of the Greater North Sea dataset by the European Marine Observation and Data Network (*EMODnet*) - where the bathymetry of the Dutch waters is provided by the Hydrographic Service of the Royal Netherlands Navy -, and, ultimately, the General Bathymetric Chart of the Oceans (*GEBCO*) by the International Hydrographic Organization and the Intergovernmental Oceanographic Commission of UNESCO. For the most detailed bathymetry at the area of interest around the island head of Schiermonnikoog, raw data from the *JarKus* measurements by Rijkswaterstaat are used. All datasets have been converted to the local reference level (*NAP*), based on the difference between reference levels at the Friesche Zeegat (Kwanten, 2007).

Only the datasets for the *Vaklodingen* and *JarKus* transects are dynamic, where all other datasets do not have varying information over the years. *Vaklodingen* from up to ten years ago have been used to reconstruct the bathymetry of the Wadden Sea and its inlets as detailed as possible. To include a detailed bathymetry of the German Wadden Islands, the *Vaklodingen* of 2005 have been used. The resulting bathymetry for 2017 and the seniority of the used data are given in Figure 4.3. The year 2017 was chosen, because a detailed scan as an extension to the *JarKus* measurements is available. This encloses the entire approaching shoal and the part of the ebb-tidal delta that are relevant for this thesis. The more recent data from 2018 includes only the parts closest to the coast. This has been excluded to prevent any unnatural 'jumps' in the bathymetric configuration.

Alternative bathymetric configurations for this model are all based on the configuration in Figure 4.3. Only locally, in the Friesche Zeegat, this has been altered to the bathymetry of a different year or to a bathymetry with a sand nourishment. Where this is the case, it is stated in the text.

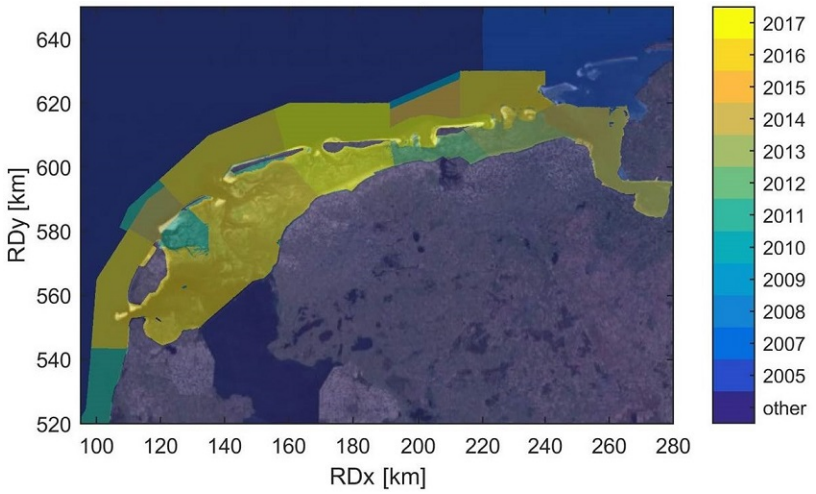

Figure 4.3: Seniority map of the used bathymetry,
where the years stand for the measurement year of the *Vaklodingen* or, in the case of the Friesche Zeegat and around Schiermonnikoog, for the *JarKus* measurements; *other* data consists of a combination of the datasets of the *AHN*, *EMODnet* and *GEBCO*

4.2.3. Input data

The year 2017, which corresponds to the used bathymetry, shows overall conditions around the Dutch average, but also experiences extremes, both in stormy weather and fair-weather conditions (Huiskamp, 2018). It is assumed that this is a representative year for the Dutch Wadden Sea (B.T. Grasmeijer, pers. comm.) and it has been used to determine all model input, such as water levels, wind and waves. Besides, this year corresponds with the recently sorted, calibrated and used input data for the Coastal Genesis II Amelander Zeegat model by Deltares (Nederhoff et al., 2019).

An impression of the wind and wave climates is given in Figure 4.4. From the wind and wave roses it follows that in 2017 the median wind speed was 6.2 m/s from the west-southwest and that the median significant wave height was 0.9 m from the northwest. Waves were higher than 1.3 m for one third of the time and higher than 2.1 m one tenth of the time.

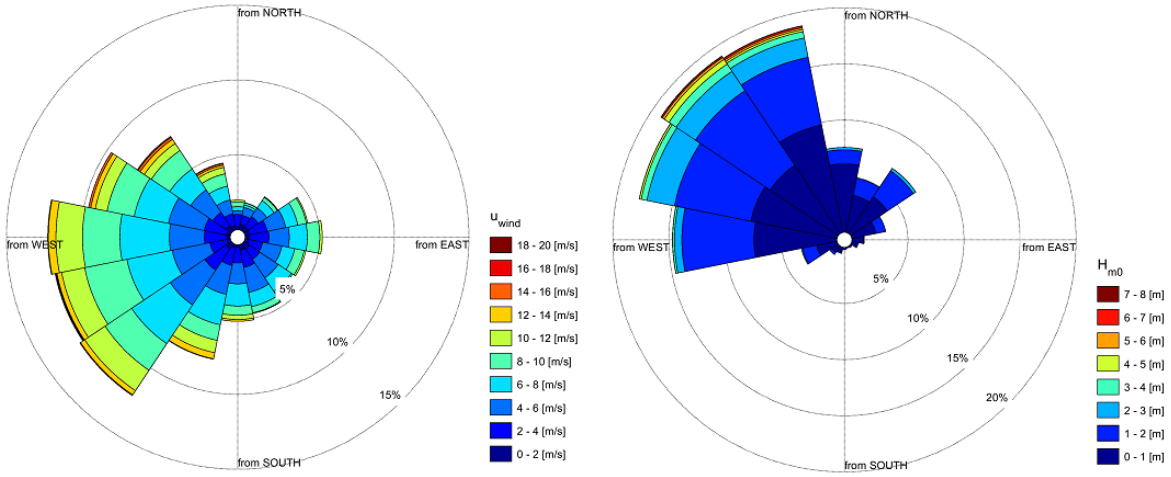

(a) Wind rose at Schiermonnikoog Noord for 2017

(b) Wave rose at Schiermonnikoog Noord for 2017

Figure 4.4: Wind and wave roses for the Friesche Zeegat

Water levels

Following Nederhoff et al. (2019), on the sea boundaries of the model water level data from the DCSMv6-ZuNov4 (Zijl et al., 2013) is derived. This input has been adjusted to account for the difference between the used mean sea level (MSL) in DCSMv6-ZuNov4 and the reference level of the bathymetric data (*NAP*) in the FM-model. The water level on the boundaries includes a tidal signal and a non-tidal residual (NTR). The latter is also known as 'surge'.

Wind

Wind and pressure conditions are taken from the ERA5 atmospheric reanalysis (Hersbach, 2016). This is the successor of the ERA-Interim model (Dee et al., 2011) by the European Centre for Medium-Range Weather Forecasts. The model provides hourly model output on winds and pressure at a resolution of 31 km (Olauson, 2018). According to Nederhoff et al. (2019) when comparing to wind observations, the ERA-Interim model for the entire year resulted in virtually the same skill score as the HIRLAM model, used in that study. With an overestimation of 13 Pa for the atmospheric pressure and an underestimation of 0.2 m/s for the wind speed magnitude, this data can confidently be used as model input. Furthermore the used wind data matches the used wave data, as is explained below. The ERA5 datasets are used for both the hydrodynamic computations and the wave computations in SWAN.

Waves

For the wave computations, the ERA5 results are put onto the large wave grid (see Figure 4.2a, which uses boundary conditions from the same ERA5 reanalysis with information on the wave height, period, direction and directional spreading. The nested wave grids use boundary conditions with calculated energy spectra from the grid above.

Waves are modeled with the D-Waves module, using the third-generation SWAN-model (Booij et al., 1999; Holthuijsen et al., 1993; Ris et al., 1999). SWAN version 3.07.00.62800 is used with the following settings:

- **Communication time step**: Stationary wave computations are conducted every 60 minutes, where wave forces follow from 3D-dissipation. At the same interval the hydrodynamic module and SWAN communicate. For the SWAN-computations, water level and velocity are taken from the results of the hydrodynamic computation. For this time step the average water level difference between two sequential SWAN computations is 33 cm. Wind speed information is taken from the same ERA5 dataset as used by the hydrodynamic computation.
- **Third generation mode**: The third generation SWAN-computation is used including wind input with wind growth, wave breaking, triad and quadruplet wave-wave interactions, whitecapping and refraction. No diffraction is included.
- **White-capping**: The Van der Westhuysen et al. (2007) formulation for a combination of wind input and saturation-based whitecapping is chosen.

- **Bed roughness**: A constant bed roughness of 0.038 $m^2 s^{-3}$ is used, which is typical for sandy bottoms.
- **Numerical accuracy**: An accuracy of 1% is set for relative wave height and period differences. At least 95% of the wet cells has to meet this requirement. The maximum number of iterations for convergence is set to 20.
- For all other settings the default values, recommended by Deltares, are used.

Surface water discharges
Discharges into the Wadden Sea from surface water by the three main sluices have been taken into account. The three largest discharge sluices in the investigated area are the *Stevin* and *Lorentz* sluices in the *Afsluitdijk* and the *R.J. Clevering* sluices in the *Lauwersmeerdam*. With up to 70×10^6 m^3 per tidal cycle for the first two (Eysink, 2003) and about 2.5×10^6 m^3 per tidal cycle for the latter (data by water board *Noorderzijlvest*), the contribution of these discharges is minimal compared to the tidal prisms in the back barrier basins (see Table 4.2). However, compared to the residual discharge over the watersheds and through the inlets (see Figure 4.6), these volumes may be of importance for sediment dynamics and sediment exchange between the North Sea to the Wadden Sea basins. Therefore, the effect on the ebb-tidal delta by the three discharge sluices will have to be investigated. The density difference between the discharged fresh water and the salt water in the Wadden Sea mainly plays a role for transport of fines, but this effect is considered to be of minor importance in the sandy ebb-tidal delta, the area of interest, and is therefore not included.

4.2.4. Further settings
Below additional hydrodynamic and sediment-related model settings are given. The settings of the wave model have been discussed earlier in Section 4.2.3.

Hydrodynamics
As mentioned before, the model is run in the Delft3D Flexible Mesh Suite, used in the depth-averaged mode. Its version is 1.1.273.59582 (D-Flow FM version 1.2.21.62800). To reduce the computation time and since the sediment in the ebb-tidal delta consist mainly of sand, no 3D-computation is used. The sediment transport for sand can usually be sufficiently represented by Delft3D in a 2DH-computation. A further discussion on this assumption can be found in Nederhoff et al. (2019).

The following settings have been applied:

- **Bed roughness**: A Manning friction coefficient of 0.020 $s/m^{1/3}$ has been used. This value results from the model calibration, as is explained in Section 4.3 and Appendix B.2.
- **Time step**: A maximum time step of 60 s is used. An average time step of 16 s followed from the model results, after conflicts with about 11.6% of cells limited by the used Courant-Friedrichs-Lewy condition of 0.7. By far most of the conflicting cells are located in the refined area of the Friesche Zeegat inlet and its back barrier basin. In that part of the grid 17.3% of the cells is limiting, which is deemed acceptable to not hold up the computational time too much. It is therefore assumed that no further optimization of the grid is required to reduce the total computation time. The calculated time step may limit the discharged water from the discharge sluices, since the flow velocities from these are limited by the CFL-condition. However, it has been observed that this is not the case.
- **Time zone**: For a smooth coupling with hydrodynamic input from the model DCSMv6-ZuNov4, the time zone of the model has been set as GMT.
- **Viscosity and diffusivity**: According to the recommendations for this grid resolution by Deltares (De Graaff, 2009), a uniform horizontal eddy viscosity of 1 m^2/s and a uniform horizontal eddy diffusivity of 1 m^2/s are used. Because no significant effect on the computed water levels is observed by altering these values, these have not been further optimized.
- **Drying and flooding**: A drying and flooding criterion for individual cells is set to 0.05 m.
- **Wind stress formulation**: Following Nederhoff et al. (2019), the Vatvani et al. (2012) wind stress formulation was used (see Table 4.1), where the middle C_d-coefficient is comparable with the recommendation by Deltares (Van Os and De Graaff, 2009), following a Charnock-value of α = 0.032.
- For all other settings the default values, recommended by Deltares, are used.

wind speed [m/s]	C_d (x 10^{-3})
0	1
25	3.0
50	1.5

Table 4.1: Wind stress formulation values by Vatvani et al. (2012) with a C_d-coefficient for specific wind speeds; in between a linear interpolation has been used

Sediment

Two sources of information for sediment near the island head of Schiermonnikoog are used, the *Sedimentatlas* of the Wadden Sea by Rijkswaterstaat and the *NCP* grain size map by TNO. From both datasets it follows that mostly sand with a median grain size of 180 µm to 220 µm is present at the area of interest. These measurements were conducted at the bottom surface in 1998. The *DINO*-cores show no major changes over the depth at Schiermonnikoog, so it is assumed that the entire profile consists of sediment of the same dimensions.

Based on these datasets, a uniform sediment is chosen as input for this model. This is sand with a specific density of ρ_s= 2650 kg/m^3, a median diameter of d_{50}= 200 µm and a 90_{th} percentile diameter of d_{90}= 300 µm. A sediment bed thickness of 5 m with an initial dry bed density of ρ_b= 1600 kg/m^3 is applied.

Since only sediment transport will be analyzed, no morphological updating is included in the model, so no additional information on the morphological settings is discussed. For sediment transport, by default, the Van Rijn (1993) formula is used. The improved Van Rijn et al. (2007) formula is not yet available in Delft3D Flexible Mesh.

4.3. Model calibration

4.3.1. Grid size and bathymetry

At first, with the aforementioned input data for hydrodynamics and wind, the original Wadden Sea model (De Graaff, 2009) has been altered to reach an optimal result. For this purpose, the observed water levels at several measurement stations in and near the Dutch Wadden Sea are compared to the model results. For the exact outcome and an overview of all locations, see Section 4.4.

The water levels have been improved by altering the bathymetry to better represent the harbors in the local grid resolution, where measurement stations are located (*Vlieland, West-Terschelling, Lauwersoog* etc.). Furthermore in the Friesche Zeegat the grid has been refined to such a level that individual gullies and channels are sufficiently represented (see Figure 4.2b). From the chosen grid size (about 100 m) onward, further refinement did not result in significantly more accurate water levels (see Figure B.1 in Appendix B.1). However, it has been refined up to 50 m at the area of interest to allow for a more detailed study of sediment transport patterns.

4.3.2. Bottom friction

Secondly, a first order (crude) calibration of the bottom friction coefficient has been conducted. The water levels and tidal constituents for all measurement locations in the model have been compared. No optimal value is found, since for the overall model, water levels are best represented with a Manning friction coefficient of 0.023 s/m$^{1/3}$, where for the Friesche Zeegat the representation is best for 0.020 s/m$^{1/3}$. This last value has been chosen for the entire model. The found root-mean-square errors can be attributed to an offshore error in the tidal propagation and/or a local error in the bathymetry. This is in agreement with the results of DCSMv6-ZuNov4. An overview of all results is given in Figure B.2 in Appendix B.2.

Due to the limited time to set up the model and the expected limited effect of a better hydrodynamic representation on the observed sediment transport patterns, no further calibration per individual tidal constituent has been conducted, nor has a spatially varying bottom friction been applied.

4.4. Model validation

In this section the skill of the model is discussed. Model results on water levels, main tidal constituents, water volumes through tidal inlets, and waves are presented. By comparing these with observations and literature the model has been validated.

4.4.1. Hydrodynamics

Total water levels

A run with exclusively hydrodynamics shows good results, when comparing the model results with the observations at several stations in the Wadden Sea. A main assessment is conducted based on the root-mean-square error between the two. This error varies between about RMSE = 9.4 cm offshore and about RMSE = 13.2 cm in the Wadden Sea, as can be seen in the overview map in Figure 4.5. The root-mean-square errors of the input data (DCSMv6-ZuNov4) are about RMSE = 8.6 cm offshore and about RMSE = 9.6 cm in the Wadden Sea. These errors are quite similar and in the area of interest the differences are negligible (see Figure B.2 in Appendix B.2). DCSMv6-ZuNov4 has a spatially varying bottom roughness and a locally altered bathymetry to represent the water levels as accurate as possible. It is satisfactory that the proposed model in this thesis, with a more realistic bathymetry and a constant bottom roughness, shows relatively similar results.

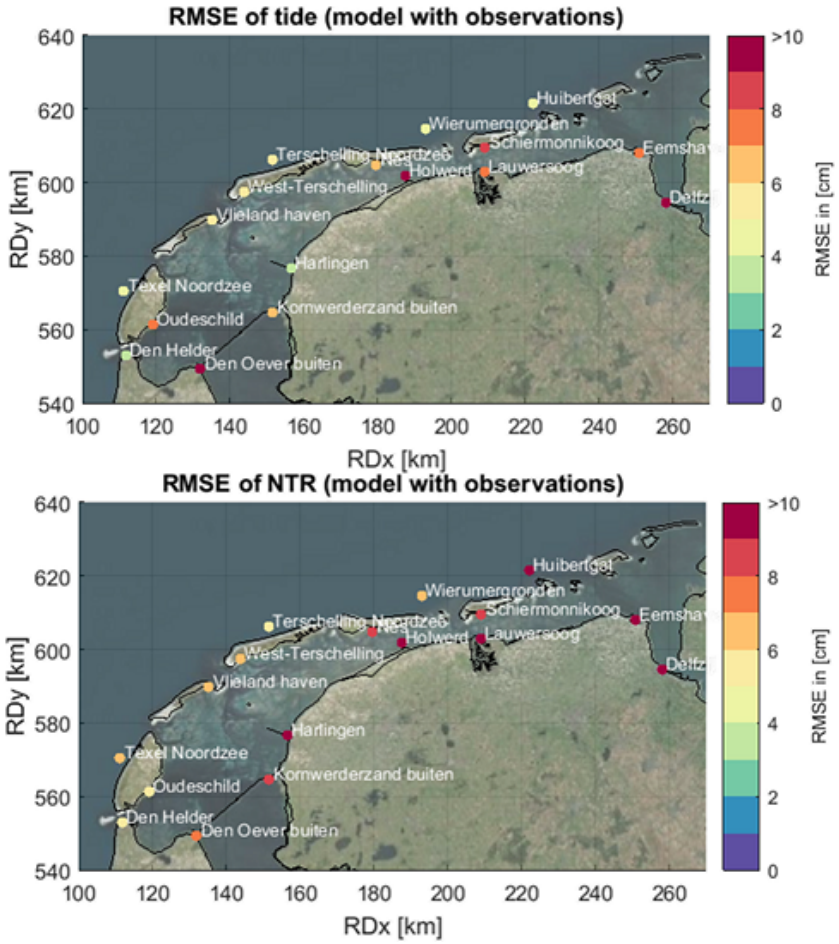

Figure 4.5: Root-mean-square errors in [cm] at measurement stations between the FM-model results and observations for the tidal water levels and the non-tidal residual (NTR)

The largest error is calculated at the measurement station in the harbor of *Delfzijl*, which is related to the poor representation of this harbor in the local grid resolution. In the area of interest both the proposed model's and the DCSMv6-ZuNov4 results are the poorest, but with root-mean-square errors around 10 cm the resemblance with the reality is fairly good. The overall water level representation is deemed acceptable for the intended use, an analysis of sediment transports and morphological

development.

The results of the measurement stations *Wierumergronden* at the western side of the Friesche Zeegat, *Schiermonnikoog* at the ferry groyne and *Lauwersoog* at the land-based ferry terminal, are visualized in Figures 4.8a, 4.8b and 4.8c respectively. The total water level has been split in a tide-related signal and a non-tidal residual (NTR). For a more detailed explanation and overview of the resulting RMSE, see Appendix B and for the results of DCSMv6-ZuNov4, see Appendix A.

Tidal constituents

From the same run with solely hydrodynamics, the main tidal constituents can be analyzed. For this purpose the amplitude ratio, of the modeled over the observed amplitude, and the difference in Greenwich phase lags are calculated. An overview for all locations is given in Table 4.5 and Figure 4.9.

Furthermore, an increase in both tidal amplitudes and Greenwich phase lags from southwest to east along the offshore measurement stations is observed. It clearly shows the propagation of the tidal wave along the Wadden Islands. A small overestimation in the west and a small underestimation in the east can be observed, but no general trend in the error is visible.

Water fluxes

Another way to evaluate how well the model represents reality is by analyzing the discharges through the tidal inlets. The sum of the average flood and ebb volumes through an inlet over a tidal cycle results in the tidal prism of the corresponding back barrier basin. From the average residual discharges it can be assessed whether the inlet in question is flood- or ebb-dominant. Subsequently this can be compared with the results from the DCSMv6-ZuNov4 model and information from literature.

A quick calculation for the hydrodynamic part of the model results in the average water volumes over the year 2017 in Table 4.2, which also includes an overview of the volumes found in literature (Louters and Gerritsen, 1994). In this publication the tidal prism has been calculated as the product of the area of the back barrier basins, based on the position of the tidal watersheds, and the average depth of the flats below the high water level. It can be concluded that the model represents the average tidal prism rather accurately.

Tidal prism (P)	***(Louters and Gerritsen, 1994)***	***DCSMv6-ZuNov4***	***FM-model***
Marsdiep	$1054 Mm^3$	$1045 Mm^3$	$1119 Mm^3$
Eierlandse Gat	$207 Mm^3$	$197 Mm^3$	$184 Mm^3$
Vlie	$1078 Mm^3$	$1018 Mm^3$	$1016 Mm^3$
Borndiep	$478 Mm^3$	$469 Mm^3$	$428 Mm^3$
Friesche Zeegat	$300 Mm^3$	$354 Mm^3$	$343 Mm^3$
Residual discharge (Q_{res})	***Dominance***	***DCSMv6-ZuNov4***	***FM-model***
Marsdiep	Ebb	$-25.9 Mm^3$	$-35.3 Mm^3$
Eierlandse Gat	Flood	$10.5 Mm^3$	$14.0 Mm^3$
Vlie	Flood	$42.5 Mm^3$	$44.6 Mm^3$
Borndiep	Ebb	$-9.6 Mm^3$	$-28.9 Mm^3$
Friesche Zeegat	Ebb	$-7.5 Mm^3$	$-3.3 Mm^3$

Table 4.2: Average water volumes through inlets from literature and computed from DCSMv6-ZuNov4 and the FM-model presented in this thesis with only hydrodynamic forcing

However, the residual discharges differ quite significantly. This does not come as a surprise, since their magnitudes are hard to determine in an exact manner due to the large dependence on wind forcing (Duran-Matute et al., 2016). Nevertheless, the resulting flood- and ebb-dominance of the inlets is correct, compared to the results of the DCSMv6-ZuNov4 model and to the study by Duran-Matute et al. (2014). This shows that the general residual flow pattern in the Wadden Sea is correctly represented.

Anticipating on the model results in Chapter 5, the sediment transport magnitudes around the island head of Schiermonnikoog NW are mainly driven by waves and only to a lesser extent by tides. Tides do play a role in determining the direction of the transport. Therefore, the correct representation of the residual flow direction is deemed of importance. However, the incorrect magnitude of the residual flow through the inlet will not affect the intended outcome of this thesis, the sediment transport at the area of interest.

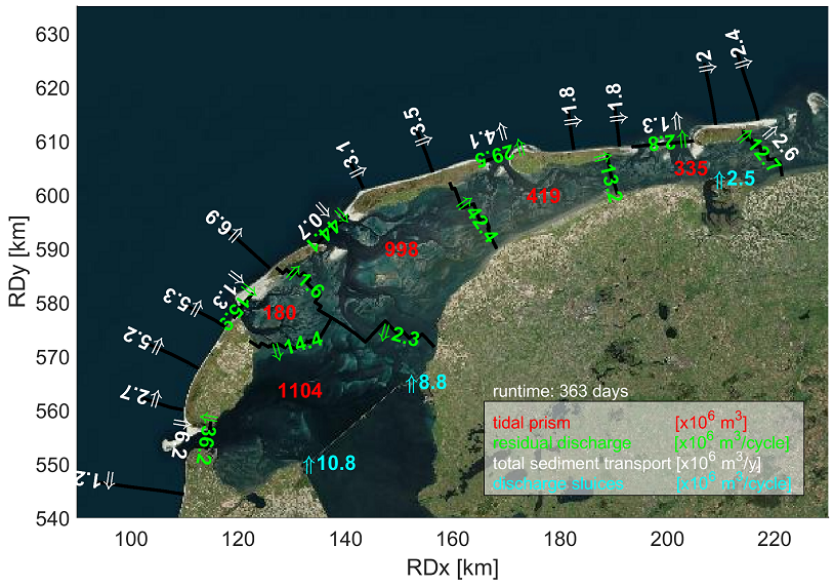

Figure 4.6: Tidal prisms, residual discharges per tidal cycle through inlets and over watersheds, main surface water discharges per tidal cycle and yearly total sediment transport from the FM-model results

4.4.2. Waves

The resulting scatter in wave heights is presented in Figure C.1 in Appendix C. Table 4.3 gives an overview on further performance of the significant wave heights at principal offshore measurement stations. These values are acceptable, when compared to other studies (Gautier et al., 2014; Van der Westhuysen, 2010). A full comparison with these and other studies is given in Appendix C.

Appendix C also includes an analysis of the effect the wave representation has on modeled sediment transports. This shows that an improvement of the root-mean-square error from a more accurate run does not bring about an improvement of the sediment transport of the same scale. It is therefore concluded that a further optimization will not significantly alter the modeled sediment transports, and that the achieved accuracy is sufficient.

Buoy	**$RMSE_{Hm0}$ [cm]**	**relative $bias_{Hm0}$ [-]**	**SCI_{Hm0} [-]**
Eierlandse Gat	33	-0.01	0.25
Amelander Zeegat 1-1	28	-0.04	0.21
Amelander Zeegat 1-2	28	0.03	0.22
AWG platform	21	-0.07	0.31
Schiermonnikoog Westgat	38	0.05	0.37
Schiermonnikoog Noord	25	0.06	0.22
Buoy	**$RMSE_\theta$ [°]**	**relative $bias_\theta$ [-]**	**SCI_θ [-]**
Eierlandse Gat	72	0.02	0.32
Amelander Zeegat 1-1	66	0.03	0.28
Amelander Zeegat 1-2	60	0.02	0.25
Schiermonnikoog Noord	73	0.02	0.30

Table 4.3: Root-mean-square errors, biases and scatter indices for the significant wave heights and directions between the observations and the FM-model at several wave buoys

4.4.3. Sediment transport

Transport through inlets

Previous studies for all inlets The computed total sediment transport[1] volumes through the inlets for 2017 is given in Figure 4.6. This has been compared with studies based on measurement data in Table 4.4. The sediment import through the Marsdiep and Vlie is roughly in line with previous studies (Elias, 2006, 2018a; Van Koningsveld et al., 2009). The import through the Eierlandse Gat is rather large, compared to the small sediment export according to Elias (2018a) and Van Koningsveld et al. (2009). The computed sediment exports through the Borndiep and Friesche Zeegat are remarkable. Other studies expect import through these inlets, with a significantly smaller magnitude (Elias, 2018b; Elias et al., 2012; Van Koningsveld et al., 2009). The found export is not unique for a numerical model study. De Fockert (2008); Teske (2013) found a similar result for the Borndiep using the Van Rijn et al. (2007) and the Van Rijn (1993) transport formulations respectively.

Inlet	Literature	FM-model
Marsdiep	$4.9 - 6.0 Mm^3/y$	$6.2 Mm^3/y$
Eierlandse Gat	$-0.2 Mm^3/y$	$1.3 Mm^3/y$
Vlie	$0.9 - 1.4 Mm^3/y$	$0.7 Mm^3/y$
Borndiep	$0.0 - 1.0 Mm^3/y$	$-4.1 Mm^3/y$
Friesche Zeegat	$0.2 - 1.1 Mm^3/y$	$-1.3 Mm^3/y$

Table 4.4: Modeled and measured sediment import and export through the tidal inlets in the Dutch Wadden Sea, where positive values stand for sediment import and negative values stand for sediment export

It is important to note that values found in the previously mentioned studies are based on field data, which mainly focuses on sedimentation and erosion found in the *Vaklodingen* bathymetric measurements. Van Ledden (2003) points out that a small measurement error in the bed level data will lead to a significant impact on calculated sediment transport. The model results follow from the cumulative sediment transport through a cross-section in the inlet. Therefore, an exact comparison of magnitudes is not possible. Furthermore, transports and volumes in these studies are based on an average over several decades, where the model results represent one specific year. This makes a comparison between the two difficult.

An overestimated sediment export for the Borndiep was also observed by Lenstra et al. (2019). Here the single grain size in the model is seen as the cause. It is likely that the same problem occurs in the model in this thesis, which also contains a single grain size.

The focus of this thesis is on the sediment transport patterns over the ebb-tidal delta and along the coast of the island head. As discussed in the results in Chapter 5, this is mainly influenced by conditions from offshore. The largely tide-driven export through the inlet is not expected to be of large influence on the modeled overall patterns.

Time series for the Zoutkamperlaag No fine sediment fraction is included in this model, because of its limited influence on ebb-tidal delta and coastal development. Therefore, the sediment transport through the Zoutkamperlaag is not entirely representing reality. However, the varying sand transport over a tidal cycle can be analyzed to asses its representation in the model.

A measured total sand and silt transport through this inlet during the spring tide of April 4, 1991 is given by Louters and Gerritsen (1994). The result is visible in Figure 4.7 where the continuous (brown) line stands for sand transport. This is compared with the transport during two spring tides for similar weather conditions in the modeled 2017, the grey and black lines. During flood, when the water level (blue line) rises, sediment import is visible, and during ebb, sediment export is visible. The magnitudes of the transport are similar for the measurements and the model results.

[1] In this thesis, the term *total sediment transport* refers to the sum of the bed load and suspended transports as defined in the Van Rijn (1993) formulation.

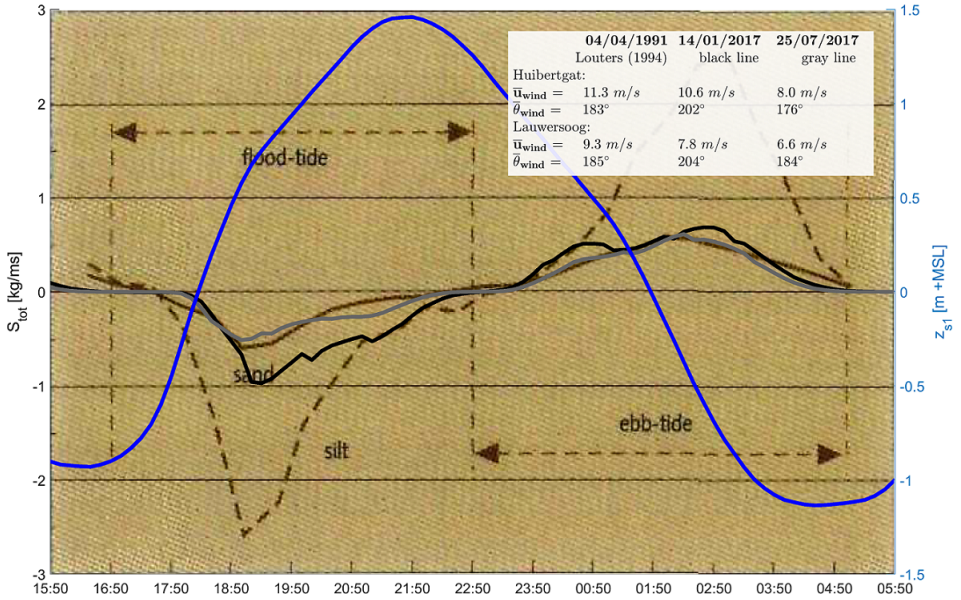

Figure 4.7: Sediment transport through the Zoutkamperlaag inlet throat as measured during a spring tide in 1991 (Louters and Gerritsen, 1994) and as calculated during two similar spring tides for 2017; in blue the water level at the northern end of the Westgat is given; wind conditions for the three tidal cycles are summarized in the table in the upper right corner

Longshore transport

Along the North Sea coastline several cross-shore cross-sections are defined between the grid boundary on the island and the NAP −20 m depth contour. The resulting cumulative sediment transport for the entire year is given in Figure 4.6. The longshore transport at the coasts of Ameland and Schiermonnikoog is with 2 Mm^3/y in line with literature (Cheung et al., 2007; Ridderinkhof et al., 2016; Steetzel, 1995), when considering that in other studies only surf zone parameters have been used. Values at more western locations seem very high. This is most likely related to a combination of problems in the used model schematization:

- the grid sizes of over 300 m are too large to properly represent the surf zone;
- the grain size diameter of d_{50}= 200 µm is too small for the coasts and ebb-tidal deltas to the west, where values of up to 450 µm are found; this results in a strong influence of a tide-driven longshore transport up to 2.5 Mm^3/y at the coasts of North Holland, Texel and Vlieland.

4.5. Chapter conclusion

In this chapter, a model grid is presented for the entire Dutch Wadden Sea with a refinement for the Friesche Zeegat and Schiermonnikoog. The model runs for the calendar year 2017 with bathymetric data from the *JarKus* and *Vaklodingen* measurements by Rijkswaterstaat, water level results from the larger DCSMv6-ZuNov4 model by Zijl et al. (2013), and wave and wind information from the worldwide atmospheric reanalysis ERA5 (Hersbach, 2016). Sediment in the model consists of only sand of a single grain size distribution. Model settings are based on recommendations by different studies by Deltares.

A calibration for the hydrodynamics has been conducted by refining the local grid size at the Friesche Zeegat, and by finding an optimal model-wide bottom friction to represent the investigated area. The bathymetry has been altered around measurement stations to include harbors where these are located. For the rest of the domain the bathymetry is based on bathymetric surveys and is as realistic as possible.

To validate the model results, a comparison to observations is made. For both hydrodynamics as waves the bias and accuracy are in line with previous studies. It has been shown that sediment transports do not significantly alter under further improvements of the water level and wave representation. The longshore sediment transport is similar to values from literature and the magnitude of the transport through the tidal inlet is comparable to available measurement data. However, the inlet is exporting sediment over the year, where literature indicates import. This is further elaborated in the discussion

in Chapter 7, but is not deemed of major importance to the overall sediment transport patterns around the island head, farther from the inlet.

Use of Delft3D Flexible Mesh

The used model set-up shows the applicability of the Delft3D Flexible Mesh Suite. The model covers a large domain, which has the benefit of omitting nearby boundary simplifications over tidal watersheds. By including these tidal watersheds, exchange between the different basins of the Dutch Wadden Sea is incorporated in the model. The possibility to locally refine the grid without radiation of the resolution to other parts of the grid - as is the case in the structured grids of the Delft3D 4 Suite - keeps the computation time for this large grid within an acceptable range, while providing detailed model results for the area of interest.

The use of larger model and reanalysis results from DCSMv6-ZuNov4 and ERA5 does not require large assumptions to be made by the programmer, is not time-consuming and is easy to apply. Additionally, in this manner, a more accurate spatially varying boundary condition is used, instead of the more common approach of scaling measurement data from a single buoy or station to the model boundary.

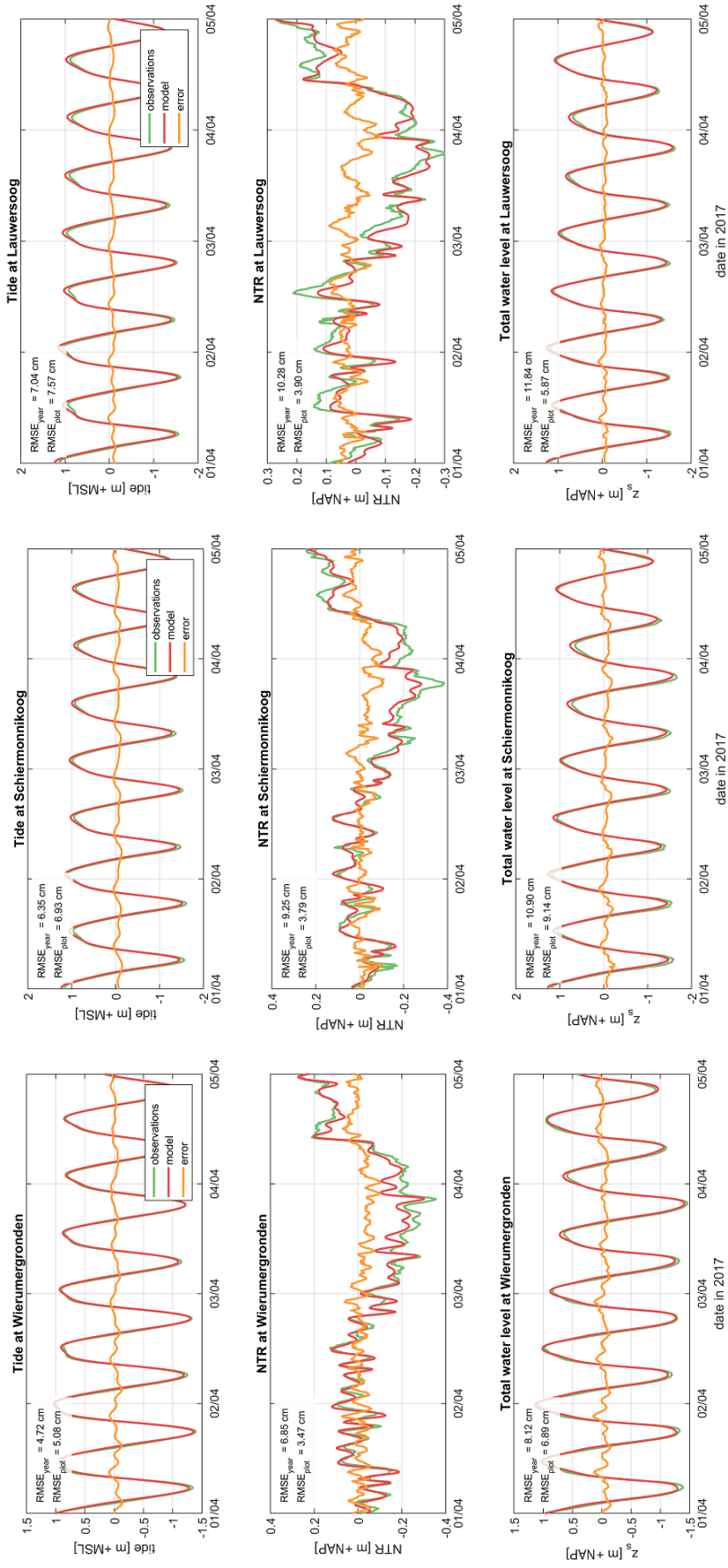

(a) Water levels at *Wierumergronden*

(b) Water levels at *Schiermonnikoog*

(c) Water levels at *Lauwersoog*

Figure 4.8: Water levels at three measurement stations in the FM-model and the observations with the RMSE in [cm] for the tidal, non-tidal residual and total water level

Station	$RMSE_{tide}$[cm]	$RMSE_{NTR}$[cm]	$RMSE_{total}$[cm]	ratio a_{M2}[-]	$\Delta\phi_{M2}$[◦]	ratio a_{S2}[-]	$\Delta\phi_{S2}$[◦]	ratio a_{M4}[-]	$\Delta\phi_{M4}$[◦]	ratio a_{N2}[-]	$\Delta\phi_{N2}$[◦]
Delfzijl	8.92	11.86	15.50	1.02	1.36	1.02	2.65	0.75	9.10	1.01	3.05
Den Helder	6.67	6.50	9.90	1.12	-0.15	1.12	0.60	1.03	0.70	1.17	1.19
Den Oever	15.84	8.46	19.70	1.27	-5.77	1.33	-4.36	1.37	2.59	1.33	-7.85
Eemshaven	4.48	9.54	10.62	1.01	0.99	0.99	2.07	0.78	-5.72	1.00	2.67
Harlingen	11.63	9.86	18.05	1.13	-5.56	1.15	-6.44	1.32	2.82	1.15	-5.72
Huibertgat	5.09	11.11	12.21	1.00	0.06	0.97	0.70	0.95	-8.23	0.97	1.93
Kornwerderzand	15.63	8.74	20.84	1.22	-6.06	1.28	-5.42	1.63	-4.86	1.27	-7.52
Lauwersoog	7.04	10.28	12.24	1.01	-0.53	0.97	-0.27	0.97	-6.70	1.03	2.94
Nes	5.75	9.43	11.42	1.02	-0.82	1.00	-0.88	0.87	-8.12	1.01	1.32
Oudeschild	11.58	6.51	14.25	1.22	-4.22	1.24	-3.83	1.15	1.29	1.29	-4.10
Schiermonnikoog	6.35	9.25	11.77	1.01	1.10	0.97	2.08	0.90	0.20	1.00	3.45
Terschelling Noordzee	6.03	6.44	8.93	1.00	2.19	0.98	1.34	1.08	-1.67	1.01	2.89
Texel Noordzee	5.87	7.09	9.22	1.02	0.67	1.05	0.17	1.12	10.51	1.07	2.14
Vlieland	9.57	6.67	12.59	1.12	-3.44	1.14	-4.72	1.24	-12.34	1.15	-3.07
West-Terschelling	10.20	7.01	13.60	1.14	-3.24	1.16	-3.51	1.29	2.11	1.17	-2.63
Wierumergronden	4.72	6.85	8.28	1.00	1.42	0.98	0.78	1.01	-4.14	1.01	1.99
Average	8.46	8.48	13.07	1.08	1.38	1.08	1.19	1.09	1.40	1.10	0.46

Table 4.5: Root-mean-square errors for the tidal, non-tidal residual and total water levels, tidal amplitude ratios and phase differences between the FM-model and the observations at several water level measurement stations

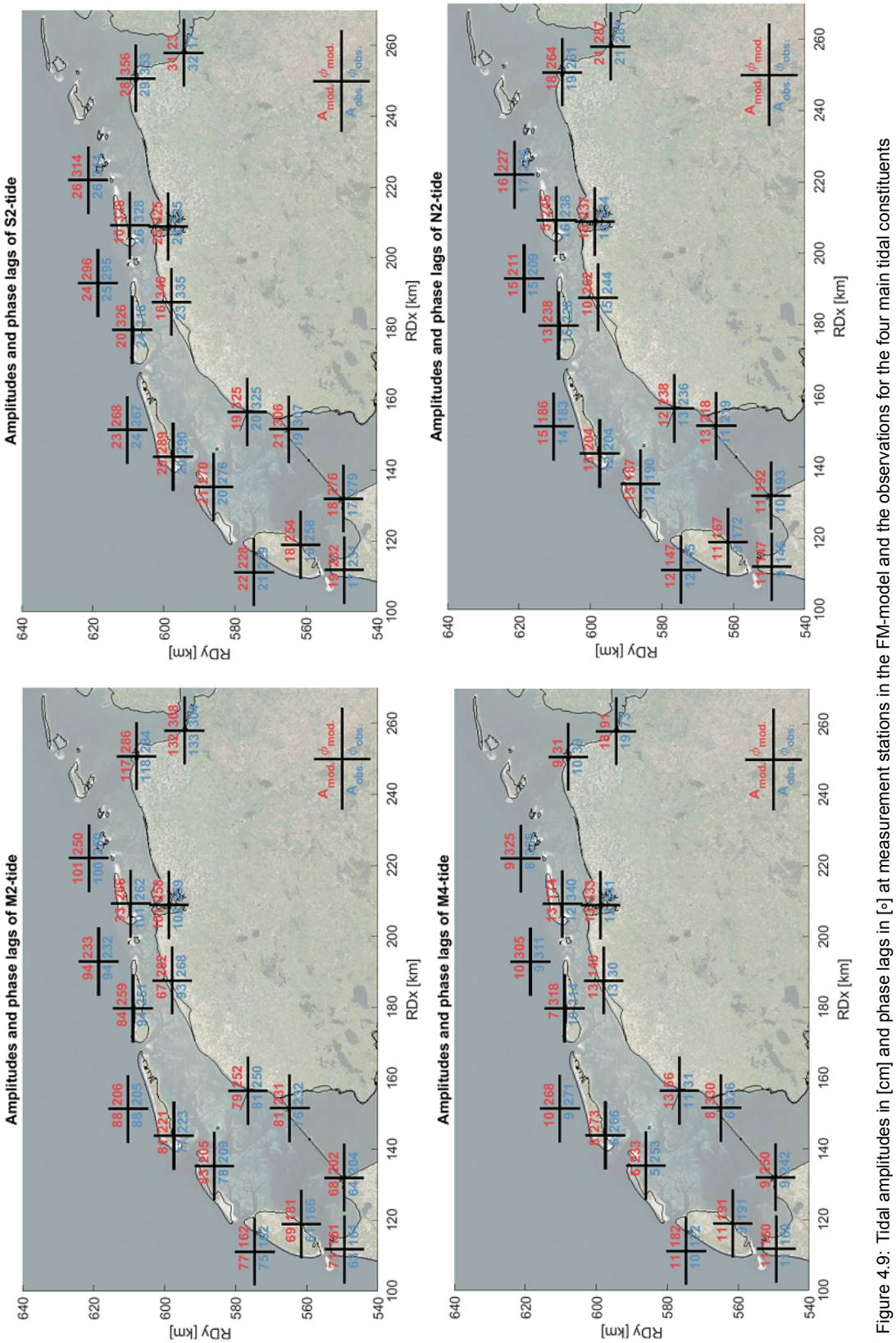

Figure 4.9: Tidal amplitudes in [cm] and phase lags in [◦] at measurement stations in the FM-model and the observations for the four main tidal constituents

5

Model results

After an overview of the conducted model runs in Section 5.1, the model results are presented by use of different topics. First of all, in Section 5.2, the hydrodynamics, waves and sediment transports are characterized. Section 5.3 describes the influence of individual processes on the occurring sediment transport. Subsequently, in Section 5.4, the development of different processes and the sediment transport over the length of the channel Plaatgat is discussed. In Section 5.5 the results for the present-day bathymetry are compared to those for the bathymetry in 2009 and to those for the present-day bathymetry with different sand nourishments in and near the Plaatgat. Section 5.6 gives an analysis of the importance of storm events. A chapter conclusion is provided in Section 5.7.

5.1. Overview of model runs

Several model runs are conducted for this thesis. To assess the importance of the driving forces of morphological changes, an evaluation of the impact of different processes on the sediment transport is made. Different model runs are conducted with the contribution of tide and discharges (run 1), tide, discharges and wind (run 2), tide, discharges and waves (run 3), tide, wind and waves (run 4), and tide, discharges, wind and waves (run 5). The discharges are those from the dewatering sluices in the Afsluitdijk and Lauwersmeerdam. In all runs tide includes the non-tidal residual (*NTR*), or *surge*, as produced by the water level forcing from DCSMv6-ZuNov4. The addition of wind stands for the addition of it to the hydrodynamic computation. Wind has been included in all wave computations to account for wave generation in the model domain.

To further analyze the importance and the role of the flood channel, different bathymetric configurations are used, while keeping the boundary conditions for 2017. In this manner more insight is obtained into the reason that the flood channel is still kept open. Therefore, the bathymetry of some years before (2009) is used (run 6), where the flood channel was still deeper (almost entirely below NAP -5 m) and shorter. It can be expected that this orientation will show a larger influence of tidal currents and will consequently transport more sediment. Other bathymetric configurations are created for the present-day situation with small sand nourishments (runs 7, 8 and 9). It is investigated, which effect these nourishments have on the channel and coast and whether these can accelerate the sand shoal attachment to the island head of Schiermonnikoog.

Summarizing, the following runs in Table 5.1 are conducted.

5.2. Model-derived characterization of processes

5.2.1. Hydrodynamics

Flow pattern

Figure 5.1 shows the flow patterns through the Zoutkamperlaag inlet and its ebb-tidal delta offshore of Schiermonnikoog northwest (NW). Starting on February 2, 2017, at 19:00h, slack water can be observed right before flood. A small outflow through the ebb channel Westgat is still present. At 21:00h, a strong inflow through the inlet is visible due to flood. The largest currents flow through the Westgat and over the shallow area north of Het Rif, the southern ebb-tidal delta. Currents through

Run	Bathymetry	Processes
1	present-day	tide and discharges
2	present-day	tide, discharges and wind
3	present-day	tide, discharges and waves
4	present-day	tide, wind and waves
5	present-day	tide, discharges, wind and waves
6	2009	all processes
7-9	sand nourishments	all processes

Table 5.1: Overview of conducted model runs, where the first five runs focus on the influence of physical processes and the last five runs on the influence of the bathymetry

the Plaatgat are small and not significant compared to currents over the approaching shoal farther offshore. At 00:00h, the currents have reduced, but are still directed inward in the entire domain. At 02:00h, right after slack water, a small outflow through the Westgat and over the southern ebb-tidal delta can be observed. Currents through the Plaatgat are still directed toward the inlet. At 04:00h, outflowing currents are present in the entire domain. The strongest currents can be found in the Westgat and over the southern ebb-tidal delta. Currents in the Plaatgat are relatively small. A bit later, at 07:00h, the tidal cycle is completed and the slack water period before flood starts again.

Figure 5.2 shows the same tidal cycle with the same moments in time. This image is zoomed in on the Plaatgat and its surrounding area to better visualize the negligible difference between currents over the approaching shoal and through the channel. The magnitude of the occurring current velocities does not suggest a clear dominance during flood, which would be suspected in a flood channel.

Residuals

The annual average ebb and flood discharges and currents, together with the annual average residuals, are given in Table 5.2. These values are relatively small for the Plaatgat compared to the Westgat, indicating its minor role as a flood channel. Furthermore, the oppositely directed residual in both sides of the channel are remarkable. This is further elaborated in Section 5.4.

Channel	$\overline{Q}$ [m^3/s]	$\overline{Q}_{\text{ebb}}$[m^3/s]	$\overline{Q}_{\text{flood}}$ [m^3/s]	$\overline{u}$ [m/s]	$\overline{u}_{\text{ebb}}$ [m/s]	$\overline{u}_{\text{flood}}$ [m/s]
inlet throat	124 (WS)	9 791	10 088	0.02 (NS)	0.48	0.45
Westgat (N)	813 (NS)	4 095	2 897	0.09 (NS)	0.38	0.24
Westgat (S)	472 (NS)	4 548	3 861	0.08 (NS)	0.57	0.45
Plaatgat (SW)	309 (WS)	952	1 264	0.04 (WS)	0.15	0.19
Plaatgat (E)	88 (NS)	781	601	0.03 (NS)	0.18	0.11

Table 5.2: Annual average residual, ebb and flood discharges and currents at cross-sections in the main channels in the Zoutkamperlaag system,
where ebb and flood refer to out- and inflow through the inlet respectively, and *NS* and *WS* stand for *toward the North Sea* and *toward the Wadden Sea* respectively; the locations of Westgat (S), Plaatgat (SW) and Plaatgat (E) are visible in Figure 5.1)

5.2.2. Waves

Significant wave height and dissipation

In Figure 5.3a the modeled annual average significant wave height in 2017 is given. A significant reduction in wave heights over the Zoutkamperlaag ebb-tidal delta and the approaching shoal can be observed. Offshore significant wave heights are on average over 1 m, where on the offshore NAP -3 m edge of the shoal around 0.8 m and in the Plaatgat around 0.6 m can be observed. Large waves can penetrate the Westgat relatively far south and also the southern ebb-tidal delta is receiving considerable wave action. A similar spatially varying wave height pattern is visible for the maximum. Maximum significant wave heights in 2017 vary from over 5 m offshore to 2 m at the island head.

Wave dissipation is clearly visible in the breaker zone along the island coast. Other dissipation hotspots are concentrated around the offshore NAP -3 m depth contours. At the northern end of the Westgat, also at greater depth, significant wave dissipation can be observed. This is likely related to the strong oppositely directed tidal currents originating from the ebb channel.

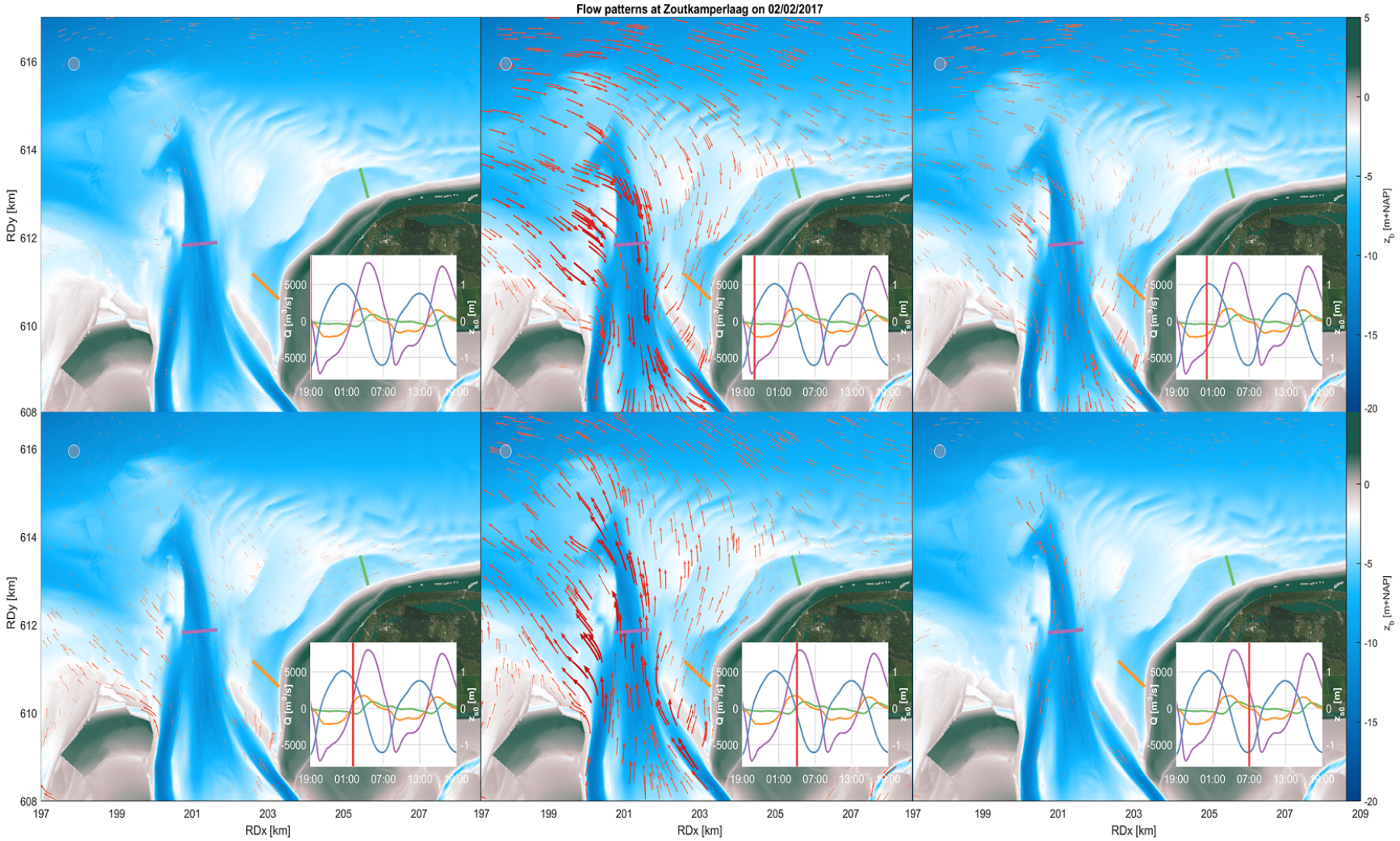

Figure 5.1: Flow patterns during flood and ebb through the Zoutkamperlaag inlet and over its ebb-tidal delta,
where the subplot on the island gives the modeled water level at the *Schiermonnikoog Westgat* buoy (blue), and the discharges through cross-sections in the Westgat (brown) and the Plaatgat (orange and green) with positive outward (ebb) and negative inward (flood) flow

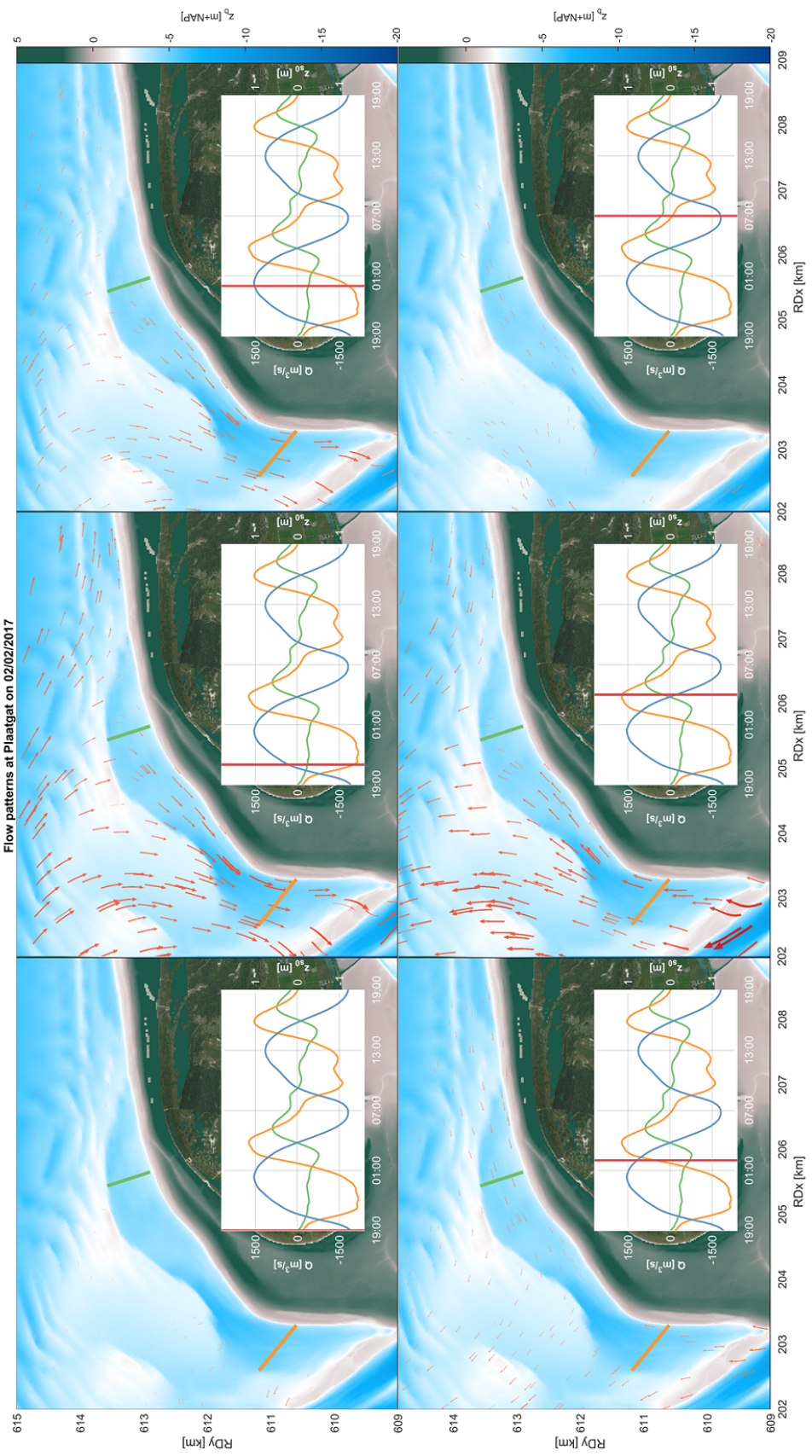

Figure 5.2: Flow patterns during flood and ebb through the Plaatgat and the surrounding area, where the subplot on the island gives the modeled water level at the *Schiermonnikoog Westgat* buoy (blue, see location in Figure 5.1), and the discharges through cross-sections in the southwestern (orange) and eastern (green) Plaatgat with positive outward (ebb) and negative inward (flood) flow

Gradient in wave height

The deep cut through the middle of the approaching shoal, the former ebb channel Oude Westgat (RDx = 203 km and RDy = 612.5 km to 614 km in Figure 5.3a), allows for a relatively large wave height near the coast around transect 303. This causes a gradient of up to 7% in the annual average significant wave height over the length of the eastern half of the Plaatgat. Farther to the east, around the attachment point of the NAP −3 m contour, the wave height is higher again due to a lower wave sheltering by the shoal and another gradient can be observed.

Gradients in wave height can often be related to gradients in sediment transport. Higher waves cause a larger sediment transport. The resulting gradient in the latter will cause coastal erosion, because locally more sediment is leaving than entering the system. For the Plaatgat, this phenomenon is further elaborated in Section 5.4.

The propagation of waves over the approaching shoal and the resulting variation in wave height in the Plaatgat due to the tidal water level are presented in Appendix E.2.

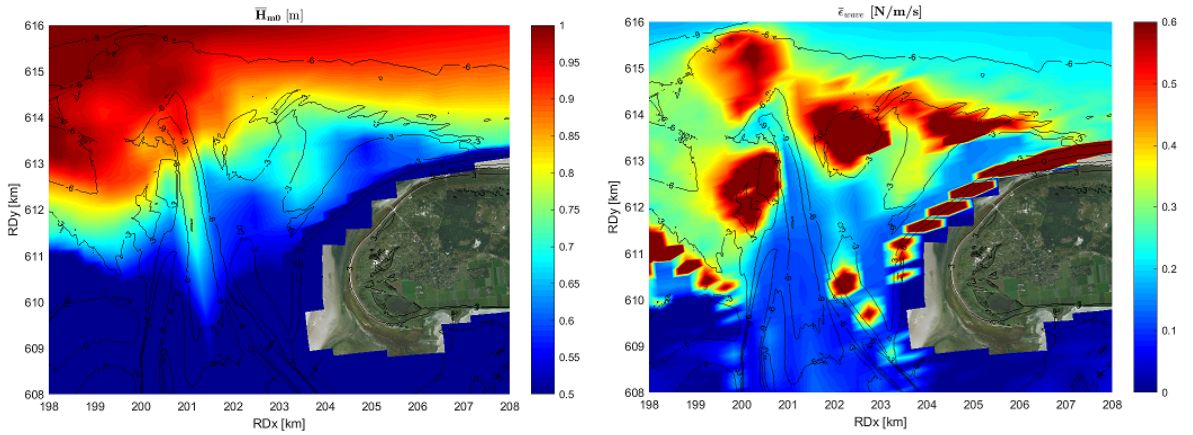

(a) Annual average significant wave height

(b) Annual average wave energy dissipation

Figure 5.3: Wave height and wave energy dissipation at the Zoutkamperlaag inlet and ebb-tidal delta

5.2.3. Sediment transport

Transport pathways

In Figure 5.4 the annual average total sediment transport as modeled for 2017 is given. Figure 5.4a shows that due to just tidal forcing sediment transport occurs only in the tidal channels. With the addition of waves, the sediment bypassing pathway of flow bypassing and bar welding is clearly visible. Following the main direction of the transport, sediment arrives in the west from the Pinkegat inlet. It follows the shallower depth contours of Het Rif toward the throat of the Zoutkamperlaag inlet. From there it is mainly transported northward, through the Westgat toward the ebb shield. Thereupon, it follows the offshore edge of the ebb-tidal delta and the approaching shoal toward the island coast of Schiermonnikoog. From here on onward it is transported by the main longshore drift toward the east of the island.

Some exceptions can be observed in the sediment transport pattern. Significant transport is present at the southern ebb-tidal delta. This is likely related to the observed large currents in this area as given in Figure 5.1. Furthermore, transport on the more exposed parts in the northwest of the approaching shoal is larger than in the more sheltered area closer to the Plaatgat and the island coast. In the Plaatgat itself sediment transport is negligible compared to the rest of the system.

In the inlet throat a strong outward directed sediment transport can be observed in the two ebb channels on the sides, the Zoutkamperlaag in the west and the Gat van Schiermonnikoog in the east. In the middle of the throat an inward directed sediment transport is visible. To the south of this location a shallower part in the inlet is visible. This resembles a typical tidal flat with two flood channels on the sides and a shallow shield between and to the south of these two. This variation in sediment transport over the inlet cross-section is further presented in Appendix E.1.

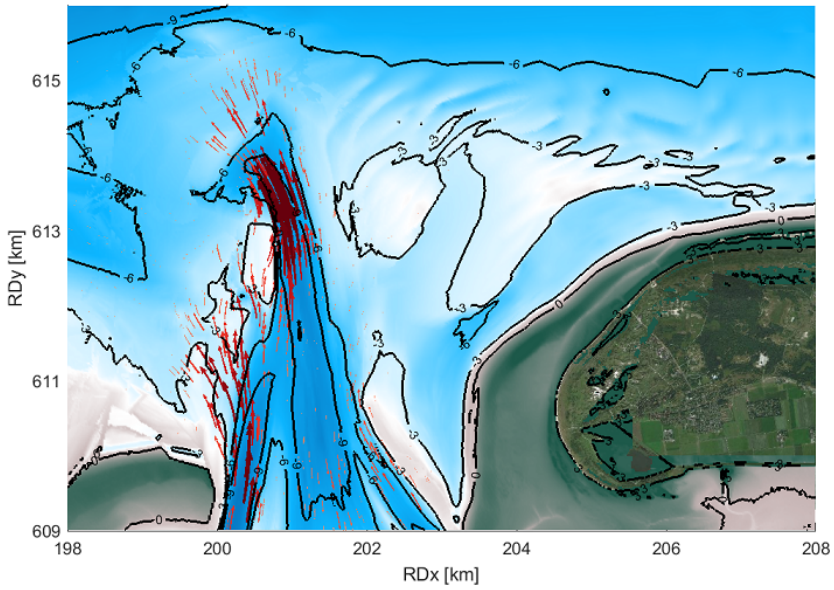

(a) For a model run with only tidal forcing (run 1)

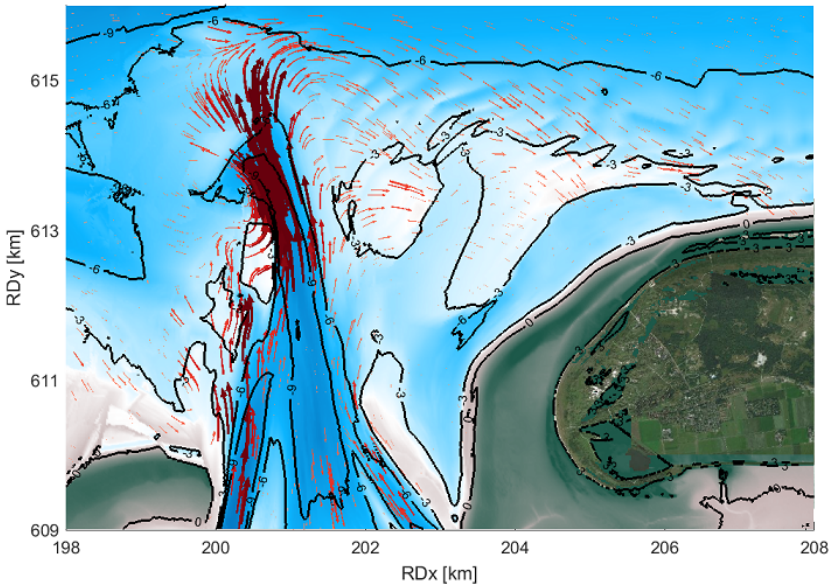

(b) For a model run with all processes included (run 5)

Figure 5.4: Annual average total sediment transport in 2017 at the Zoutkamperlaag inlet and ebb-tidal delta

Contribution of waves

By comparing the described sediment transport pattern with a model run with purely hydrodynamic forcing (see Figure 5.4a), the driving process behind different parts of the transport pathways can be determined. With only tidal action, the large lateral transports in the Westgat and over the southern ebb-tidal delta are still present. This confirms the link between the observed strong flow patterns and the resulting sediment transport in these sections. However, the longshore component disappears in this run. This indicates that the bypassing of sediment over the inlet is driven by wave action. Also the propagation of the approaching shoal, the bar welding, is thus mainly driven by waves.

Furthermore, the addition of waves causes an overall increase in the magnitude of sediment transport. This can be related to the effect of wave breaking. Wave action brings sediment in suspension. When in the water column, this sediment can be transported by the currents present in the system.

Contribution of winds
An addition of wind to the model shows a minor effect on the sediment transport pattern. At the northern end of the Westgat a small deflection of the sediment transport toward the east can be observed. Furthermore, wind causes an increase in the magnitude of the sediment transport to the east and thereby enhances the effect of wave action. Sediment transport to the west is dampened by wind. These effects can easily be explained by the significant wind direction from the west and southwest, as given in Figure 4.4. Opposing winds dampen and equally directed winds enhance sediment transport. Similar to Figure 5.4a, in Appendix E.3 the sediment transport pathways for a model run without waves and for a model run without wind are presented for a full comparison.

Moreover, the addition of wind results in an increase in the water level set-up. This allows larger waves to propagate farther toward the coast over the shallow parts of the ebb-tidal delta. Wave breaking occurs closer to the coast and causes a significant increase in sediment transport in otherwise more sheltered areas.

The varying sediment transport pathways in the Plaatgat during a tidal cycle and for a storm event are presented in Appendix E.2.

5.3. Unraveling dominant processes

The previous analysis of the contribution per physical process is further studied in depth in this section. Firstly, this focuses on the spatial variation in the influence that individual processes have on the sediment transport. Secondly, the effect per process on the cumulative total sediment transport is assessed for representative cross-sections in the area of interest. Finally, using these same cross-sections the modeled erosion and sedimentation pattern of this area is given and compared to observations.

5.3.1. Spatial variation in influence

To visualize the spatial variation in the influence of the individual physical processes, the percentage of the occurring total sediment transport for the lowest 80% magnitudes per process is calculated and plotted on a map per individual grid cell. The magnitude of every process has been averaged over the tidal periods and subsequently been sorted in an ascending order. The corresponding tide-averaged total sediment transport is sorted in the same order. The cumulative of this sorted transport shows the influence of peaks in the corresponding process. Where the 80% lowest magnitudes of the process lead to about 80% of the cumulative total sediment transport, the influence is negligible. The lower this last percentage, the larger the influence peaks in the physical process have on the sediment transport. After all, this indicates that the highest 20% of the process has a relatively large impact on the occurring sediment transport.

In Figure 5.5 the contribution of peaks in the current, wind speed and wave height on the occurring sediment transport is given. The blue areas indicate locations where the contribution is minimal. The red areas indicate locations where the contribution is large. It has to be taken into account that this indicates the relative importance and should be related to the magnitude of the sediment transport itself (see Figure 5.4b).

The largest spatial variation in the relative importance of the peak magnitudes is clearly observed for the **wave height** (Figure 5.5c). This shows no major influence in the deeper channels in the inlet (and the basin), where the currents are more dominant (Figure 5.5a). However, on the shallower parts of the ebb-tidal delta and in the Plaatgat the 20% tidal periods with highest waves contribute to over 50% of the total sediment transport.

The pattern of the relative importance of large **wind speeds** (Figure 5.5b) is similar. However, the effect on the total sediment transport by the highest 20% is less significant. The similarity between the effect of large wind speeds and large wave heights can be attributed to wave generation by winds, which causes a strong correlation. Furthermore, a water level set-up due to wind will increase the impact of waves on sediment transport by allowing for a deeper penetration over the shallow parts of the ebb-tidal delta (see Appendix E.2).

The relative importance of **currents** shows a different pattern (Figure 5.5a). Compared to wave height and wind speed the peaks have a larger influence on sediment transport in the deeper channels. The influence of peaks in currents is relatively small on the northwestern part of the ebb-tidal delta, the shallower area to the west of the ebb channel. In the Plaatgat, the influence of currents seems rather

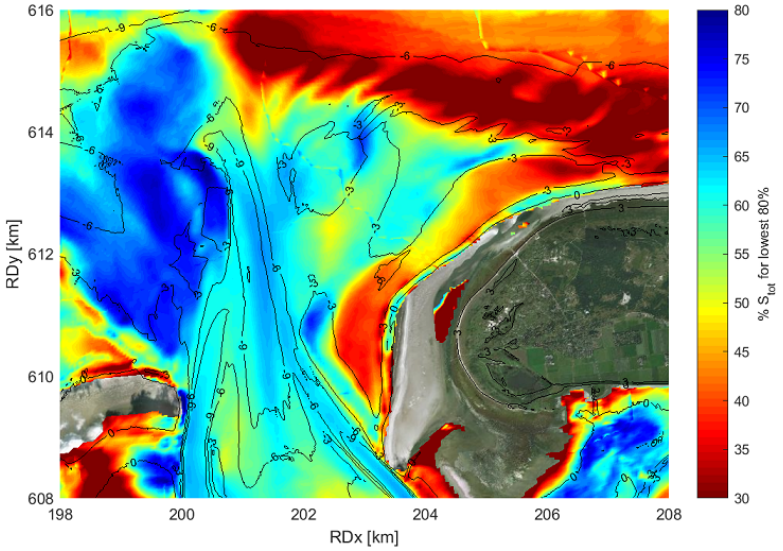

(a) Relative importance of the currents (due to both tide and waves)

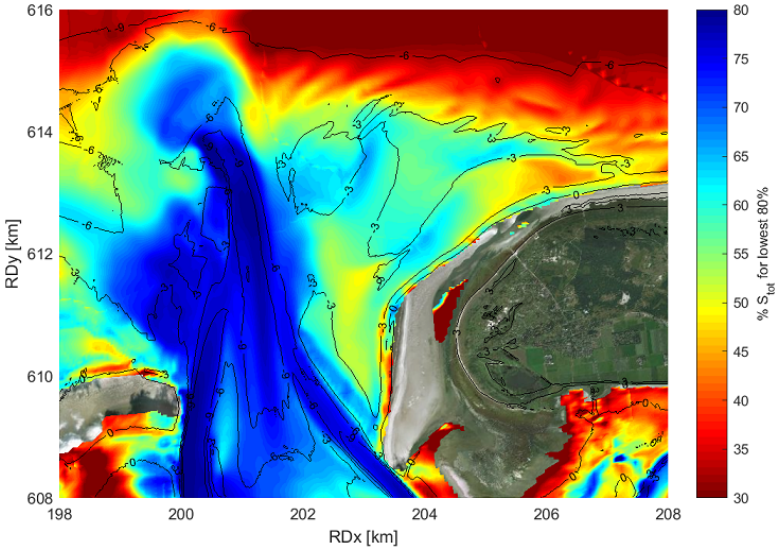

(b) Relative importance of the wind speed

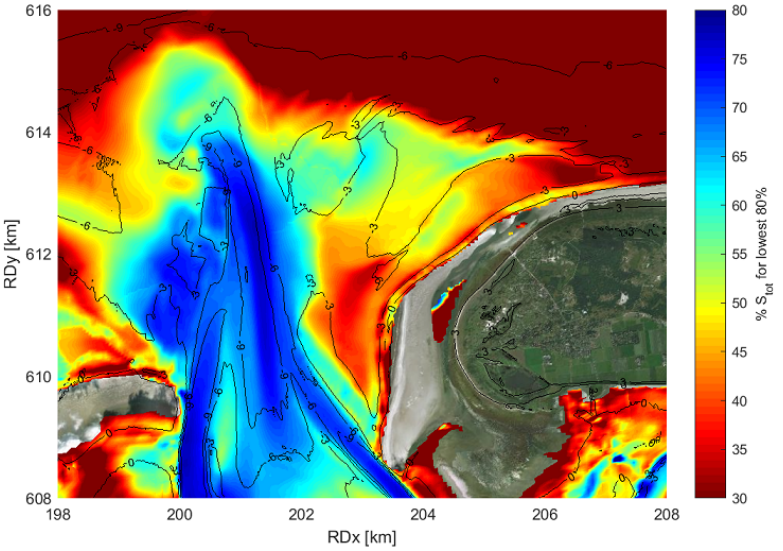

(c) Relative importance of the significant wave height

Figure 5.5: Contribution of the lowest 80% of tide-averaged processes to the cumulative total sediment transport,
where a blue color stands for a minimal contribution and a red color stands for a large contribution; *the inconsistencies in the color pattern are related to the model partition boundaries and have no effect on the overall pattern*

large, especially in the southwestern half. However, it has to be taken into account that this includes both tide- and wave-generated currents.

The sediment transport in the more offshore, deeper parts is entirely dependent on peaks in the magnitude of all processes (storm events). Under calm conditions no sediment transport can be observed in this area. In part, this is also the case for the Plaatgat, where peak events are required to bring about significant sediment transport.

5.3.2. Sediment transport over cross-sections

To analyze the morphological development of the ebb-tidal delta of the Zoutkamperlaag, several cross-sections are defined in the model. The position of these cross-sections (given in Figure 5.7) is based on the bathymetric contour lines. Additionally, several cross-sections through the main channels have been defined. For every cross-section the cumulative bed load sediment transport and the cumulative suspended sediment transport is calculated. The cumulative total sediment transport for four main cross-sections is given in Figure 5.6. In this figure the results of different model runs with varying sets of processes are given. This gives an overview of the effect the addition of a certain process has on the transport through these cross-sections.

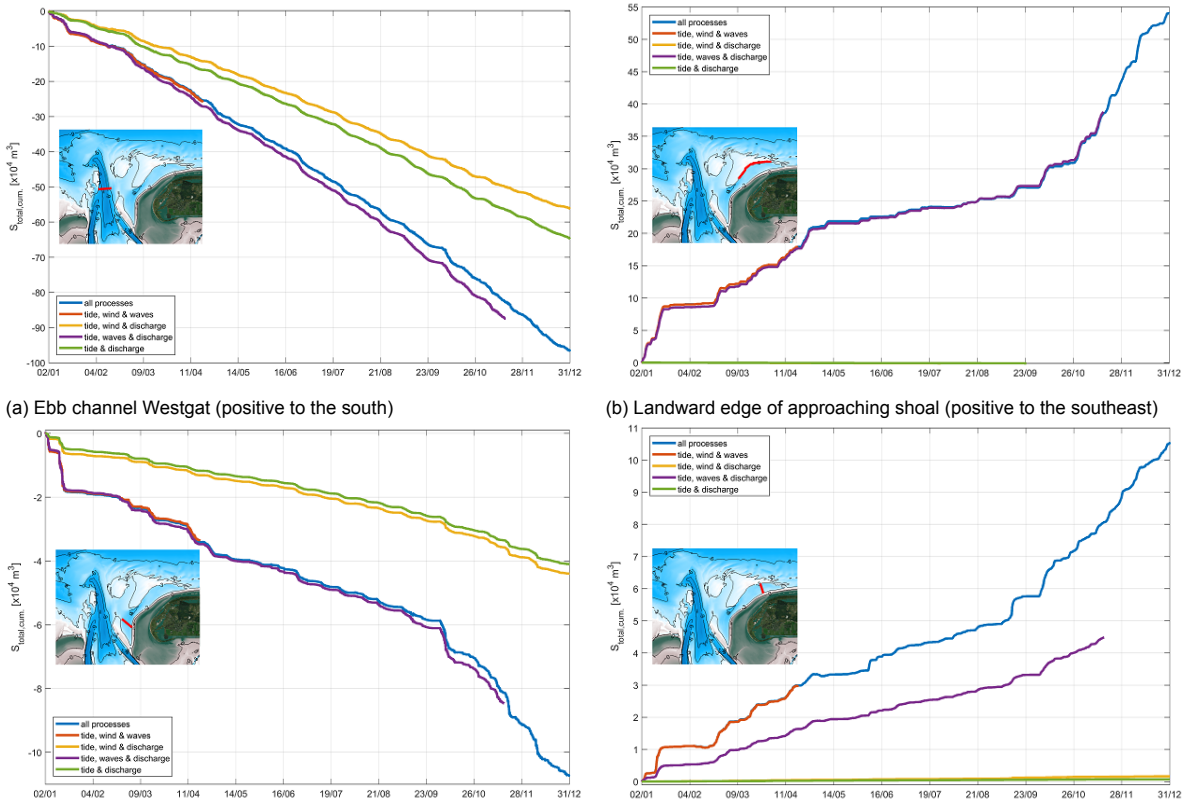

(a) Ebb channel Westgat (positive to the south)

(b) Landward edge of approaching shoal (positive to the southeast)

(c) Plaatgat West (positive to the northeast)

(d) Plaatgat East (positive to the east)

Figure 5.6: Cumulative total sediment transports for the modeled year 2017 through 4 characteristic cross-sections for model runs 1 to 5 with different physical processes included; *some runs do not cover the entire year due to modeling difficulties (see Section 7.1.1)*

Discharge from Lauwersmeer

The addition of a discharge from the sluices in the Lauwersmeerdam (blue, run 5) shows no significant effect on the sediment transports in the area of interest. It is visible in Figure 5.6 that the omission of this discharge (red, run 4) has almost no effect on the sediment transport through any of the cross-sections. The earlier made assumption that this is mainly of importance to processes in the basin and for finer sediment particles seems to be valid. Therefore, this has not been investigated further.

Tide
A model run with only tidal action (green, run 1), which also includes the non-tidal residual (or 'surge'), shows a strong northward transport through the Westgat. This proves the large influence of tides in this ebb channel. However, no major sediment transport on and around the approaching shoal can be seen. In the Plaatgat, sediment transport is visible in the western half, although only limited. The eastern half of the channel shows almost no sediment transport under only tidal forcing.

Waves
The addition of waves to the model (purple, run 3) results in the most significant effect on the total sediment transports. In the Westgat, the already occurring export of sediment is strongly enhanced by waves. This is mainly due to the increase in suspended sediment transport. With no increased currents in the channel, this indicates that wave action brings more sediment in suspension.

The sediment transport over the approaching shoal and through the eastern half of the Plaatgat is almost entirely caused by waves. Also in the western half of the Plaatgat the sediment transport is strongly increased by waves.

Another important aspect in Figure 5.6 is the strong influence of storm events on the sediment transport in model runs with wave-action. All major 'jumps' in the graphs correspond with extremes in the observed offshore wave heights. The sediment transport on the approaching shoal (Figure 5.6b) is mainly driven by these storm events, but also in the Plaatgat (Figure 5.6c and 5.6d) the influence is significant.

Wind
The influence of wind is limited compared to the influence of waves. By itself wind does not cause significant sediment transport (yellow, run 2). However, it can enhance or limit the resulting sediment transport. In shallow areas, a large increase in wave-driven sediment transport can be brought about by a wind-driven water level set-up, as mentioned before (compare purple, run 3, and blue, run 5 in Figure 5.6d).

Furthermore, a change in magnitude is related to the wind direction with respect to the already occurring sediment transport. In the Westgat the northwestward sediment transport is slightly reduced after the addition of the generally opposing wind, where in the Plaatgat and on the approaching shoal wind enhances the already occurring eastward sediment transport. The influence of wind on the landward edge of the shoal is limited.

5.3.3. Resulting erosion and sedimentation

A group of cross-sections encircles a characteristic segment in the area of interest. By combining the resulting modeled sediment transports, a sediment volume that has been deposited in that segment over the year 2017 is found. By dividing the result by area of the segment, a bed level change is found. This value can subsequently be compared to the morphological development, according to the *JarKus* measurements of 2017 and 2018. It has to be noted that these measurements have been conducted in May of both years, where the model runs for the calendar year of 2017.

Comparing the calculated bed level changes in Figure 5.7, the following similarities are found:

- a channel is developing to the west of the ebb channel Westgat, just north of Het Rif, due to strong currents (see Figure 5.1);
- the Westgat is farther rotating clockwise and translating to the east. This causes erosion on the west side of the approaching shoal;
- the approaching shoal is increasing in size and slowly filling in the Plaatgat;
- a strong infilling of the deep cut through the shoal, the previous ebb channel Oude Westgat, is observed. However, in the model this is mainly visible on the northwestern part of the shoal due to the lack of feedback in the morphostatic run.

Some developments from the 2018 measurements are not clearly visible in the model results:

- the erosion of the deeper, seaward parts of the approaching shoal;
- the erosion of the eastern half of the approaching shoal;
- the north-eastward shift of the south-to-north spit at the western end of the island head;

- the continuing coastal erosion and resulting landward shift of the waterline. Sediment transport and erosion are visible along the waterline, but due to the morphostatic modeling no feedback is included. Furthermore, onshore processes are not included in Delft3D, which explains the lack of beach development.

To visualize the spatial sedimentation and erosion from the model, besides the resulting volumes from the cross-sections, a run with bottom updating has been conducted. To not let an incorrectly changing bathymetry affect the model results, a morphological factor of 0.01 has been used. The resulting sedimentation and erosion have been scaled back to be able to compare these to observations.

Figure 5.7b shows a minor modeled sedimentation and erosion pattern compared to the observations as given in Figure 5.7a. This is in line with the expected underrepresentation of the exact morphodynamics as described in Section 2.3.2. Similar as for the observations, most modeled sedimentation and erosion takes place on the west of the Westgat. Furthermore, the wave-like pattern of sedimentation and erosion along the periphery of the ebb-tidal delta is present in both the observations and the model. Sedimentation on the edges of the Oude Westgat and of the Plaatgat and erosion along the shoreline are visible. However, the resulting volumes are significantly smaller for the modeled pattern, even in proportion to the volumes in the rest of the system. This shows that the morphodynamics for shallow area of the ebb-tidal delta near the coast are not well incorporated in the model. A further elaboration on this shortcoming is given in Section 7.1.3.

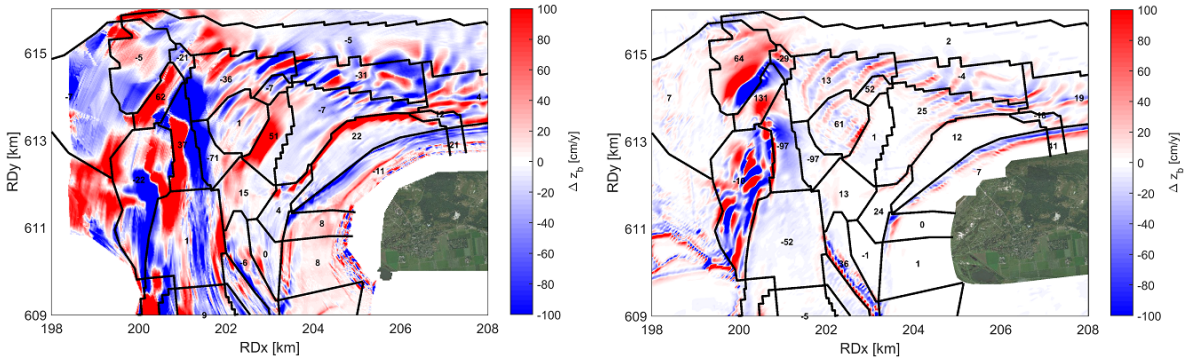

(a) Observed change between the *JarKus* measurements in May 2017 and May 2018

(b) Modeled change from the sediment transports over cross-sections with a sedimentation and erosion pattern from a morphodynamic run during calendar year 2017

Figure 5.7: Observed and modeled bed level change in cm per segment with sedimentation and erosion in red and blue respectively

Total sediment transport on a grid

The sedimentation and erosion patterns in Figure 5.7b give an overview of the changes per bed form. However, from this figure it is not straightforward to interpret the sediment transport and resulting erosion and sedimentation along the coast. For this purpose, the total sediment transport is interpolated onto a structured grid of cross-sections, following the curvature of the Plaatgat and the coastline. Figure 5.8 shows the result and helps to further analyze the parts of the ebb-tidal delta in front of Schiermonnikoog NW that undergo sedimentation or erosion.

In what follows, the morphological development is described from the island head toward the offshore parts, as observed in Figure 5.8. This pattern shows coastal erosion over the NAP −1 m contour in the eastern half and accretion on the southwestern half. In the Plaatgat, the eastern half shows mainly sedimentation toward the attachment point of the NAP −3 m contour. Near the attachment point the patterns seems more dynamic with some erosion, as well. The southwestern half shows more erosion with some sedimentation where the south-to-north spit migrates closer to the coast. The landward part of the approaching shoal shows erosion in the shallower part in the middle and sedimentation on the more landward pointing sides. The latter is most pronounced at the eastern end. The deep cut through the shoal is filling up at a fast pace. Also the part of the shoal in the northwest is experiencing sedimentation. The offshore quadrangles show a varying pattern of sedimentation and erosion which might hint at the occurrence of sand waves, as observed in the patterns in Figure 5.7.

Overall, the described pattern is in line with the pattern from the previous analysis per bed form. Additionally, this analysis shows the previously missing similarity between the model and the measurement as given in Figure 5.7: the coastal erosion and the development of the shape of the shoal. The agreement of the sediment transport patterns in the model with the *JarKus* measurements makes the resulting pattern trustworthy. However, the morphological development and the corresponding sediment transport magnitudes are not exact.

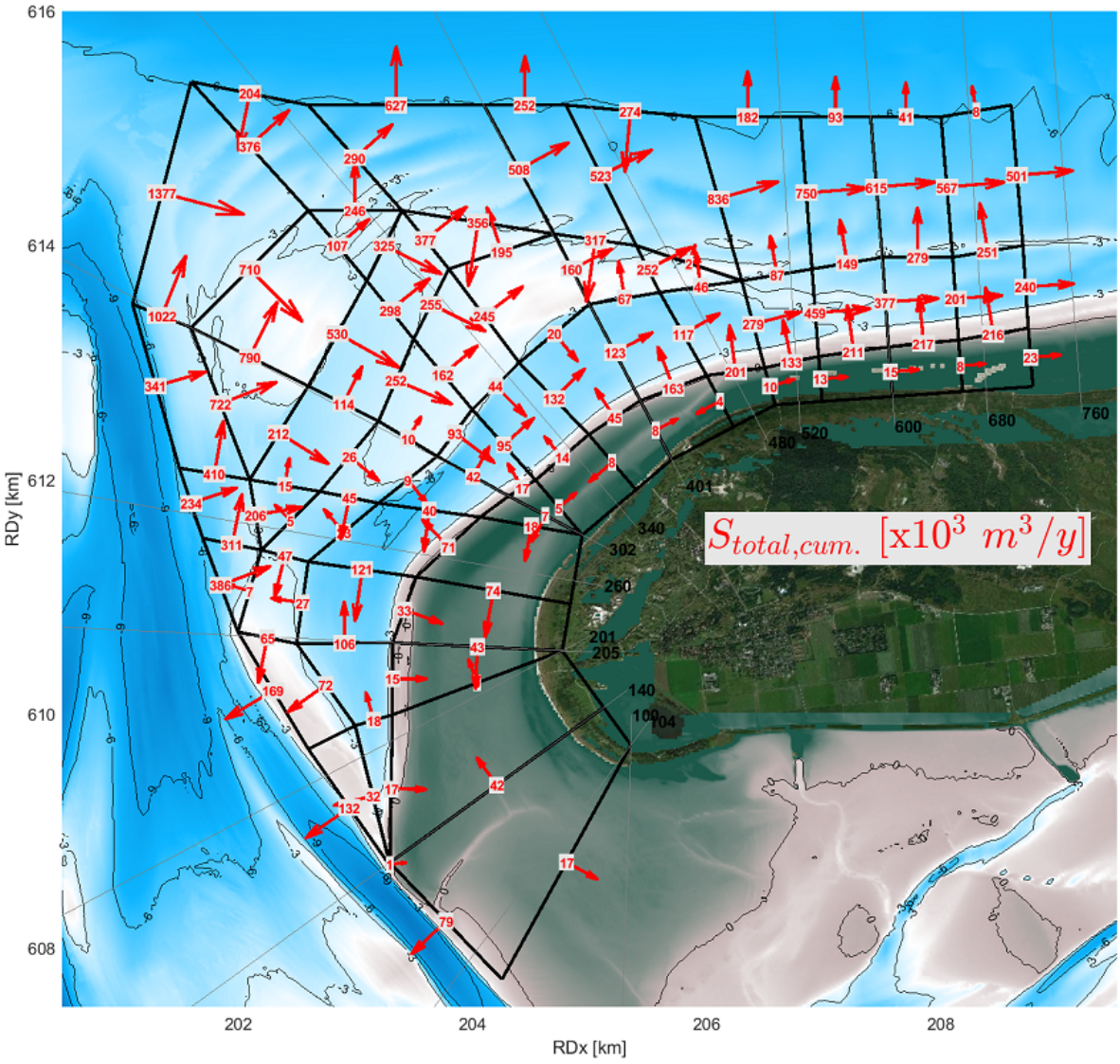

Figure 5.8: Annual cumulative total sediment transport[1] along the Plaatgat and its surroundings on a structured grid

5.4. Interpretation of processes in the Plaatgat

At Schiermonnikoog, the most problematic erosion occurs on the beach section between transects 400 and 500, where the basal coastline (*BKL*) is almost exceeded near transect 500 (see Figure 3.1). These transects are located at the eastern part of the former flood channel Plaatgat and therefore a further analysis into the behavior of this channel is required.

[1] The given volume fluxes in this thesis represent a volume without pores. It is directly derived from the modeled mass flux.

5.4.1. Processes and sediment transport

Figure 5.9a clearly shows that the Plaatgat no longer functions as a flood channel. Not everywhere along the channel the currents are directed toward the inlet and, as mentioned in Section 5.2.1, the velocities are very small. Larger annual average velocities toward the inlet are visible around the curve the channel makes around the island head. These currents are mainly generated by tidal action. An addition of wind and waves results in a slight decrease in magnitude. Large annual average velocities toward the east are visible closer to the attachment point of the NAP -3 m contour around transect 540. These currents are mainly generated by wave action. Also the addition of wind increases the annual average current toward the east due to the increased wave action after the resulting water level set-up.

At the deepest part of the Plaatgat between transects 302 and 320, where the southernmost point of the approaching shoal is located relatively close to the shore, a clear transition of mainly eastward currents to the east and mainly southwestward currents to the southwest is visible. This same transition is visible in the direction of the annual average total sediment transport (see Figure 5.9d). The same point corresponds with the largest flow and sediment transport over the approaching shoal (see Figure 5.8), and with the largest wave heights on the approaching shoal and in the Plaatgat (see Figures 5.3a and 5.9c).

In Figure 5.9d, the effect of different processes on the sediment transport in the Plaatgat is presented. In the southwestern half, tides cause a significant portion of the occurring transport. This is strongly enhanced by the addition of wave action. In the eastern half of the Plaatgat, no sediment transport can be observed without wave action. The addition of wind enhances the sediment transport in this part. This is due to the occurring water level set-up, which allows larger waves to reach over the ebb-tidal delta. Figure 5.9c clearly confirms this by showing overall larger wave heights in the channel, when wind is added to the computation. More model results regarding this set-up are given in Appendix E.2.

5.4.2. Comparison to observed erosion

In Figure 5.10, the development of the momentary coastline *MKL* between 2017 and 2018 is given to compare the presented model results to observations. Figure 5.9d has a positive sediment transport gradient at the locations with the largest wave heights between transects 220 and 380, and 460 and 540. These sections largely agree with the observed erosion in Figure 5.10a. Also the accretion south of transect 206 can be connected to the negative sediment transport gradient in this area. The negative gradient east of transect 540 corresponds with the accretion at the attachment point of the NAP -3 m contour.

From the *JarKus* transects of the years 2017 and 2018 the volume change is calculated between the main beach pole and the approaching shoal. These volume changes between 2017 and 2018 are somewhere between -200 and $200\,\mathrm{m^2/m/y}$. Yearly volume changes in Figure 5.8 and 5.9d are of the same order of magnitude. In Figure 5.10b the resulting changes from the transects and from the sediment transport gradient in Figure 5.9d are plotted. A relatively good agreement between the data is visible, considering that the transects and modeled cross-sections are not everywhere positioned at the same angle.

5.5. Impact of different bathymetric configurations

5.5.1. Bathymetry of 2009

In 2009 the Plaatgat was still deeper and shorter. Only recently the NAP -5 m contour of the approaching shoal had attached to the coast of Schiermonnikoog. Furthermore the flood channel was more oriented toward the northeast, instead of the current position toward the east, along the coastline. A model run (run 6) with this bathymetric configuration has been conducted to analyze whether this shows a larger influence of currents in the channel. This can confirm that the Plaatgat is already being abandoned and only of marginal importance with respect to tidal action in 2017.

In Figure 5.11 the flow patterns for the bathymetry of the Plaatgat in 2017 and in 2009 are visible. Currents through the channel are larger for 2009 than for 2017 (see Tables 5.2 and 5.3). Also, for 2009 the currents through the channel are larger compared to the surrounding area, where for 2017 no significant difference can be observed. This indicates that between the bathymetric configuration of 2009 and of 2017 the channel has lost its role as a tidal channel. For 2009 the southwestern half of the

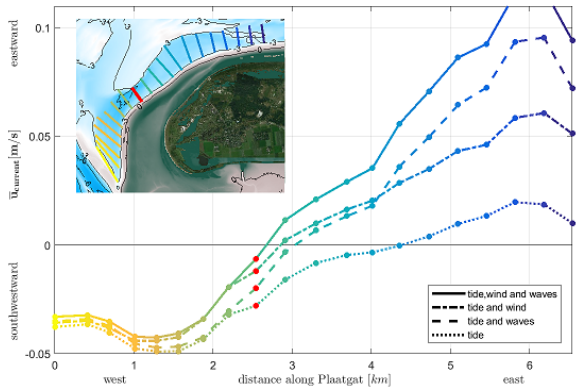

(a) Annual average current

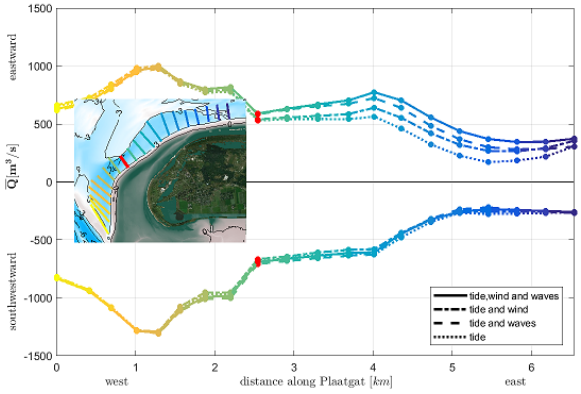

(b) Annual average flood (southwestward) and ebb (eastward) discharges

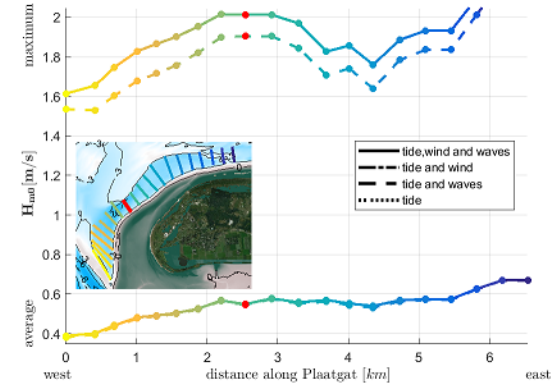

(c) Annual average and maximum significant wave heights

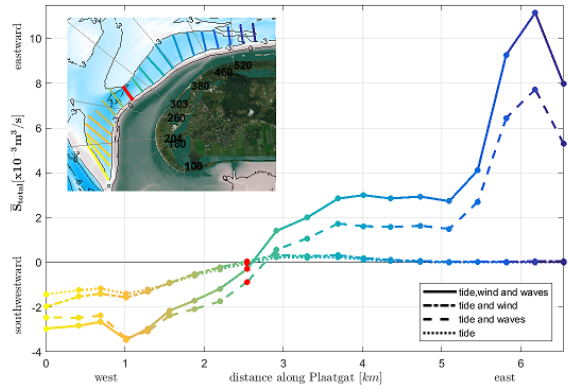

(d) Annual average total sediment transport, with *JarKus* transects plotted in the map in the subfigure

Figure 5.9: Development of the current, discharge, wave height and total sediment transport along the Plaatgat, where the color of the line corresponds with the cross-sections on the map, the style of the line corresponds with a combination of physical processes (runs 1, 2, 3 and 5), and the red dot and cross-section represent the divergence point

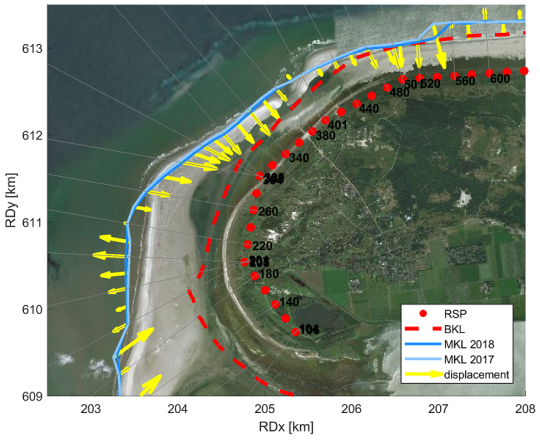

(a) Displacement of the momentary coastline (*MKL*)

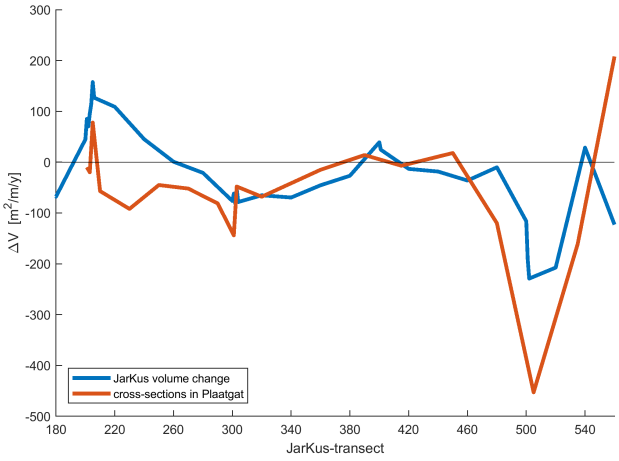

(b) Volume change of the transects between the main beach pole and the approaching shoal (blue) and from the sediment transport gradient in Figure 5.9d (red)

Figure 5.10: Development of the *JarKus* transects at Schiermonnikoog NW between the measurements in 2017 and 2018

Plaatgat shows a clear flood-dominance, where water movement in the eastern half is mainly to the east. However, the values in the latter half are significantly lower and likely generated by wave action. For 2017 the currents and discharges are more of the same magnitude in both halves of the channel.

Overall it can be concluded that the southwestern Plaatgat was still mainly a flood channel in 2009, but the influence of waves on the direction of the current can already be observed in the east.

Channel	$\overline{Q}$ [m^3/s]	$\overline{Q}_{ebb}$[m^3/s]	$\overline{Q}_{flood}$ [m^3/s]	$\overline{u}$ [m/s]	$\overline{u}_{ebb}$ [m/s]	$\overline{u}_{flood}$ [m/s]
inlet throat	119 (WS)	9 781	10 031	0.01 (NS)	0.47	0.44
Westgat (W)	160 (NS)	4 979	4 894	0.04 (NS)	0.45	0.39
Westgat (S)	329 (NS)	5 738	5 387	0.05 (NS)	0.54	0.47
Plaatgat (SW)	159 (WS)	2 826	2 953	0.00	0.24	0.22
Plaatgat (E)	398 (NS)	669	431	0.11 (NS)	0.19	0.10

Table 5.3: Annual average residual, ebb and flood discharges and currents at cross-sections in main channels in the Zoutkamperlaag system for 2009,
where ebb and flood refer to out- and inflow through the inlet respectively, and *NS* and *WS* stand for *toward the North Sea* and *toward the Wadden Sea* respectively

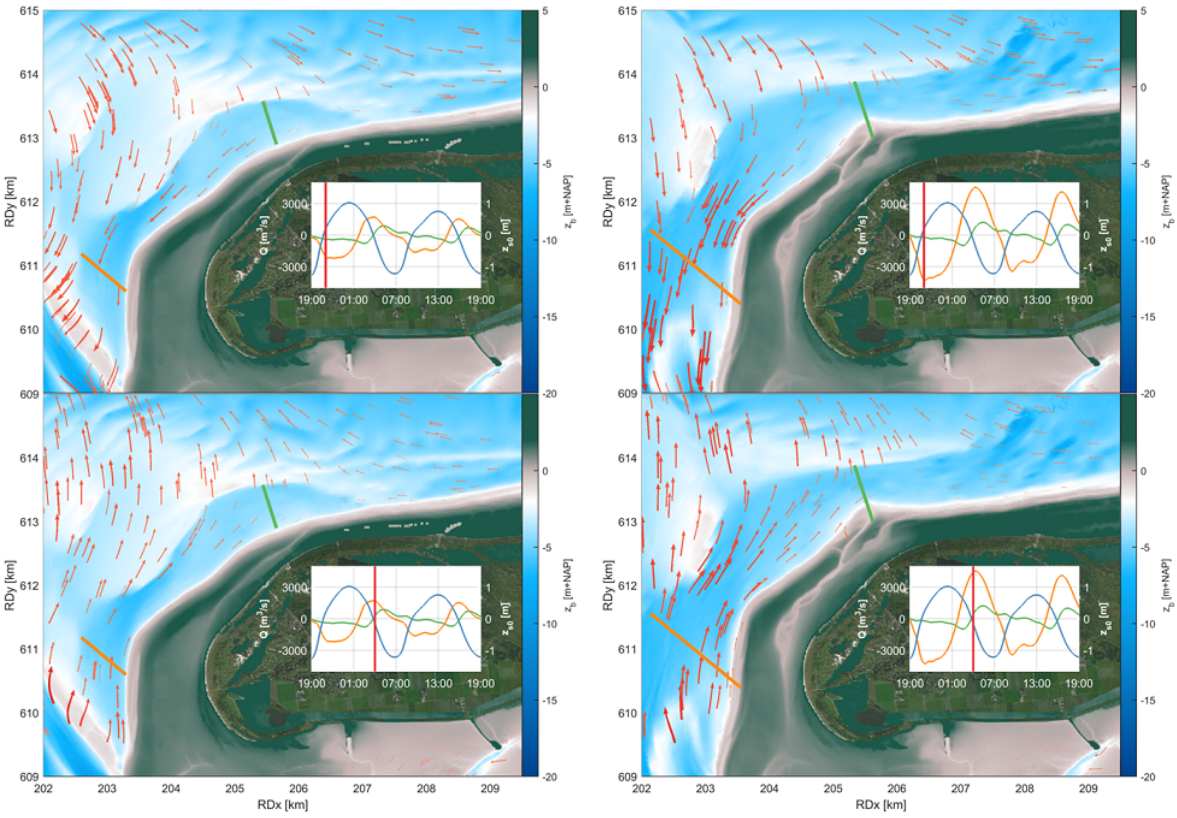

(a) For 2017

(b) For 2009

Figure 5.11: Flow patterns during ebb and flood in Plaatgat, showing the difference between the magnitude of the (tidal) currents through the channel under different bathymetric configurations; the discharge and water levels in the subfigure are as in Figure 5.2

5.5.2. Sand nourishments

Interventions in the Dutch ebb-tidal deltas have been conducted and are being investigated only recently. Until now, sand nourishments are limited to the coastal areas of the Wadden Islands. More knowledge is currently being acquired by conducting and monitoring a pilot nourishment on the ebb shield of the Borndiep ebb-tidal delta at neighboring Ameland (Ministerie van Infrastructuur en Waterstaat, 2018).

To further analyze the effect of the bathymetry on the individual physical processes, model runs with alterations in the original bathymetry are conducted. For this purpose sand nourishments are placed in the bathymetry of 2017. This includes a nourishment in the Plaatgat at the divergence point,

a nourishment in the deep cut (Oude Westgat) and a nourishment on the shoal at the divergence point. The nourishments are relatively small with volumes of 815 000 m^3, 413 000 m^3 and 229 000 m^3, to depths of NAP 0 m to NAP -3m, -2 m and -2 m respectively. The purpose of these nourishments is to assess the effect different locations have on the behavior of the Plaatgat. The aim is not to come up with a perfect design. Figure 5.12 shows the development of the modeled annual average current, discharge, wave height and sediment transport along the Plaatgat for the original bathymetry in 2017 and for the same bathymetry with the different sand nourishments.

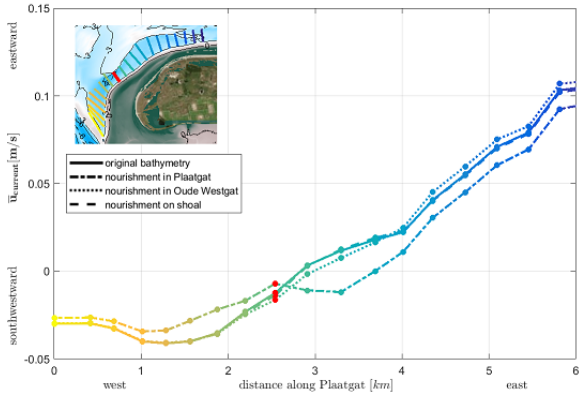

(a) Annual average current

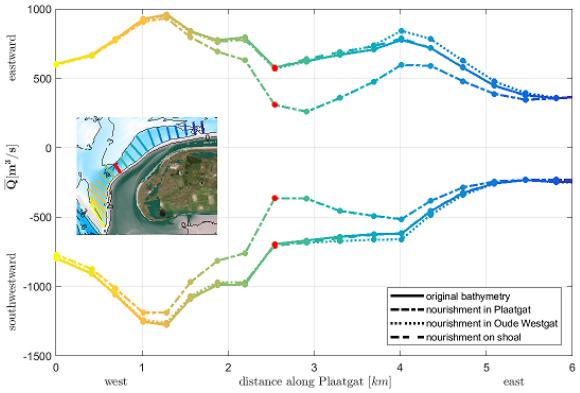

(b) Annual average flood (southwestward) and ebb (eastward) discharges

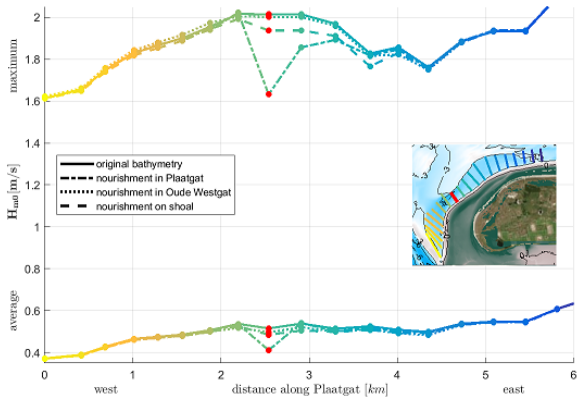

(c) Annual average and maximum significant wave heights

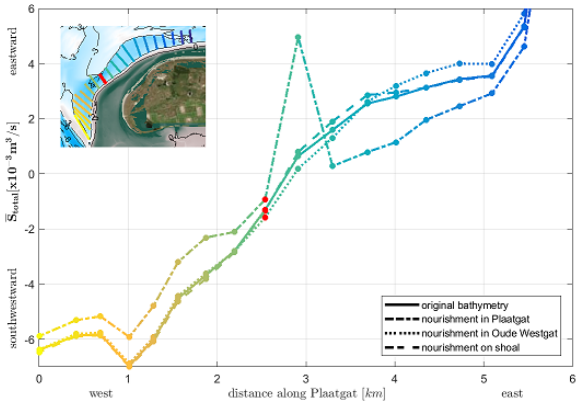

(d) Annual average total sediment transport

Figure 5.12: Development of the current, wave height and total sediment transport along the Plaatgat, where the color of the line corresponds with the cross-sections on the map, the style of the line corresponds with a bathymetric configuration, and the red dot and cross-section represent the divergence point for the original bathymetry of 2017

In Figure 5.12b, it is visible that for the nourishment in the Plaatgat the discharge through the Plaatgat is strongly reduced during both ebb and flood flow. This does not come as a surprise, because this intervention blocks the currents in the channel. The nourishment blocking the Oude Westgat results in a slight increase in the discharge through the eastern half of the Plaatgat. This indicates that a part of the tidal flow can no longer follow the original route over the shoal, but is deviated through the Plaatgat. A nourishment on the shoal shows no impact on the occurring currents in the Plaatgat. Furthermore, the related annual average current in Figure 5.12a shows a similar change due to the different nourishments.

Figure 5.12c shows the development of the annual maximum and average significant wave height along the Plaatgat. The maximum wave height is impacted most by a nourishment in the Plaatgat. The reduced depth does not allow large waves to be present at the site of the nourishment. A nourishment on the shoal lowers the maximum wave to pass over it into the Plaatgat. This brings about a decreased maximum significant wave height along this intervention. A nourishment in the Oude Westgat has only a limited effect on the maximum wave height. The annual average wave height is locally strongly reduced by a nourishment in the Plaatgat, but the effect is limited along the rest of the channel. Nourishments in the Oude Westgat and on the shoal reduce the average wave height over a longer stretch, where

the latter results in the largest decrease of the gradient in the wave height along the Plaatgat (see also Figure 5.13a).

For the resulting sediment transport along the Plaatgat in Figure 5.12d, one should look at the gradient of the line, because this can be related to erosion and sedimentation. The gradient along the area of interest (between 4 and 5 km) is mainly impacted by a nourishment on the shoal. Other nourishments show changes in the sediment transport, which may be significant, but still a strong gradient is present.

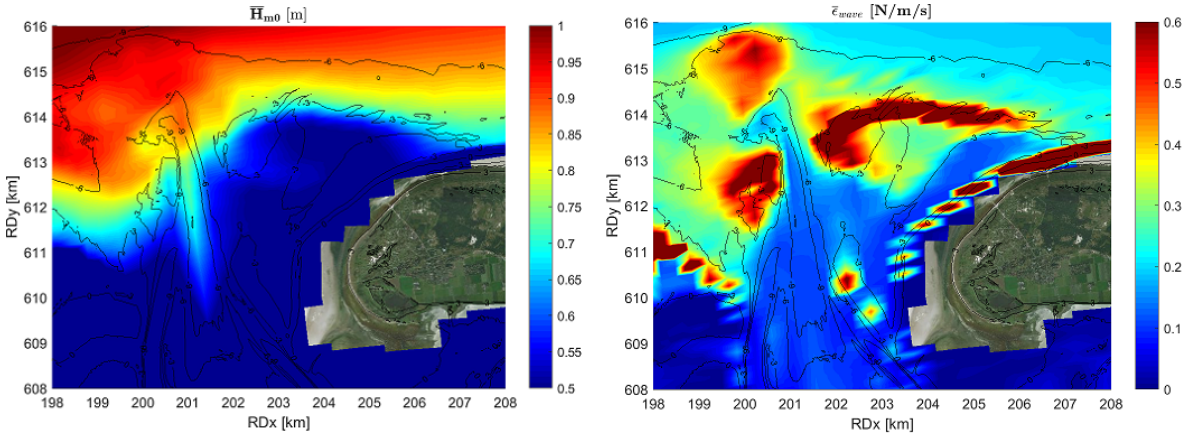

(a) Annual average significant wave height

(b) Annual average wave energy dissipation

Figure 5.13: Wave height and wave energy dissipation at the Zoutkamperlaag inlet and ebb-tidal delta for a smoothed sand shoal

5.6. Storms

In Figure 5.6b, a strong step-wise pattern is visible, where the largest portion of the cumulative sediment transport is caused in the more energetic periods of the year with the largest wave heights. This is roughly from January till April and from October till December. The calmer period from half January till half February 2017 is an exception on this energetic period, because the small wave heights result in no significant increase in the cumulative sediment transport.

Storm events can cause a wind-driven water level set-up in the model of up to 0.45 m at the island coast. According to Duran-Matute et al. (2016) this set-up can be even larger. The largest set-up is visible with winds from western directions, from which the fetch is the longest. Furthermore, the wind speeds from these directions are generally larger than from eastern directions. The resulting set-up increases the largest wave heights that can penetrate over the shallow shoal toward the coast, which in their turn result in a larger sediment transport in the shallower areas by bringing more sediment in suspension. In the shallower area a local (near-shore) root-mean-square wave height of 0.6 m and higher seems to be a threshold for significant sediment transport in the model. This value may be lower in reality, because the modeled morphological response in this area seems underrepresented (see Section 7.1.3).

The used model set-up does not allow for a detailed analysis of single storm events. Besides the underrepresented sediment transport magnitude on the approaching shoal, other factors are missing. For example, long waves are not included and no schematization of waves and winds from different directions is used. However, an overall analysis of the impact of storms in 2017 on the sediment transports on the shoal can be made.

The wind rose in Figure 4.4a shows that the main wind direction in 2017 was from the west-southwest (WSW), but the largest storms - just like the largest waves - came from the northwest (NW). In the cumulative sediment transport over the shoal and through the eastern half of the Plaatgat (in Figure 5.6b and 5.6d) large jumps are visible for the following events, where the first number is the maximum hourly average wind speed and the second number is the maximum wind gust:

- January 4, 2017: 17 m/s to 26 m/s from the NNW
- January 13, 2017: 20 m/s to 27 m/s from the NW
- February 23, 2017: 16 m/s to 24 m/s from the WSW
- April 22, 2017: 13 m/s to 19 m/s from the NW
- June 6, 2017: 13 m/s to 23 m/s from the WSW
- September 13, 2017: 19 m/s to 29 m/s from the WSW
- October 5, 2017: 22 m/s to 31 m/s from the WNW
- October 29, 2017: 22 m/s to 29 m/s from the NNW
- November 19, 2017: 16 m/s to 24 m/s from the NW
- November 23, 2017: 13 m/s to 20 m/s from the SSW
- November 27, 2017: 10 m/s to 20 m/s from the SW
- December 8, 2017: 14 m/s to 23 m/s from the W

All the events coincide with a significant wave height of over 1.4 m offshore. Strong winds from more eastern directions generate lower waves and have only a limited effect on the sediment transport. Examples are:

- February 8, 2017: 13 m/s to 15 m/s from the E
- February 12, 2017: 13 m/s to 16 m/s from the E
- May 4, 2017: 14 m/s to 19 m/s from the ENE

Summarizing, the effect of single storm events seems significant. However, the cumulative sediment transport is not entirely driven by these events. Also under average conditions transport is visible. Transport causes migration of the approaching shoal. Therefore, it can be concluded that the shoal is constantly migrating, but large changes are driven by storm events.

5.7. Chapter conclusion

The modeled currents, wave heights and sediment transports follow the expected patterns. The most important result is the insignificance of tidal currents in the former flood channel Plaatgat. An analysis of the hydrodynamics shows that the tide follows a different path toward the inlet, and that currents over the shoal and through the channel are of the same magnitude. The sediment transport magnitudes behind the shoal are small compared to those at its offshore edges. This is contrary to the recent assumption that flood currents keep the Plaatgat open and therewith cause coastal erosion (Van der Lugt et al., 2018), but similar to other numerical model studies (Elias, 2016; Nederhoff et al., 2016).

A further analysis of the influence of different processes on the sediment transports shows that waves are more important than tides in the area on the shoal and around the island head. The effect of waves in the Plaatgat and at the shoreline is increased by a wind-driven water level set-up, which allows for larger waves to penetrate over the shoal. This increases the sediment transports.

The modeled sediment transports are compared to the observed morphological changes. The mass balance per channel, shoal or other bed form corresponds with the pattern of erosion and sedimentation in the *JarKus* measurements. Along the Plaatgat the gradients in the sediment transport neatly coincide with the observed erosion and accretion of the momentary coastline (*MKL*).

At the coast and in the Plaatgat, the large variation in wave sheltering of Schiermonnikoog NW by the approaching shoal causes alongshore gradients in wave height. Consequently, these bring about gradients in the sediment transport. The modeled transport is small, but the gradients are persisting during the year. This causes the observed ongoing coastal erosion. An altered shape of the shoal can reduce these gradients and the resulting erosion. These findings are further elaborated as a conceptual model in Chapter 6.

In the shallow parts of the system, the influence of storm events is large. Mainly storms from western directions have a large influence, as they generate the largest waves and water level set-up. The sediment transport over the shoal and through the Plaatgat is constantly present, but strongly increased during storms.

6

Conceptual model

Based on the model results of this thesis and on previous studies, a conceptual model for the final stage of a flood channel before its abandonment is set-up. For this purpose, in Section 6.1 three stages are described for ebb-tidal deltas in front of the Dutch Wadden Islands of Texel, Ameland and Schiermonnikoog. Subsequently, these three cases are used to describe a more general conceptual model in Section 6.2.

6.1. Three case studies

Below a generalized description of physical processes and the morphological development of flood channels at three Dutch Wadden Islands is presented. The developments of these systems show a clear similarity. After the typical case, where tidal currents dominate the flood channel, the influence of waves becomes more important. Eventually, this dominates the morphodynamics of the shoal, channel and coast. Resulting coastal erosion will decrease when the morphology in front of the island head has become smoother.

6.1.1. Texel

The Marsdiep tidal inlet is located between the mainland of Noord-Holland and the Wadden Island Texel. The ebb channel toward the southwest and the flood channel Molengat toward the north-northwest are separated by the uninhabited island Noorderhaaks. Sediment transport follows the flow bypassing and bar welding mechanism. Large sand shoal attachments to the downdrift island of Texel occur about every 130 years (Ridderinkhof et al., 2016), but smaller shoals attaches on a more regular basis. At present, a small elongated shoal north of Noorderhaaks is migrating towards the island coast.

A conceptual model is presented in Figure 6.1. In this model, the combination of tidal currents (red) and waves (black) cause a sediment transport (yellow). Stars give the main erosion hotspots at the coastline.

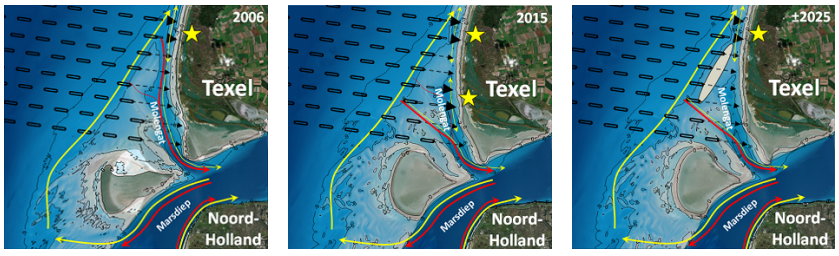

(a) Stage 1: Molengat as a flood channel

(b) Stage 2: Northern Molengat no longer a flood channel and erosion due to a gradient in wave heights

(c) Stage 3: No longer a gradient in wave heights due to a more even foreshore

Figure 6.1: Conceptual model for Texel SW,
where residual tidal currents are given in red, waves in black, sediment transport in yellow and erosional hotspots are given as a star

For the bathymetry around the southern island head of Texel, Cleveringa (2001) described the tidal current pathways and wave-driven shoal development. Until 2006 the channel Molengat between the approaching shoal and the island coast was functioning as a typical flood channel (Figure 6.1a). North of the ebb-tidal delta, where the alongshore transport and the flood-driven transport diverge, an erosion hotspot was present. The erosion is partially caused by the reduced wave sheltering at the northern tip of the ebb-tidal delta.

Due to the recent underwater attachment of the northern tip of the shoal, currents in the northern half of the channel have decreased and found a new path farther to the south. Subsequently, the northern part of the channel has started to fill in and wave action became more important (Figure 6.1b).

Since 2009, the shape of the attaching shoal in front of the southern coast of Texel caused wave-driven erosion. A study by Elias (2016) shows that gradients in wave heights follow from the asymmetrical bathymetry of the migrating shoal. The subsequent sediment transport gradients result in erosional hotspots along the coastline. This will continue until the shoal attaches in its entirety to the island and obtains a more symmetrical shape (Figure 6.1c). The new shape can reduce or stop the occurrence of gradients in the wave height.

6.1.2. Ameland

The tidal inlet Borndiep is located between the Wadden Islands of Terschelling and Ameland. The ebb channel Westgat and the flood channel Oostgat are separated by a large migrating shoal. Shoal attachments occur every 59 years (Ridderinkhof et al., 2016). Figure 6.2 gives a conceptual model of the tidal currents, waves and sediment transports.

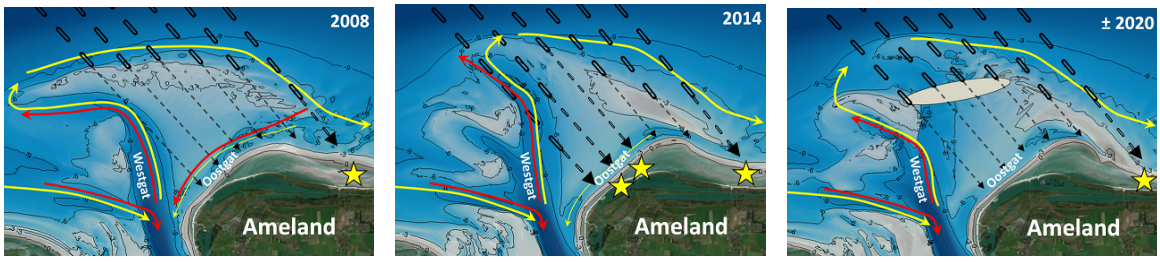

(a) Stage 1: Oostgat as a flood channel

(b) Stage 2: Oostgat no longer a flood channel and erosion due to a gradient in wave heights

(c) Stage 3: No longer a gradient in wave heights due to a more even foreshore

Figure 6.2: Conceptual model for Ameland NW,
where residual tidal currents are given in red, waves in black, sediment transport in yellow and erosional hotspots are given as a star

In 2008 and before, the system showed typical behavior with a tide-dominated ebb and flood channel (Figure 6.2a). The flow bypassing and bar welding sediment transport mechanism is dominant, with sediment import through the Oostgat.

Recently, in 2016, a shoal attached to the coast of Ameland NW. A model study on the area has been conducted for the situation just before the attachment (Figure 6.2b) due to significant coastal erosion (Section 2.2.1, Nederhoff et al., 2016). The resulting hydrodynamics for the bathymetry in 2014 show that the flood channel Oostgat between the coast and the shoal no longer experiences large currents. No clear distinction between the current velocities through this channel and over the shoal is visible. Furthermore, the direction of the currents varies over the length of the channel. All together it can be concluded that tidal action in this area is limited, as is expected due to the hydraulic inefficiency of this long channel just before the upcoming attachment of the shoal.

Just like the case at Schiermonnikoog, a divergence point was present at a straight coastline section due to a gradient in the wave heights. This gradient is caused by the unfavorable orientation of the ebb channel Westgat. This channel is parallel to the main wave direction, which enables large waves to reach the coast of Ameland NW. In addition, the shallow parts of the approaching sand shoal are mainly located toward the east. Wave dissipation in the west is significantly smaller than in the east. In the study by Nederhoff et al. (2016), it is pointed out that the local wave height gradient causes a sediment transport gradient and subsequent erosion at the western half of the island head.

Eventually, the migration of a new shoal from the ebb-tidal delta and the closure of the unfavorably

oriented Westgat will reduce the occurring gradients and the erosion. In recent bathymetric measurements this development is already visible (Figure 6.2c).

6.1.3. Schiermonnikoog

The tidal inlet Zoutkamperlaag between the Engelsmanplaat and the Wadden Island Schiermonnikoog has been discussed in length in this thesis. Based on the model results from Chapter 5, a conceptual model similar to the previous two cases has been set up (Figure 6.3).

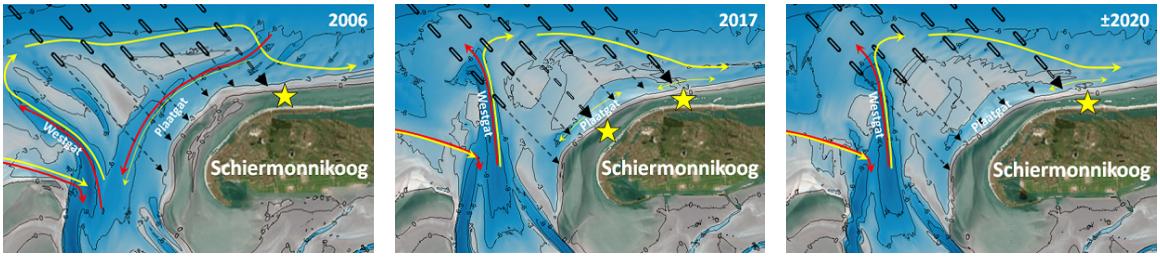

(a) Stage 1: Plaatgat as a flood channel

(b) Stage 2: Plaatgat no longer a flood channel and erosion due to a gradient in wave heights

(c) Stage 3: No longer a gradient in wave heights due to a more even foreshore

Figure 6.3: Conceptual model for Schiermonnikoog NW,
where residual tidal currents are given in red, waves in black, sediment transport in yellow and erosional hotspots are given as a star

Before 2009, the ebb-tidal delta of the Zoutkamperlaag consisted of the tide-dominated ebb channel Westgat and flood channel Plaatgat (Figure 6.3a), separated by a migrating sand shoal. Sediment transport follows the flow bypassing and bar welding mechanism with sediment transport toward the inlet through the Plaatgat.

The diverging sediment transport pathways and the significant influence of waves in the Plaatgat are described in Section 5.4. At Schiermonnikoog it is visible in the model results, that in the eastern part of the Plaatgat a gradient – and sediment transport in general – only occurs with the addition of wave action. The ongoing coastal erosion is caused by a gradient in the wave height (Figure 6.3b).

The investigated nourishments at different locations in the system show the effect of different bathymetric configurations on the gradient in the wave height and sediment transport along the coastline. This indicates that the shape of the approaching shoal is governing. In the bathymetric measurements of 2018 it can be seen that the sediment in the approaching shoal is slowly spreading out. The ends of the shoal are becoming shallower and the deep cut through the middle is filling in. This development will eventually reduce the occurring gradient of the wave height and reduce the coastal erosion (Figure 6.3c).

6.2. General case

The importance of the gradient in wave heights after the reduction of tidal currents through a flood channel has been observed at different sites in the Wadden Sea. It can be concluded that after the reduction of tidal currents in a flood channel, the dominant role of gradients in the wave height is not unique. This phenomenon causes local coastal erosion at many sites near abandoning flood channels. A generic conceptual model for the abandonment of a flood channel and the subsequent attachment of a sand shoal to the downdrift island coast is given in Figure 6.4.

This conceptual model consists of three stages. The first stage with a functioning flood channel is partially based on the conceptual model by Cleveringa (2001) and on the widely used schematization of an ebb-tidal delta. The second stage with a wave-dominated channel and surroundings follows from the presented model results and the study of Ameland in 2014 (Nederhoff et al., 2016) and of Texel in 2015 (Elias, 2016). The third stage is the eventual abandonment of the channel based on morphological observations at Ameland and Schiermonnikoog, and on the resulting effect on the wave action and sediment transports.

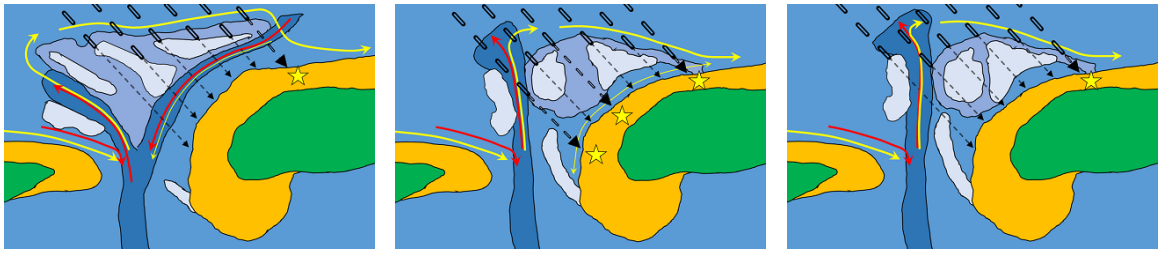

(a) Stage 1: Regular flood channel

(b) Stage 2: No longer a flood channel and erosion due to a gradient in wave heights

(c) Stage 3: No longer a gradient in wave heights due to a more even foreshore

Figure 6.4: Conceptual model for a general case,
where residual tidal currents are given in red, waves in black, sediment transport in yellow and erosional hotspots are given as a star

Stage 1: Tide-dominance
In the first stage (Figure 6.4a), the flood channel fulfills its typical role with dominating currents toward the tidal inlet and resulting inward directed sediment transport. In combination with an oppositely directed longshore sediment transport farther downdrift, this will result in a typical erosional hotspot downdrift of the ebb-tidal delta, where the sediment transports diverge. From the ebb-tidal delta, a sand shoal is migrating downdrift and toward the island head due to wave action. The landward migration slowly forces the flood channel toward the coast and the downdrift migration results in an elongation of the flood channel. At this point, the currents through the flood channel are still strong enough to keep it open. The landward migration will result in coastal erosion and the elongation will result in a slowly decreasing hydraulic efficiency. Additionally, other factors in the ebb-tidal delta development can contribute to this decrease. For example, at Schiermonnikoog, the development of bars at the ends of the channel reduced the flood currents. Gradually the decreasing hydraulic efficiency will force flood currents to find another path toward the inlet. This will increase the relative influence of waves in the area.

Stage 2: Wave-dominance
In the second stage (Figure 6.4b), tidal action in the flood channel is no longer the main driver in keeping the channel open, only wave action will determine the occurring sediment transport. If the currents reduce, the channel will gradually silt up with sediments from the ebb-tidal delta. The shape of the ebb-tidal delta is of importance during this stage. An asymmetrical bathymetry of the approaching shoal and its surroundings may result from remains of former channels (Oude Westgat at Schiermonnikoog), the orientation of the ebb-channel (Westgat at Ameland) or numerous other factors. This asymmetry may cause a persisting gradient in the wave heights in the channel and along the coast. This gradient will result in a gradient in sediment transport over the length of the channel, which, in its turn, can keep the channel open and cause ongoing coastal erosion. This holds back an attachment of the sand shoal to the island head.

Stage 3: Abandonment
The shape of the shoal will constantly be reworked by wave action. Over time, asymmetries that cause a wave height gradient will be filled in or flattened. Subsequently, the sediment transport gradients will move, decrease or disappear (Figure 6.4c). When this results in sedimentation in the flood channel and a cease of coastal erosion, the sand shoal can attach to the coast.

The attachment of a shoal does not happen over the entire length of the coast at once, and locally wave action can still cause erosion. An example is the ongoing erosion at the western half of the island head of Ameland, while the tip of the shoal has already attached in the east.

After the shoal attachment, a new flood channel will present itself in front of the island head. This channel is forced into its position by the formation and migration of new shoals from the updrift parts of the ebb-tidal delta. Often, this flood channel will be a previous ebb channel. Subsequently, the cycle starts over with stage 1 (Figure 6.4a).

7

Discussion

The discussion is split into two parts. Section 7.1 discusses the uncertainties in the used software and in the model set-up. Subsequently, in Section 7.2, the model results are discussed. This elaborates on the accuracy of the modeled hydrodynamics, waves and sediment transports.

7.1. Software and model set-up

The use of a larger grid in the Delft3D Flexible Mesh Suite (Deltares, 2018) with a local refinement of a subsystem has been successful. The performance and results of the model are good and no large assumptions have to be made to include model boundaries. The latter is further simplified by using boundary conditions from the larger stable model DCSMv6-ZuNov4 and reanalysis ERA5.

7.1.1. Software

The computation time for 1 year of about 5 days on 4 computational nodes with 4 cores each was acceptable. With this run time it is feasible to produce model results in a decent time frame. The combination of running both the hydrodynamic and the wave computations in parallel is very promising. This has contributed to a large reduction in computation time. However, the software development of this feature is still in an early stage. This requires a close cooperation with the developers and is therefore rather time-consuming. This could cause problems for a quick set-up of a model in other projects.

The coupling of parallel computations for both hydrodynamics and waves still experiences some bugs. This led to runs that aborted before the entire modeled year was completed. This is visible in, for example, Figure 5.6. To compare results of different runs *ceteris paribus*, the lowest run time has been used. E.g. if one run ended in October, results for November and December of the other runs are not taken into account in the comparison. This problem may, however, have excluded some relevant storms in the more active maritime winter months.

Another point related to the ongoing development of the Delft3D Flexible Mesh Suite has to do with the available sediment transport models. For this thesis, the formulation by Van Rijn (1993) has been used, where a distinction is made between bed load and suspended load transport. In the future the formulation by Van Rijn et al. (2007) will be included, which additionally distinguishes between roughness heights for different bed forms. This will likely result in a better representation of the sediment transport and morphodynamics, because it includes a changing roughness over time by means of a roughness predictor. Brière and Walstra (2006) showed improved results for bar dynamics, when using this formulation.

Furthermore, the software version used for this thesis does not yet produce a so-called 'running mean' output for sediment transport in the map results. This poses a limitation of this thesis. The given values in the presented results are snapshots in time at every output time step. It is assumed that averaging the hourly output over the entire year results in a sufficiently accurate value to draw conclusions on the observed patterns. However, by including the 'running mean' output, a better result can be obtained. This is now included in a more recent release.

7.1.2. Representation of processes

The hydrodynamics in the developed model are sufficient for the intended purpose, the modeling of sediment transport patterns. This can be further improved by applying a spatially varying bottom roughness and by calibrating the tide from the offshore boundary. Due to a lack of time, this has not been done, but it can result in a better water level representation. Furthermore, for a better comparison of measured and modeled water levels the grid can be refined around observation stations to better represent the local bathymetry and therewith the tidal propagation.

The model is able to properly represent the sediment transport patterns of sand. Magnitudes in the area of interest are of the same order as expected from literature and measurements. To better represent the sediment transports different sediment fractions should be included. For the transport through the inlets and in the basins the addition of a fine, cohesive sediment fraction is required. The sediment bypassing mechanism over the tidal inlet will be different for different grain sizes. To determine the total bypassed volumes more accurately the availability of different grain sizes has to be included. For a better longshore sediment transport representation a spatially varying grain size for sand should be included along the coast. The latter can be further improved by refining the grid cells along the entire coast. It is assumed that the overestimation of the occurring longshore transport at other islands is mainly caused by a poor representation of the surf zone.

The transport of fines in the basin and through the inlets has to go hand-in-hand with a difference between salt water in the system and fresh water discharged from sluices into the Wadden Sea to include the effects of estuarine circulation. Additionally, other minor discharge sluices can be implemented. It is shown that the discharge volumes are significant with respect to residual discharges over the watersheds and through the inlets and therefore these have to be taken into account for an analysis of processes in the basins.

7.1.3. Sedimentation and erosion on the ebb-tidal delta

A better representation of waves can be achieved by further refining the grid resolution. The current resolution in the area of interest is 150 m. This value cannot be reduced much further, because a smooth scaling between the nested grids has to be used. This means that a fourth nested wave grid may be needed. This helps to more accurately represent the wave heights on the approaching shoal and in the Plaatgat.

The sedimentation and erosion pattern in Figure 5.7b is too weak compared to the observations from the *JarKus* measurements. Part of this can be related to the lack of feedback by using a morphological factor of 0.01. Strong sedimentation at the eastern edges of the shoals indicates their migration. However, since the volumes are too small, this migration with the associated wider sedimentation zones is not occurring.

Another difference in the pattern is the lack of significant sedimentation and erosion on the shallower parts of the ebb-tidal delta near the coast. It has been found that wave action is of importance in this area. Therefore, it can be the case that waves break too soon on the periphery of the delta. Not enough energy is left in the remainder of the waves to work the part closer to the coast. A solution to this problem may lay in using a breaker-delay parameter to better represent bar migration, as proposed by Walstra et al. (2012). This addition could not be implemented, calibrated and evaluated in the time span of this graduation project.

Other causes for this problem can be related to the used grain size, the use of a single grain size or the lack of 3D-effects such as bed streaming. The latter is likely responsible for the less pronounced changes in the cross-shore beach profile.

7.2. Model results

7.2.1. Hydrodynamics

The hydrodynamic representation of the model is satisfactory. Considering the relatively simple approach in model set-up, linking the boundaries to results from a larger scale model (DCSMv6-ZuNov4), the resemblance of the modeled and observed water levels in the Wadden Sea is good. The same goes for the resulting tidal prisms per basin. Observed current patterns at the Friesche Zeegat seem realistic when compared to literature. The in- and outflowing current pathways strongly agree with the patterns as described by Sha (1989b). Difficulties arise with the quantification of the flood channel in the ebb-tidal delta. Where a clear ebb-dominance is observed in the ebb channel, this is not the case

with flood-dominance in the (expected) flood channel. A clear difference in importance of the channel is visible by comparing the results of different bathymetries, but the residual discharges show no clearly prevailing direction over the entire length of the channel. The question remains, whether this is in line with the reality at Schiermonnikoog, or whether this is a demerit of the model. Unfortunately, no measurement data of the currents in the investigated channels is available to further analyze this matter.

7.2.2. Waves

The wave representation is of a similar skill as in other studies. A full comparison is given in Appendix C.2. Once again considering the used simple approach by linking the boundaries to larger scale reanalysis results (ERA5), the similarity between the model and observations is fortifying. The used grid resolution suffices to represent wave patterns, such as dissipation and the observed wave height (gradient) near the coast of Schiermonnikoog. However, a finer grid size will produce a more exact value for every point. The current resolution shows minor disruptions in the patterns. For example, the wave dissipation in the surf zone contains 'gaps', where the wave computation cannot properly follow the beach slope. For the final results, it is important to note that these missing points do not appear to affect the modeled overall sediment transport patterns nor magnitudes.

7.2.3. Sediment transport

Through the inlet

The sediment transport pathways and their changes under the addition or omission of different physical processes can clearly be explained from literature and are as expected, but the sediment import through the inlets of the Wadden Sea basins is not present for the Borndiep and Friesche Zeegat. In these inlets export is observed. A similar result is found by De Fockert (2008) and by Teske (2013), who modeled the Borndiep, for both the Van Rijn (1993) and the Van Rijn et al. (2007) formulations. A possible cause for the observed export is in the used sediment transport formulations. A better representation, yet not perfect, can be obtained by using the Van Rijn et al. (2007) instead of the Van Rijn (1993) formulation (Elias et al., 2015; Wang et al., 2016). However, this has not yet been implemented in the used software.

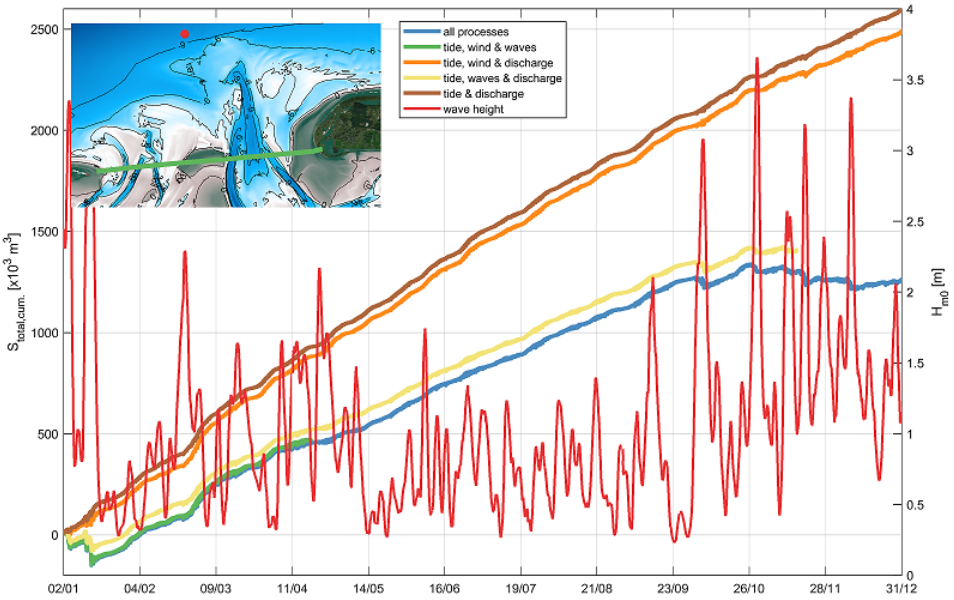

Figure 7.1: Cumulative total sediment transports for the modeled year 2017 through the Friesche Zeegat for model runs with different physical processes,
where a running mean wave height offshore of the Westgat is given in red and the cross-section is given in green; *some runs do not cover the entire year due to modeling difficulties (see Section 7.1.1)*

For a cross-section through the inlet throat of the Friesche Zeegat the cumulative sediment transport has been plotted in Figure 7.1. This total sediment transport consists of bed load and suspended transport. The first is of minor importance, but shows a constant import through the inlet. The latter has

a larger magnitude and shows more fluctuation. The tide drives a strong export of suspended sediment, but this is reduced during storms. Figure 5.6a for the transport through the ebb channel Westgat shows an increased export after the addition of waves, bringing sediment in suspension. Therefore, the reduced cumulative export over the entire inlet is likely caused by an even larger increase in import over the shallower areas. The underrepresentation of morphological development and sediment transport due to wave action in these shallow areas, as discussed in Section 7.1.3, can be the problem. Waves are not able to penetrate the system deep enough to counteract the tide-driven export.

Bypassing the inlet
The sediment transport pathway of sediment bypassing the inlet is exactly as expected. Literature suggests, based on the tide-dominance (Bruun and Gerritsen, 1959) and on the grain size distribution (Herrling and Winter, 2018), that flow bypassing through the ebb channel and bar welding over the ebb-tidal delta will occur. This pattern is clearly visible in Figure 5.4b and therewith it gives confidence in the correctness of the overall sediment transport pathways. Furthermore, the magnitude of the longshore transport is in agreement with values from literature.

At Schiermonnikoog NW
The sediment transport pathways and variation at Schiermonnikoog northwest (NW) can clearly be explained from the influence of tides and waves. Without dominating flood currents through the Plaatgat, the governing eastward transport is credible. This follows directly from the prevailing wave direction from the NW. Furthermore, the modeled variation in sediment transport magnitudes can be connected to the amount of wave sheltering by the ebb-tidal delta. Transports behind shallow areas are smaller than for locations that are more exposed to waves from the NW. Closer to the inlet, where tides still have some influence and the angle of the coastline results in an oppositely directed wave-driven sediment transport, the transport is directed inward.

Besides the sensible connection between driving processes and the modeled sediment transports, the model results also correspond well with the observed patterns. Positive sediment transport gradients in the model are located where coastal erosion has been observed and vice versa for negative gradients. The order of magnitude of the coastal erosion in 2017 is more or less in line with the modeled transport gradients in the Plaatgat. However, the morphological development and transport magnitudes on the shoal are not well represented (see Section 7.1.3).

8

Conclusions

Concluding this thesis, Section 8.1 offers answers to the main research question and subquestions as stated in Section 1.3. After the conclusion, several recommendations are given in Section 8.2. These are recommendations for further research and for future sand nourishments.

8.1. Conclusions

In this thesis, two objectives are presented in Section 1.3. The first is on the driving mechanisms for the development of Schiermonnikoog northwest (NW) and its relation to the adjacent ebb-tidal delta. This objective contains the main research question and five subquestions. The second objective is on the applicability of the Delft3D Flexible Mesh Suite (Deltares, 2018) to analyze a subsystem within a larger system. A conclusion on these objectives is presented below.

8.1.1. Development at Schiermonnikoog NW

Analysis of observed changes

The first subquestion is: *Which changes in the morphology of the coast and ebb-tidal delta occurred at the island head of Schiermonnikoog?*

The ebb-tidal delta of the Zoutkamperlaag shows a clear cyclic behavior with the landing of channels and sand shoals on the downdrift (eastern) beach at Schiermonnikoog NW. These morphological patterns result in an alternation of periods of erosion and accretion. For several decades the landing of a large sand shoal in 1972 has contributed to a large seaward extension of the coastline, but in recent years this volume has eroded. Currently, the basal coastline (*BKL*) is almost transgressed around *JarKus* transect 500. This site approximately corresponds with the attachment point of the NAP -3 m contour of the new approaching sand shoal from the ebb-tidal delta. The coastline retraction around transect 500 seems to have reduced in the last years, because the surroundings of the attachment point are getting shallower. To the west of this location significant erosion continues.

The area of the Plaatgat below NAP -3 m has reduced since 2005 and at both ends of the channel bars have developed, which are obstructing the flow. However, in the last years the cross-sectional area of the channel has been stable around 1000 m^2. A landward movement of the shoal and channel is visible, which is in line with the measured coastline retreat. These observations indicate that the Plaatgat is not yet silting up, but forced onshore by the migrating sand shoal. Tidal action in this area is likely to reduce under the future development of the rest of the ebb-tidal delta. Flood currents will start to use the more north-northeastward-oriented ebb channel Westgat and a newly opening flood channel in the west. Migration speeds are decreasing over time, but still significant. Based on the observed rates of shoal migration and coastline retreat, an attachment of the shoal to the coast can be expected in 5 to 10 years from now.

The volume of sediment present in the approaching shoal is about the same order of magnitude as during the last attachment in 1972. Nevertheless, the sediment is located at larger depths, which could indicate that a smaller volume is available for beach accretion in the upcoming attachment.

Explanation of changes from literature

The second subquestion is: *How can the recent morphological changes be explained from literature, focusing on dominant processes and the relation with the development of the tidal inlet system?*

The cyclic behavior of the ebb-tidal delta is expected to repeat itself more or less every 26 years (Ridderinkhof et al., 2016). Mainly the migration of shoals forces channels to migrate clockwise from west to east, following the ebb-tidal delta breaching conceptual model (FitzGerald, 1988). This shoal migration can be related to the sediment transport pattern over the ebb-tidal delta. According to Oost (1995), this pattern is flow bypassing and bar welding. This bypassing scheme is to be expected, based on the tide-dominance (Bruun and Gerritsen, 1959) and local grain sizes (Herrling and Winter, 2018). Significant changes in the ebb-tidal delta bathymetry are mainly caused by storm events (Herrling and Winter, 2014; Winkelmolen and Veenstra, 1980).

When a flood channel reaches the downdrift coastline, it will elongate and become hydraulically inefficient. This will result in a gradual infilling of the channel as flood currents will find another path into the inlet (FitzGerald, 1988). The Plaatgat is believed to have reached this stage (Oost et al., 2015), but the ongoing infilling of the channel seems to have halted. Most likely the eventual abandonment of the channel is related to the opening of a new flood channel in the west of the system (Oost, 1995). Oost et al. (2015) expect this abandonment and the related shoal attachment to take place in 10 to 20 years from now.

The large volume of the shoal attachment in 1972 is caused by excess sediment after a reduction of the ebb-tidal delta volume (Oost and De Haas, 1992). In particular, the reduced tidal prism of the Friesche Zeegat after the closure of the Lauwerszee embayment made the ebb-tidal delta too large for the system. At present, the inlet and basin have stabilized and have reached a new equilibrium (Elias et al., 2012; Steijn, 1991). Future attachments are expected to occur more often, closer to the inlet and in lower volumes (Elias et al., 2012; Ridderinkhof et al., 2016).

Main processes for development

The third subquestion is: *Which processes at northwestern Schiermonnikoog contribute most to the development of the current situation?*

Sediment transport pathways over the ebb-tidal delta clearly follow the expected flow bypassing and bar welding scheme. The northward directed transport through the ebb channel Westgat is mainly driven by tidal action. Waves are responsible for an eastward component in the transport direction. They cause a strong transport along the periphery of the ebb-tidal delta. Furthermore, without wave action the shallow areas of the ebb-tidal delta experience no significant sediment transport. The influence of wind is mainly an enhancement of eastward and a reduction of westward directed transport. This is in line with the main wind direction. Additionally, the increased water level set-up by wind allows relatively large waves to penetrate deeper over the shoals, which increases the transport in shallow areas. The effect of storm events on the sediment transport in shallower areas is significant. Therefore, it is likely that single events will cause the eventual attachment of the shoal.

A striking result is the behavior of the Plaatgat. For the bathymetry of 2017, no significant contribution of tidal action can be observed in both the currents and sediment transport. Currents are not significantly larger through the channel than over the approaching shoal. The southwestern half shows a minor tide-related southwestward sediment transport, but the eastern half in front of the heavily eroding beach section shows no significant current and no sediment transport related to tidal action. The addition of wave action to the model increases the southwestward transport in the southwestern half and causes an even larger transport toward the east in the eastern half. This sediment transport is deemed to be responsible for keeping the channel open and the resulting coastal erosion due its landward migration. Compared to other areas of the ebb-tidal delta and the offshore edges of the approaching shoal, this transport is small. However, a persistent year-round transport in a single direction can cause significant erosion.

The wave height shows a gradient of about 7% along the Plaatgat over the entire year with its maximum height around transect 303, where a clear divergence point in current and sediment transport directions is found. The cause of this gradient is a deep cut through the middle of the approaching shoal, the former ebb channel Oude Westgat. This results in a gradient in the sediment transports along the Plaatgat and a subsequent erosion and sedimentation pattern. Similarly, a gradient is visible toward the eastern end of the shoal, where the sheltering of the ebb-tidal delta reduces.

Relation of processes with bathymetry

The fourth subquestion is: *What is the relation between the influence of the driving processes and the bathymetry?*

The deeper and shorter Plaatgat in 2009 clearly shows a larger influence of tidal action and flood-dominance in the southwestern half of the channel. However, no significant (direction of the) currents can be observed in the eastern half. The difference in the influence of tidal action confirms that the present-day Plaatgat is no longer part of the main in- and outflow channels of this system, but an abandonment is delayed by a different process, namely wave action.

This conclusion is supported by the minor influence of a sand nourishment in the middle of the Plaatgat on the occurring sediment transport. The purpose of such an intervention is the blockage of currents through the channel. However, this has no effect, because these currents are insignificant and do not cause the gradient in the sediment transport. If it is desired to place a nourishment as a structural solution, this should be done on the approaching shoal. A smoothing of its bathymetry will prevent the occurrence of a wave height gradient and its subsequent sediment transport gradient and erosion.

Conceptual model

The final subquestion is: *What is a correct conceptual model for the system behavior at northwestern Schiermonnikoog and how does this relate to similar locations?*

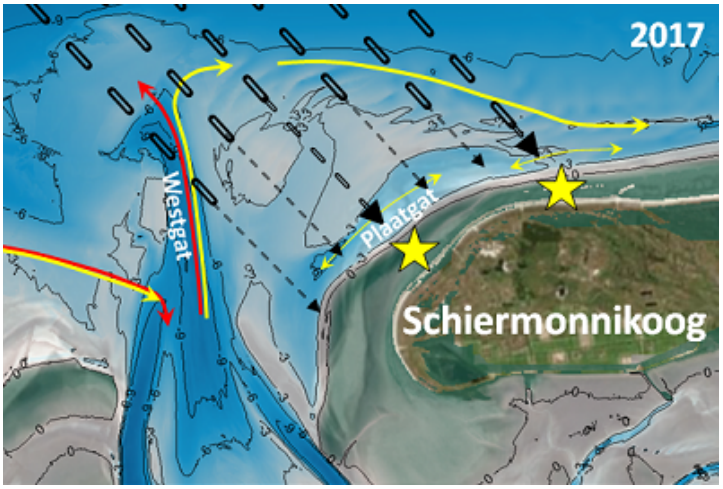

Figure 8.1: Stage 2 of the conceptual model for the present-day behavior of the Plaatgat,
where residual tidal currents are given in red, waves in black, sediment transport in yellow and erosional hotspots are given as a star

The observed gradient in the wave height at Schiermonnikoog NW with the resulting sediment transport gradient and erosion is caused by the uneven wave sheltering by the ebb-tidal delta. At Texel SW the same phenomenon has been observed, where the shape of an approaching sand shoal causes local erosion hotspots (Elias, 2016). Furthermore, a similar case is the variation in wave sheltering due to the ebb channel orientation at Ameland NW (Nederhoff et al., 2016). From these three cases, a more general conceptual model is developed for the abandoning stage of a flood channel (Chapter 6).

When a flood channel approaches the downdrift barrier island, it will elongate as it curves around the island head and as the attaching sand shoal spreads out in front of the island coast. This will reduce its hydraulic efficiency and tidal currents will start to find other paths toward the inlet. Consequently, the channel starts to gradually fill in. Together with the reducing tidal currents, the relative influence of wave action is increasing. Eventually this will determine the occurring sediment transports and erosion and sedimentation patterns entirely. The local bathymetry is of large importance for this pattern. Offshore features, such as an uneven shape of the shoal or an unfavorable orientation of another channel, can cause persisting gradients in the wave height and subsequently in the longshore sediment transport. The resulting erosion is able to delay a shoal attachment by keeping the former flood channel open and is able to cause local coastal erosion.

Final conclusion: *Future development*
With the answers to the five subquestions, the main research question can be answered. This question is: *What determines the possible future development of the northwestern part of the island head of Schiermonnikoog and the adjacent ebb-tidal delta in the upcoming years up to two decades?*

The approaching shoal at Schiermonnikoog NW is expected to attach to the coast within 10 years. This is likely to occur around transect 500, where at present the NAP −3 m contour has attached. The eventual attachment is likely to be caused by a storm event, because this generates the largest sediment transports on, and migration of the shallow sand shoal. At least until the attachment, the ongoing coastline retreat will continue. This will be largest between transects 303 and 480, where a positive gradient in the longshore sediment transport is found. Around the attachment point sedimentation is likely to occur, related to the found negative gradient in the sediment transport.

The development of the shape of the shoal is of importance to the coastal erosion. In the most recent *JarKus* measurements of 2018 it can be observed that the deep cut of the Oude Westgat is silting up. This will reduce the gradient in wave heights and subsequent erosion as explained above. When the shape of the shoal no longer allows a gradient to occur, it is likely that the Plaatgat will start silting up at a faster pace, and thus speeding up the shoal attachment.

Strong tidal currents north of Het Rif, in combination with large modeled sediment transports and observed erosion in the last *JarKus* measurements, indicate the opening of a possible new flood channel to the west of the ebb-tidal delta of the Zoutkamperlaag. This is in line with the cycle of morphological development as described by Oost et al. (2015). During flood, water will be able to enter the inlet through this newly formed channel. This contributes to the oncoming abandonment of the Plaatgat by reducing tidal action in the eastern part of the ebb-tidal delta even further.

8.1.2. Applicability of Delft3D-FM
With respect to the secondary objective of this thesis, the Delft3D Flexible Mesh Suite allows for an easy transition from coarser to finer grid resolutions. The set-up of the model in this thesis has shown that with this functionality it is possible to solve a small subsystem in detail. It is relatively easy to 'zoom in' on different locations in the model grid by refining the local resolution. This can be done without affecting the overall computation time by increasing the grid resolution of other parts in the domain due to radiation.

The main advantage of this method is the inclusion of a large coarser domain around the investigated area. With this, no uncertain nearby model boundaries have to be considered. In the Wadden Sea, a clear example of a difficult boundary to incorporate in a model is a tidal watershed. In this model, tidal watersheds formed no boundaries near the investigated area. This required no simplifications - with their related errors and uncertainties - regarding these to be made.

By using the results from validated, even larger scale models and datasets as boundary conditions instead of data from single measurement points in the system, further uncertainties due to assumptions made by the programmer can be prevented. Any errors in the output of these larger scale models and datasets will still have an effect on the developed model, but in general this approach is more objective and easier to apply.

8.2. Recommendations
In this thesis, the influence of different physical processes in the ebb-tidal delta at Schiermonnikoog NW is presented. This gives an overview of the contribution of individual processes and helps to improve the existing knowledge on this inlet system and the behavior of flood channels in their final stage before abandonment. The results and the use and development of the model also form a basis for further research. Suggestions regarding this are given below. Additionally, a recommendation for Rijkswaterstaat is given regarding the possible sand nourishment.

8.2.1. Further research
Cycle of morphological development
More model runs for the different stages in the cycle of morphological development of the Zoutkamperlaag ebb-tidal delta may result in a better understanding of the system. This can help to evaluate how the influence of processes and the occurring sediment transport patterns change over time. In this manner, also the effect of the shape of the approaching shoal on the development of the Plaatgat can

be analyzed. It is likely that the occurring gradient in wave heights, causing the currents and sediment transport that prevent the abandonment of this channel, will change under different bathymetric configurations. Furthermore, these model runs will help to better evaluate the future development of the area.

Storm events
Runs with a schematization of different wind and wave conditions will help to determine the effect of individual storms on the development of the approaching shoal and the Plaatgat. This quantifies the storm event required to cause an attachment of the approaching shoal. With this threshold and with information on the probability of the occurrence of different storm events, a better estimation of the development and eventual landing of the shoal can be made.

Historical flood channel behavior
A study of historical data and literature can help to further investigate the behavior of flood channels before their abandonment. By comparing these findings with the observed wave, current and sediment transport patterns, and the conceptual model presented in this thesis, the latter can be evaluated and improved. This analysis mainly has to focus on the occurrence of gradients in the wave height and whether these are caused by the local bathymetry. Similar situations might be found, where deep cuts parallel to the main wave direction result in a delay of the shoal attachment to the downdrift coast. This can result in valuable insight into the abandonment of flood channels, which helps to better understand erosion problems at island heads.

Measurement campaign
To verify the presented model results and the conceptual model in Chapter 6, measurement data is required. To evaluate the role of tidal currents in and around the Plaatgat, flow velocities through this channel and over the shoal have to be measured. Furthermore, the spatial variation of wave heights in the area can be measured with several wave buoys and a tracer study can be used to determine the prevailing sediment transport direction along the coastline. Together, these measurements will help to check the correctness of the modeled divergence point and the conceptual model. An attempt to measure the modeled sediment transport gradient can be made, though this is challenging, for a final verification of the conclusions of this thesis.

Comparison to other modeling software and approaches
To obtain a more comprehensive insight into the applicability, advantages and disadvantages of the used model set-up, it is advisable to look into the differences with more conventional model set-ups. This should focus on the difference in model results, computational efficiency and user-friendliness between different nested grids and the used locally changing grid resolution, between boundary conditions from measurement data and the used boundary conditions from a larger scale model, and between assuming a nearby boundary on the tidal watershed and the used larger grid without assumptions regarding these boundaries. The used model set-up showed promising results, but without the addition of these comparisons, no clear advice for an optimal modeling approach can be given. Studying the differences between approaches can result in a useful guideline for future modeling projects with Delft3D Flexible Mesh.

8.2.2. Possible sand nourishments

Rijkswaterstaat foresees to conduct a beach nourishment of about 600 000 m^3 between transects 400 and 500 in 2020 or 2021. At present, this intervention is being discussed with the stakeholders and no final decision has been made. This nourishment will prevent a transgression of the basal coastline in the upcoming years. It is realistic that with the currently occurring coastline retreat velocity no further nourishments will be required until the upcoming accretionary period after the shoal attachment.

Nevertheless, a more structural solution to the problem at Schiermonnikoog seems to be a sand nourishment on the approaching shoal. It is interesting to further investigate how nourishments in the ebb-tidal delta affect the development of the downdrift barrier island coast. The situation, as described in the conceptual model in Chapter 6, seems not unique and may be a common phenomenon in the cyclic development of ebb-tidal deltas. For situations where the flood channel is no longer dominated by tidal action, island head erosion problems could be solved by tactically placing sand nourishments

on or next to the approaching shoal. This would then reduce coastal erosion and speed up the final stage of the channel abandonment and shoal attachment by reducing wave-driven longshore transport and the effects of gradients in the wave heights.

More in general, a thorough understanding of the dominant drivers of occurring erosion is required to place an effective nourishment. Determining functions of channels and other bed forms in the highly dynamic environment of a tidal inlet is not straightforward. A modeling study or in situ measurements are required to assess the influence of tides and waves. Common tide related interventions, such as channel wall dredging or nourishments or the closure of a channel, will prove ineffective in cases where a channel is already in its final stage before abandonment. For a wave-driven erosion problem reshaping the bathymetry will be more effective. A smoother and shallower foreshore will decrease gradients in the wave height and their magnitude respectively. Consequently, the sediment transport gradients and magnitude will decrease, stopping or decreasing the coastal erosion.

Bibliography

N. Booij, R.C. Ris, and L.H. Holthuijsen. A third-generation wave model for coastal regions 1. Model description and validation. *Journal of Geophysical Research*, 104(C4):7649–7666, 1999.

C. Brière and D.J.R. Walstra. Modelling of bar dynamics. Technical report, WL|Delft Hydraulics, Delft, 2006.

P. Bruun and F. Gerritsen. Natural By-Passing of Sand at Coastal Inlets. *Journal of the Waterways and Harbors Division*, 85(4):75–108, 1959.

L. Cavaleri, S. Abdalla, A. Benetazzo, L. Bertotti, J.R. Bidlot, O. Breivik, S. Carniel, R.E. Jensen, J. Portilla-Yandun, W.E. Rogers, A. Roland, A. Sanchez-Arcilla, J.M. Smith, J. Staneva, Y. Toledo, G.Ph. van Vledder, and A.J. van der Westhuysen. Wave modelling in coastal and inner seas. *Progress in Oceanography*, 167:164–233, 2018.

K.F. Cheung, F. Gerritsen, and J. Cleveringa. Morphodynamics and Sand Bypassing at Ameland Inlet, The Netherlands. *Journal of Coastal Research*, 231:106–118, 2007.

J. Cleveringa. Zand voor zuidwest Texel: Technisch advies RIKZ over vier mogelijke ingrepen in het Zeegat van Texel. Technical report, Rijksinstituut voor Kust en Zee, Den Haag, 2001.

D.P. Dee, S.M. Uppala, A.J. Simmons, P. Berrisford, P. Poli, S. Kobayashi, U. Andrae, M.A. Balmaseda, G. Balsamo, P. Bauer, P. Bechtold, A.C.M. Beljaars, L. van de Berg, J.R. Bidlot, N. Bormann, C. Delsol, R. Dragani, M. Fuentes, A.J. Geer, L. Haimberger, S.B. Healy, H. Hersbach, E.V. Hólm, L. Isaksen, P. Kållberg, M. Köhler, M. Matricardi, A.P. McNally, B.M. Monge-Sanz, J.J. Morcrette, B. K. Park, C. Peubey, P. de Rosnay, C. Tavolato, J.N. Thépaut, and F. Vitart. The ERA-Interim reanalysis: Configuration and performance of the data assimilation system. *Quarterly Journal of the Royal Meteorological Society*, 137(656):553–597, 2011.

Deltares. Delft3D Flexible Mesh Suite: Technical Reference Manual, 2018.

P. Doornenbal, A.P. Oost, A. Bruens, and J.J. van der Werf. Memo: Regionale Kustlijnzorg advisering Schiermonnikoog. Technical report, 2011.

M. Duran-Matute, T. Gerkema, G.J. de, J.J. Nauw, and U. Gräwe. Residual circulation and freshwater transport in the Dutch Wadden Sea: A numerical modelling study. *Ocean Science*, 10(4):611–632, 2014.

M. Duran-Matute, T. Gerkema, and M. Sassi. Quantifying the residual volume transport through a multiple-inlet system in response to wind forcing: The case of the western Dutch Wadden Sea. *Journal of Geophysical Research*, 121:8888–8903, 2016.

E.P.L. Elias. *Morphodynamics of Texel Inlet*. PhD thesis, Delft University of Technology, 2006.

E.P.L. Elias. Verkenning morfologische effecten (geulwand)suppletie Paal 10, Texel. Technical report, Deltares, Delft, 2016.

E.P.L. Elias. Een actuele sedimentbalans van de Westelijke Waddenzee (1933-2015). Technical report, Deltares, Delft, 2018a.

E.P.L. Elias. Een actuele sedimentbalans van het Friesche Zeegat (1926-2012). Technical report, Deltares, Delft, 2018b.

E.P.L. Elias, A.J.F. van der Spek, Z.B. Wang, and J.G. de Ronde. Morphodynamic development and sediment budget of the Dutch Wadden Sea over the last century. *Geologie en Mijnbouw/Netherlands Journal of Geosciences*, 91(3):293–310, 2012.

E.P.L. Elias, R. Teske, A.J.F. van der Spek, and M. Lazar. Modelling tidal-inlet morphodynamics on medium time scales. In *Coastal Sediments*, page 14, San Diego, 2015.

F. Engelund and E. Hansen. A monograph on sediment transport in alluvial streams. Technical report, Technical University of Denmark, Hydraulic Laboratory, Copenhagen, 1967.

W.D. Eysink. Extra spuisluis in de Afsluitdijk; Effect op onderhoud havens. Technical report, WL|Delft Hydraulics, Delft, 2003.

D.M. FitzGerald. Shoreline erosional-depositional processes associated with tidal inlets. In *Lecture Notes on Coastal and Estuarine Studies*, number 29, pages 186–225. Springer Verlag, New York, 1988.

D.M. Fitzgerald, S. Penland, and D. Nummedal. Control of Barrier Island Shape by Inlet Sediment Bypassing: East Frisian Islands, West Germany. *Marine Geology*, 60:355–376, 1984.

D.M. Fitzgerald, N.C. Kraus, and E.B. Hands. Natural Mechanisms of Sediment Bypassing at Tidal Inlets. Technical report, U.S. Army Engineer Research and Development Center, Vicksburg, 2000.

A. de Fockert. Impact of Relative Sea Level Rise on the Amelander Inlet Morphology. Master's thesis, Delft University of Technology, 2008.

C. Gautier and S. Caires. Operational wave forecasts in the southern North Sea. In *IAHR World Congress*, page 4, 2015.

C. Gautier and A.J. van der Westhuysen. Wave propagation under influence of currents. Technical report, Deltares, Delft, 2010.

C. Gautier, A. Camarena, and J.C.C. van Nieuwkoop. SWAN hindcasts Wadden Sea, December 2013: Tidal inlet of Ameland and eastern Wadden Sea. Technical report, Deltares, Delft, 2014.

M.A. van Goor, T.J. Zitman, Z.B. Wang, and M.J.F. Stive. Impact of sea-level rise on the morphological equilibrium state of tidal inlets. *Marine Geology*, 202(3-4):211–227, 2003.

R.F. de Graaff. SBW Wadden Sea, water level modelling; Calibration hydrodynamic model. Technical report, Deltares, Delft, 2009.

M.O. Hayes. Morphology of sand accumlation in estuaries: An introduction to the symposium. In L.E. Cronin, editor, *Estuarine Research*, page 20, New York, 1975. Academic Press.

J.B. Herbich and L.B. Hales. The Effect of Tidal Inlet Currents on the Characteristics and Energy Propagation Of Ocean Waves. In *Offshore Technology*, 1972.

G. Herrling and C. Winter. Morphological and sedimentological response of a mixed-energy barrier island tidal inlet to storm and fair-weather conditions. *Earth Surface Dynamics*, 2(1):363–382, 2014.

G. Herrling and C. Winter. Tidal inlet sediment bypassing at mixed-energy barrier islands. *Coastal Engineering*, 140:342–354, 2018.

H. Hersbach. The ERA5 Atmospheric Reanalysis. *AGU Fall Meeting Abstracts*, 2016.

A. Hibma, H.J. de Vriend, and M.J.F. Stive. Numerical modelling of shoal pattern formation in well-mixed elongated estuaries. *Estuarine, Coastal and Shelf Science*, 57(5-6):981–991, 2003a.

A. Hibma, H.M. Schuttelaars, and Z.B. Wang. Comparison of longitudinal equilibrium profiles of estuaries in idealized and process-based models. *Ocean Dynamics*, 53(3):252–269, 2003b.

A. Hibma, H.M. Schuttelaars, and H.J. de Vriend. Initial formation and long-term evolution of channel-shoal patterns. *Continental Shelf Research*, 24(15):1637–1650, 2004.

L.H. Holthuijsen, N. Booij, and R.C. Ris. A spectral wave model for the coastal zone. In *Ocean Wave Measurement and Analysis*, pages 630–641, New Orleans, 1993. ASCE.

A. Huiskamp. Jaaroverzicht van het weer in Nederland; 2017. Technical report, Koninklijk Nederlands Meteorologisch Instituut, de Bilt, 2018.

H.W.J. Kernkamp, A. van Dam, G.S. Stelling, and E.D. de Goede. Efficient scheme for the shallow water equations on unstructured grids with application to the Continental Shelf. *Ocean Dynamics*, 61(8):1175–1188, 2011.

M. van Koningsveld, B. de Sonneville, Z.B. Wang, and L.C. van Rijn. Sediment Budget Analysis of the Dutch Coastal System a Focus on the Wadden Sea. In *Coastal Engineering*, page 15, Hamburg, 2009.

N.G. Kragtwijk, T.J. Zitman, M.J.F. Stive, and Z.B. Wang. Morphological response of tidal basins to human interventions. *Coastal Engineering*, 51:207–221, 2004.

M.C. Kwanten. Memorie: Noordzee reductiematrix 2006. Technical report, Koninklijke Marine, Dienst Hydrografie, Den Haag, 2007.

F. Ladage, C. Meyer, Stephan H.-J., and H.D. Niemeyer. Morphologische Entwicklung im Seegat Otzumer Balje und seinem Einzugsgebiet. Technical report, Niedersächsischer Landesbetrieb für Wasser- wirtschaft, Küsten- und Naturschutz, Norderney, 2006.

M. van Ledden. *Sand-mud segregation in estuaries and tidal basins*. PhD thesis, Delft University of Technology, 2003.

K.J.H. Lenstra, S.R.P.M. Pluis, W. Ridderinkhof, G. Ruessink, and M. van der Vegt. Cyclic channel-shoal dynamics at the Ameland inlet: the impact on waves, tides, and sediment transport. *Ocean Dynamics*, pages 409–425, 2019.

G.R. Lesser, J.A. Roelvink, J.A.T.M. van Kester, and G.S. Stelling. Development and validation of a three-dimensional morphological model. *Coastal Engineering*, 51:883–915, 2004.

M.A.M. Löffler, C.C. de Leeuw, M.E. ten Haaf, S.K. Verbeek, A.P. Oost, A.P. Grootjans, E.J. Lammerts, and R.M.K. Haring. *Eilanden natuurlijk: Natuurlijke ontwikkeling en veerkracht op de Waddeneilanden*. Het Grafisch Huis, Groningen, 2008.

T. Louters and F. Gerritsen. The Riddle of the Sands; a tidal system's answer to a rising sea level. Technical report, National Institute for Coastal and Marine Management/RIKZ, Den Haag, 1994.

M.A. van der Lugt, T. Vermaas, and A.J.F. van der Spek. Aanlanding zandplaat Schiermonnikoog NW. Technical report, Deltares, Delft, 2018.

R. Marciano, Z.B. Wang, A. Hibma, H.J. de Vriend, and A. Defina. Modeling of channel patterns in short tidal basins. *Journal of Geophysical Research*, 110(1):1–13, 2005.

Ministerie van Infrastructuur en Milieu. Bestuursakkoord Water. Technical report, Den Haag, 2011.

Ministerie van Infrastructuur en Milieu. Basiskustlijn 2012: Herziening Basiskustlijn. Technical report, Den Haag, 2012.

Ministerie van Infrastructuur en Waterstaat. Pilotsuppletie Buitendelta Amelander Zeegat, 2018.

C.M. Nederhoff, E.P.L. Elias, and T. Vermaas. Erosie op Ameland Noordwest; Modelstudie: simulaties met Delft3D en XBeach. Technical report, Deltares, Delft, 2016.

C.M. Nederhoff, R. Schrijvershof, P.K. Tonnon, and J.J. van der Werf. The Coastal Genesis II Terschelling-Ameland inlet (CGII-TA) model: Model setup, calibration and validation of a hydrodynamic wave model. Technical report, Deltares, Delft, 2019.

P. Noordstra. Zandhaak Schiermonnikoog, volumebepaling. Technical report, Rijkswaterstaat, directie Friesland, Leeuwarden, 1989.

M. Olabarrieta, W.R. Geyer, and N. Kumar. The role of morphology and wave-current interaction at tidal inlets: An idealized modeling analysis. *Journal of Geophysical Research*, 119:8818–8837, 2014.

J. Olauson. ERA5: The new champion of wind power modelling? *Renewable Energy*, 126:322–331, 2018.

A.P. Oost. *Dynamics and Sedimentary Development of the Dutch Wadden Sea with Emphasis on the Frisian Inlet: a study of the barrier islands, ebb-tidal deltas and drainage basins*. PhD thesis, Universiteit Utrecht, Utrecht, 1995.

A.P. Oost and K.S. Dijkema. Effecten van bodemdaling door gaswinning in de Waddenzee. Technical report, DLO-Instituut voor Bos- en Natuuronderzoek, Den Burg, 1993.

A.P. Oost and H. de Haas. Het Friesche Zeegat - Morfologisch-Sedimentologische veranderingen in de perioden 1970-1987 Deel 1. Technical report, Faculteit Aardwetenschappen Universiteit Utrecht, Utrecht, 1992.

A.P. Oost, H. de Haas, F. IJnsen, J.M. van den Boogert, and P.L. de Boer. The 18.6 yr nodal cycle and its impact on tidal sedimentation. *Sedimentary Geology*, 87(1-2):1–11, 1993.

A.P. Oost, T. Vermaas, and L.M. Vonhögen-Peeters. Morfologische beschouwing ontwikkeling vaarweg buitendelta Zoutkamperlaag. Technical report, Deltares, Delft, 2015.

A.P. Oost, R. van Buren, and A. Kieftenburg. Overview of the hydromorphology of ebb-tidal deltas of the trilateral Wadden Sea. Technical report, Deltares, Delft, 2017.

A.P. Oost, C.M. Nederhoff, B. van der Valk, and M. Maarse. Beheerbibliotheek Schiermonnikoog: Beschrijvingen van het kustvak ter ondersteuning van het beheer en onderhoud van de kust. Technical report, Deltares, Delft, 2018.

J.J.A.M. van Os and R.F. de Graaff. SBW Wadden Sea, water level modelling; Study on improvement of wind input. Technical report, Deltares, Delft, 2009.

W. Ridderinkhof, P. Hoekstra, M. van der Vegt, and H.E. de Swart. Cyclic behavior of sandy shoals on the ebb-tidal deltas of theWadden Sea. *Continental Shelf Research*, 115:1351–1372, 2016.

L.C. van Rijn. Sediment transport, part I: bed-load transport. *Journal of Hydraulic Engineering*, 110 (10):1431–1456, 1984.

L.C. van Rijn. *Principles of Sediment Transport in Rivers , Estuaries and Coastal Seas*. Aqua Publications, Amsterdam, 1993.

L.C. van Rijn, D.J.R. Walstra, and M. van Ormondt. Unified View of Sediment Transport by Currents and Waves. IV: Application of Morphodynamic Model. *Journal of Hydraulic Engineering*, 133(7): 776–793, 2007.

R.C. Ris, L.H. Holthuijsen, and N. Booij. A third-generation wave model for coastal regions 2. Verification. *Journal of Geophysical Research*, 104(C4):7667–7681, 1999.

L.P. Sha. Variation in ebb-delta morphologies along the West and East Frisian Islands, The Netherlands and Germany. *Marine Geology*, 89(1-2):11–28, 1989a.

L.P. Sha. Sand transport patterns in the ebb-tidal delta off Texel Inlet, Wadden Sea, The Netherlands. *Marine Geology*, 86(2-3):137–154, 1989b.

L.P. Sha and P.L. de Boer. Ebb-tidal delta deposits along the west Frisian Islands (the Netherlands): processes, facies architecture and preservation. *Clastic tidal sedimentology*, 16:199–218, 1991.

D. van Sijp. Correcties op gemeten eb- en vloedvolume bij de omrekening naar gemiddeld getij, in het Friese Zeegat. Technical report, Rijkswaterstaat, directie Friesland, Leeuwarden, 1989.

C.S. Son, B.W. Flemming, and A. Bartholomä. Evidence for sediment recirculation on an ebb-tidal delta of the East Frisian barrier-island system, southern North Sea. *Geo-Marine Letters*, 31(2):87–100, 2011.

A.J.F. van der Spek. *Large-scale evolution of Holocene tidal basins in the Netherlands*. PhD thesis, Universiteit Utrecht, 1994.

H.J. Steetzel. Voorspelling ontwikkeling kustlijn en buitendelta's Waddenkust over de periode 1990-2040. Technical report, Waterloopkundig Laboratorium, Delft, 1995.

R.C. Steijn. Some Considerations on Tidal inlets: A literature survey on hydrodynamic and morphodynamic characteristics of tidal inlets with special attention to Het Friesche Zeegat. Technical report, WL|Delft Hydraulics, Delft, 1991.

R.C. Steijn and G. Hartsuiker. Morphodynamic Response of a Tidal Inlet after a Reduction in Basin Area: Numerical simulation of hydro- and morphodynamics of the mesotidal inlet "Het Friesche Zeegat". Technical report, WL|Delft Hydraulics, Delft, 1992.

R.C. Steijn and T. Louters. Hydro- and Morphodynamics of a Mesotidal Inlet in the Dutch Wadden Sea. In *Oceanology*, page 18, Brighton, 1992. Directoraat-Generaal Rijkswaterstaat.

M.J.F. Stive and Z.B. Wang. Chapter 13 Morphodynamic modeling of tidal basins and coastal inlets. *Elsevier Oceanography Series*, 67(C):367–392, 2003.

M.J.F. Stive, Z.B. Wang, M. Capobianco, P. Ruol, and M.C. Buijsman. Morphodynamics of a tidal lagoon and the adjacent coast. In *Physics of Estuarine and Coastal Seas*, pages 355–362, The Hague, 1998.

J. Sutherland, A.H. Peet, and R.L. Soulsby. Evaluating the performance of morphological models. *Coastal Engineering*, 51:917–939, 2004.

R. Teske. Tidal inlet channel stability in long term process based modelling. Technical report, Deltares, Delft, 2013.

D. Vatvani, N.C. Zweers, M. van Ormondt, A.J. Smale, H. de Vries, and V.K. Makin. Storm surge and wave simulations in the Gulf of Mexico using a consistent drag relation for atmospheric and storm surge models. *Natural Hazards and Earth System Science*, 12(7):2399–2410, 2012.

J. van Veen. *Onderzoekingen in de Hoofden: in verband met de gesteldheid der Nederlandsche kust*. PhD thesis, Rijksuniversiteit Leiden, 1936.

D.J.R. Walstra, A.J.H.M. Reniers, R. Ranasinghe, J.A. Roelvink, and B.G. Ruessink. On bar growth and decay during interannual net offshore migration. *Coastal Engineering*, 60:190–200, 2012.

Y. Wang, Q. Yu, J. Jiao, P.K Tonnon, Z.B. Wang, and S. Gao. Coupling bedform roughness and sediment grain-size sorting in modelling of tidal inlet incision. *Marine Geology*, 381:128–141, 2016.

Z.B. Wang, T. Louters, and H.J. de Vriend. Morphodynamic modelling for a tidal inlet in the Wadden Sea. *Marine Geology*, 126(1-4):289–300, 1995.

Z.B. Wang, P. Hoekstra, H. Burchard, H. Ridderinkhof, H.E. de Swart, and M.J.F. Stive. Morphodynamics of the Wadden Sea and its barrier island system. *Ocean and Coastal Management*, 68:39–57, 2012.

M. van der Wegen and J.A. Roelvink. Long-term morphodynamic evolution of a tidal embayment using a two-dimensional, process-based model. *Journal of Geophysical Research*, 113(3):49, 2008.

A.J. van der Westhuysen. Modeling of depth-induced wave breaking under finite depth wave growth conditions. *Journal of Geophysical Research*, 115(1):1–19, 2010.

A.J. van der Westhuysen, M. Zijlema, and J.A. Battjes. Nonlinear saturation-based whitecapping dissipation in SWAN for deep and shallow water. *Coastal Engineering*, 54:151–170, 2007.

Wetterskip Fryslân. Watergebiedsplan Schiermonnikoog. Technical report, Leeuwarden, 2011.

A.M. Winkelmolen and H.J. Veenstra. The Effect of a Storm Surge on Near-shore Sediments in the Ameland-Schiermonnikoog Area (N. Netherlands). *Geologie en Mijnbouw/Netherlands Journal of Geosciences*, 59(2):97–111, 1980.

F. Zijl, M. Verlaan, and H. Gerritsen. Improved water-level forecasting for the Northwest European Shelf and North Sea through direct modelling of tide, surge and non-linear interaction. *Ocean Dynamics*, 63(7):823–847, 2013.

F. Zijl, J. Sumihar, and M. Verlaan. Application of data assimilation for improved operational water level forecasting on the northwest European shelf and North Sea. *Ocean Dynamics*, 65(12):1699–1716, 2015.

A

DCSMv6-ZuNov4

The first version of the Dutch Continental Shelf Model (DCSM) has been developed in the 1980s to accurately forecast hydrodynamics and surges at the Dutch coast. In this model results of the meteorological high-resolution limited area model (HiRLAM) are used. Over the years, the model has been improved till the current, sixth version, where an astronomical correction does not yield a more accurate water-level result (Zijl et al., 2013).

To improve the accuracy of the water-level representation the model has been calibrated by altering the local bathymetry to improve the tidal phase lag and by using a spatially variable bed roughness to improve the tidal amplitude (Zijl et al., 2013). For an even better representation in the Dutch coastal waters, a more detailed model grid has been nested into the existing DCSMv6. This addition of the *Zuidelijke Noordzee* model (ZuNov4 (Zijl et al., 2015)) results in the commonly used DCSMv6-ZuNov4 model, which has been used as water level input data on the boundaries of the FM-model developed for this thesis.

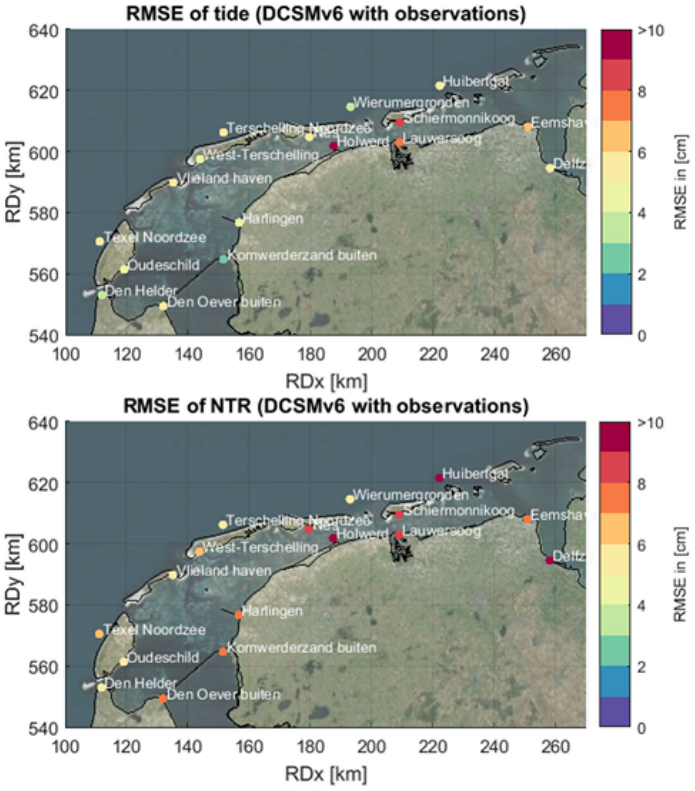

Figure A.1: Root-mean-square errors in [cm] at measurement stations between DCSMv6-ZuNov4 and observations for the tidal water levels and the non-tidal residual

The accuracy of the DCSMv6-ZuNov4 model in the area of interest of this thesis is given in Figure A.1. It can be concluded that the root-mean-square errors in the water-level representation are similar to the ones in the developed FM-model (also see Figure 4.5 and B.2). It is therefore concluded that both models perform equally well with respect to hydrodynamics in the area of interest, where the FM-model uses a more accurate bathymetry from measurements and a constant bed roughness. Both aspects may limit an optimal representation of the tide.

B

Model set-up and calibration

B.1. WadSea 2009 grid optimization

The Wadden Sea model of 2009 (WadSea 2009) by Deltares (De Graaff, 2009) is a further calibrated version of model set-up for the SBW 2008 project. This calibration has been conducted, among other aspects, with respect to the computational grid. This resulted in a grid size of about 200 m in the inlets, which was about the limit for the computational capacities at the time.

This well-calibrated grid has formed the basis of the adapted grid for the developed FM-model. Subsequently this grid has been coarsened offshore to decrease computational time, a possibility that was not available in the structured Delft3D 4 Suite in 2009. Furthermore, the grid has been refined in the Friesche Zeegat inlet. The higher resolution resulted in a better representation of gullies and shoals in this area, which resulted in a better representation of water-levels at local measurement stations. At a resolution of about 100 m in the inlet, this has largely converged. However, since computational time allowed so, an even more detailed grid of 50 m is applied at the approaching shoal from the ebb-tidal delta and the coast of Schiermonnikoog NW. This will allow for a more detailed analysis at the area of interest. Results of the convergence of the root-mean-square error are given in Figure B.1.

n	DCSMv6	WadSea	100 m	50 m	DCSMv6	WadSea	100 m	50 m	DCSMv6	WadSea	100 m	50 m
Station	ZuNov4	org. bath	$RMSE_{tide}$		ZuNov4	org. bath	$RMSE_{NTR}$		ZuNov4	org. bath	$RMSE_{total}$	
Delfzijl	5.77	42.28	17.18	17.12	10.06	23.06	12.48	12.39	11.51	46.80	21.01	20.98
Den Helder	3.96	3.93	4.45	4.47	6.36	6.42	6.43	6.43	7.25	7.33	7.57	7.59
Den Oever buiten	5.72	9.07	9.61	9.73	7.73	8.26	8.31	8.40	9.39	11.99	12.35	12.40
Eemshaven	6.93	7.27	7.93	7.88	8.44	9.54	9.56	9.56	10.54	11.66	12.15	12.11
Harlingen	4.55	4.55	4.34	4.36	7.54	9.54	9.63	9.65	8.74	10.37	10.34	10.35
Huibertgat	5.60	5.29	5.38	5.38	10.38	11.05	11.05	11.05	11.77	12.10	12.13	12.14
Kornwerderzand buiten	3.07	6.26	6.53	6.62	7.53	8.57	8.61	8.61	7.93	10.38	10.56	10.61
Lauwersoog	8.31	10.88	8.40	8.10	9.47	10.52	10.35	10.23	12.05	14.35	12.60	12.42
Nes	6.00	7.96	6.97	6.69	8.78	9.38	9.39	9.38	10.15	11.91	11.30	11.11
Oudeschild	5.32	6.75	7.44	7.79	6.30	6.41	6.44	6.45	7.85	8.99	9.50	9.78
Schiermonnikoog	8.87	29.79	12.59	8.83	8.76	14.41	9.62	9.13	11.79	32.26	15.61	12.43
Terschelling Noordzee	5.77	5.42	5.63	5.65	5.83	6.29	6.31	6.31	8.07	8.16	8.32	8.33
Texel Noordzee	5.72	5.23	5.32	5.36	6.64	6.88	6.97	6.99	8.54	8.48	8.59	8.63
Vlieland haven	5.82	16.03	6.41	6.46	6.32	12.16	6.51	6.52	8.15	19.31	8.76	8.80
West-Terschelling	4.73	32.25	5.86	5.86	6.55	16.52	6.84	6.85	7.62	35.08	8.63	8.64
Wierumergronden	4.38	4.46	4.68	4.69	5.98	6.75	6.76	6.76	7.24	7.84	7.98	7.99
Average	5.66	12.34	7.42	7.19	7.67	10.36	8.45	8.42	9.29	16.06	11.09	10.89
Average Offshore	5.09	4.87	5.09	5.11	7.04	7.48	7.50	7.51	8.57	8.78	8.92	8.94
Average Basins	5.92	15.74	8.48	8.13	7.95	11.67	8.89	8.83	9.61	19.37	12.07	11.78
Average Frisian Inlet	*7.19*	*15.04*	*8.56*	*7.21*	*8.07*	*10.56*	*8.91*	*8.71*	*10.36*	*18.15*	*12.06*	*10.95*
Minimum	3.07	3.93	4.34	4.36	5.83	6.29	6.31	6.31	7.24	7.33	7.57	7.59
Maximum	8.87	42.28	17.18	17.12	10.38	23.06	12.48	12.39	12.05	46.80	21.01	20.98

Figure B.1: Root-mean-square errors for the tidal, non-tidal residual and total water levels for different grid resolutions; every second column is for the original WadSea-model with an unaltered bathymetry in the harbors, every third and fourth column is for an increased grid resolution around the Friesche Zeegat and its basin

B.2. Manning friction coefficient

The full results for the purely hydrodynamic model runs with Manning friction coefficients between $n = 0.018\,\mathrm{s/m^{1/3}}$ to $0.025\,\mathrm{s/m^{1/3}}$ is given below. It can be concluded that for the model as a whole $n = 0.023\,\mathrm{s/m^{1/3}}$ gives the most promising water level results, but for the Friesche Zeegat in particular a smaller value of $n = 0.020\,\mathrm{s/m^{1/3}}$ is more suitable. Since the focus of this thesis is on that location, the latter value has been selected. Overall it can be concluded that the difference is minor and all root-mean-square errors sufficiently small for an investigation of sediment transports. Ideally, a spatially varying bed roughness would have been applied, but the implementation was deemed too time-consuming.

Furthermore, it is visible that the differences in phase lag between the observations and the model are not significantly affected by a changing bed roughness. This is more commonly influenced by local bathymetry effects. For the amplitude ratios of the model over the observations a similar trend

is observed as for the root-mean-square error in water levels. This confirms the choice made for the friction coefficient.

Station	DCSMv6 ZuNov4 RMSE$_{tide}$ 0.018	0.019	0.02	0.021	**0.022**	0.023	0.024	0.025	DCSMv6 ZuNov4 RMSE$_{NTR}$ 0.018	0.019	0.02	0.021	**0.022**	0.023	0.024	0.025	DCSMv6 ZuNov4 RMSE$_{total}$ 0.018	0.019	0.02	0.021	**0.022**	0.023	0.024	0.025
Delfzijl	5.77	12.18	10.03	8.92	10.40	13.04	16.08	20.21	23.19	10.06	11.93	12.02	11.86	11.83	12.04	12.16	12.65	12.74	11.51	16.99	15.50	14.64	15.64	17.55	19.96	23.62	26.28
Den Helder	3.96	8.75	7.66	6.67	5.79	5.04	4.45	4.04	3.84	6.36	6.60	6.54	6.50	6.47	6.44	6.43	6.42	6.41	7.25	10.79	9.90	9.12	8.47	7.95	7.57	7.33	7.22
Den Oever buiten	5.72	20.70	18.18	15.84	13.57	11.48	9.56	7.82	6.47	7.73	8.62	8.53	8.46	8.38	8.33	8.29	8.27	8.36	9.39	22.03	19.70	17.56	15.60	13.86	12.35	11.11	10.16
Eemshaven	6.93	7.13	5.17	4.48	5.50	6.91	8.79	9.89	5.81	8.44	9.65	9.58	9.54	9.70	9.54	9.56	9.59	6.42	10.54	11.74	10.62	10.32	10.69	11.56	12.76	13.51	8.31
Harlingen	4.55	18.97	15.16	11.63	8.48	5.88	4.34	4.65	5.18	7.54	10.23	10.01	9.86	9.75	9.68	9.63	9.62	6.90	8.74	21.45	18.05	15.11	12.75	11.11	10.34	10.44	8.47
Huibertgat	5.60	5.37	5.18	5.09	5.10	5.20	5.38	5.64	6.29	10.38	11.21	11.15	11.11	11.08	11.06	11.04	11.04	9.63	11.77	12.34	12.21	12.12	12.08	12.08	12.13	12.23	11.26
Kornwerderzand buiten	3.07	22.89	19.14	15.63	12.36	9.31	6.53	4.09	5.52	7.53	8.97	8.84	8.74	8.68	8.63	8.61	8.60	6.47	7.93	24.32	20.84	17.67	14.86	12.46	10.56	9.29	8.10
Lauwersoog	8.31	8.72	7.61	7.04	6.97	7.47	8.39	9.64	4.41	9.47	10.42	10.33	10.28	10.24	10.23	10.35	10.26	6.81	12.05	13.00	12.24	11.84	11.75	12.02	12.59	13.43	7.71
Nes	6.00	9.14	7.18	5.75	5.21	5.73	6.97	8.57	5.64	8.78	9.61	9.50	9.43	9.39	9.38	9.39	9.43	6.29	10.15	12.76	11.42	10.57	10.29	10.56	11.30	12.37	8.30
Oudeschild	5.32	14.69	12.96	11.58	10.12	8.82	7.69	6.51	10.31	6.30	6.60	6.55	6.51	6.48	6.45	6.43	6.42	9.47	7.85	15.85	14.25	13.00	11.71	10.60	9.68	8.80	13.65
Schiermonnikoog	8.87	7.23	7.30	6.35	7.06	8.30	9.83	14.37	37.22	8.76	9.70	9.63	9.25	9.23	9.24	9.26	9.67	18.56	11.79	11.74	11.77	10.90	11.33	12.14	13.24	17.08	40.72
Terschelling Noordzee	5.77	6.54	6.26	6.03	5.85	5.71	5.64	5.61	4.99	5.83	6.62	6.52	6.44	6.38	6.34	6.31	6.29	6.76	8.07	9.21	8.93	8.70	8.53	8.40	8.32	8.29	8.14
Texel Noordzee	5.72	6.43	6.14	5.87	5.65	5.46	5.32	5.23	11.04	6.64	7.19	7.14	7.09	7.05	7.01	6.97	6.93	10.29	8.54	9.45	9.22	9.01	8.84	8.70	8.59	8.51	14.45
Vlieland haven	5.82	12.44	10.95	9.57	8.33	7.27	6.41	5.81	16.17	6.32	6.85	6.75	6.67	6.60	6.55	6.51	6.49	9.73	8.15	13.95	12.59	11.37	10.30	9.43	8.76	8.32	18.62
West-Terschelling	4.73	13.80	11.96	10.20	8.58	7.11	5.86	4.93	5.97	6.55	7.23	7.11	7.01	6.93	6.88	6.84	6.82	11.03	7.62	15.29	13.60	12.06	10.69	9.53	8.63	8.02	12.36
Wieumergronden	4.38	5.12	4.88	4.72	4.63	4.61	4.67	4.80	11.86	5.98	7.00	6.92	6.85	6.81	6.78	6.76	6.75	9.63	7.24	8.49	8.28	8.12	8.02	7.97	7.98	8.04	15.01
Average	5.66	11.26	9.74	8.46	7.72	7.33	7.24	7.61	10.24	7.67	8.65	8.57	8.48	8.44	8.41	8.41	8.45	9.09	9.29	14.34	13.07	12.01	11.35	10.99	10.92	11.27	13.67
Average Offshore	5.09	6.44	6.03	5.68	5.40	5.21	5.09	5.07	7.60	7.04	7.72	7.65	7.60	7.56	7.52	7.50	7.49	8.54	8.57	10.06	9.71	9.41	9.19	9.02	8.92	8.88	11.22
Average Basins	5.92	13.44	11.42	9.73	8.78	8.30	8.22	8.77	11.44	7.95	9.07	8.99	8.87	8.84	8.81	8.82	8.89	9.34	9.61	16.29	14.60	13.18	12.33	11.89	11.83	12.36	14.79
Average Frisian Inlet	*7.19*	*7.02*	*6.60*	*6.04*	*6.22*	*6.79*	*7.63*	*9.60*	*17.83*	*8.07*	*9.04*	*8.96*	*8.80*	*8.76*	*8.75*	*8.79*	*8.90*	*11.67*	*10.36*	*11.08*	*10.76*	*10.28*	*10.37*	*10.71*	*11.27*	*12.85*	*21.15*
Minimum	3.07	5.12	4.88	4.48	4.63	4.61	4.34	4.04	3.84	5.83	6.60	6.52	6.44	6.38	6.34	6.31	6.29	6.29	7.24	8.49	8.28	8.12	8.02	7.95	7.57	7.33	7.22
Maximum	8.87	22.89	19.14	15.84	13.57	13.04	16.08	20.21	37.22	10.38	11.93	12.02	11.86	11.83	12.04	12.16	12.65	18.56	12.05	24.32	20.84	17.67	15.64	17.55	19.96	23.62	40.72

(a) Root-mean-square errors for the tidal, non-tidal residual and total water levels for different Manning friction coefficients

Station	ratio$_{A,M2}$ 0.018	0.019	0.02	0.021	**0.022**	0.023	0.024	0.025	ratio$_{A,S2}$ 0.018	0.019	0.02	0.021	**0.022**	0.023	0.024	0.025	ratio$_{A,M4}$ 0.018	0.019	0.02	0.021	**0.022**	0.023	0.024	0.025	ratio$_{A,N2}$ 0.018	0.019	0.02	0.021	**0.022**	0.023	0.024	0.025
Delfzijl	1.08	1.05	1.02	**0.99**	0.96	0.93	0.90	0.88	1.09	1.05	1.02	0.98	0.95	0.91	0.88	0.85	0.94	0.89	0.75	0.71	0.67	0.63	0.68	0.64	1.08	1.05	1.01	0.98	0.95	0.92	0.89	0.86
Den Helder	1.16	1.14	1.12	1.10	1.08	1.06	1.04	1.02	1.17	1.15	1.12	1.10	1.08	1.06	1.04	1.02	**0.99**	1.01	1.03	1.05	1.06	1.07	1.08	1.08	1.23	1.20	1.17	1.15	1.12	1.10	1.08	1.06
Den Oever buiten	1.37	1.32	1.27	1.23	1.19	1.15	1.11	1.08	1.43	1.38	1.33	1.29	1.24	1.20	1.16	1.13	1.42	1.40	1.37	1.35	1.32	1.29	1.27	1.24	1.44	1.38	1.33	1.29	1.24	1.20	1.16	1.12
Eemshaven	1.06	1.04	**1.01**	0.99	0.96	0.94	0.92	1.06	1.05	1.02	0.99	0.96	0.94	0.91	0.89	1.07	0.89	0.84	0.78	0.74	0.70	0.68	0.66	1.14	1.05	1.03	**1.00**	0.98	0.95	0.93	0.91	1.11
Harlingen	1.22	1.18	1.13	1.09	1.05	1.01	0.98	0.98	1.25	1.20	1.15	1.11	1.06	1.02	0.98	**1.01**	1.50	1.41	1.32	1.24	1.16	1.09	1.03	1.10	1.25	1.20	1.15	1.11	1.07	1.03	0.99	1.02
Huibertgat	1.02	1.01	**1.00**	**1.00**	0.99	0.98	0.97	0.94	0.98	0.97	0.97	0.96	0.95	0.94	0.93	0.95	0.95	0.95	0.95	0.95	0.95	0.95	0.95	0.97	0.98	0.98	0.97	0.96	0.95	0.94	0.93	0.95
Kornwerderzand buiten	1.32	1.27	1.22	1.17	1.12	1.08	1.04	**1.00**	1.39	1.33	1.28	1.22	1.17	1.13	1.08	**1.01**	1.89	1.75	1.63	1.52	1.42	1.33	1.25	1.27	1.39	1.33	1.27	1.22	1.17	1.12	1.08	1.02
Lauwersoog	1.05	1.03	1.01	**0.99**	0.98	0.96	0.94	**1.01**	1.01	0.99	0.97	0.95	0.93	0.91	0.89	1.01	0.95	0.96	0.97	0.98	0.98	0.97	0.97	1.29	1.07	1.05	1.03	**1.01**	**0.99**	0.97	0.95	1.02
Nes	1.08	1.05	1.02	**1.00**	0.97	0.95	0.92	0.97	1.07	1.04	**1.00**	0.97	0.94	0.91	0.89	0.95	0.82	0.85	0.87	0.88	0.89	0.89	0.88	1.06	1.07	1.04	1.01	0.99	0.96	0.93	0.90	0.97
Oudeschild	1.29	1.25	1.22	1.18	1.15	1.12	1.08	0.90	1.33	1.28	1.24	1.21	1.17	1.14	1.10	0.86	1.10	1.12	1.15	1.16	1.16	1.16	1.14	0.87	1.38	1.33	1.29	1.25	1.21	1.17	1.14	0.88
Schiermonnikoog	1.03	1.02	**1.01**	0.99	0.97	0.95	0.92	0.70	0.99	0.97	0.97	0.95	0.92	0.90	0.86	0.64	0.81	0.82	0.90	0.90	0.90	0.90	0.83	0.98	1.02	**1.00**	**1.00**	0.98	0.96	0.94	0.90	0.63
Terschelling Noordzee	**1.01**	**1.00**	**1.00**	**0.99**	0.99	0.98	0.97	0.97	**0.99**	0.99	0.98	0.97	0.97	0.96	0.96	0.94	1.09	1.09	1.08	1.08	1.08	1.07	1.07	1.01	1.02	1.01	**1.01**	**1.00**	**0.99**	0.99	0.98	0.97
Texel Noordzee	1.04	1.03	1.02	1.01	**1.01**	**1.00**	0.99	0.92	1.06	1.05	1.05	1.04	1.03	1.02	1.02	0.87	1.13	1.12	1.12	1.12	1.11	1.11	1.11	0.96	1.09	1.08	1.07	1.06	1.05	1.04	1.03	0.93
Vlieland haven	1.17	1.14	1.12	1.09	1.07	1.05	1.02	0.90	1.20	1.17	1.14	1.11	1.08	1.06	1.03	0.84	1.17	1.21	1.24	1.26	1.27	1.28	1.28	0.82	1.20	1.17	1.15	1.12	1.09	1.07	1.04	0.88
West-Terschelling	1.20	1.17	1.14	1.11	1.08	1.06	1.03	0.96	1.23	1.20	1.16	1.13	1.10	1.07	1.04	0.92	1.24	1.27	1.29	1.30	1.31	1.31	1.30	0.95	1.23	1.20	1.17	1.14	1.11	1.08	1.05	0.93
Wierumergronden	1.01	**1.01**	**1.00**	**0.99**	0.99	0.98	0.97	0.90	**0.99**	0.99	0.98	0.97	0.96	0.96	0.95	0.87	**1.00**	**1.00**	**1.01**	**1.01**	**1.01**	1.01	1.01	0.64	1.02	1.02	**1.01**	**1.00**	**0.99**	0.99	0.98	0.89
Average	1.13	1.11	1.08	1.06	1.03	1.01	0.99	0.95	1.14	1.11	1.08	1.06	1.03	**1.01**	0.98	0.93	1.12	1.11	1.09	1.08	1.06	1.05	1.03	**1.00**	1.16	1.13	1.10	1.08	1.05	1.03	**1.00**	0.95
Average Offshore	1.05	1.04	1.03	1.02	**1.01**	**1.00**	0.99	0.95	1.04	1.03	1.02	**1.01**	**1.00**	0.99	0.98	0.93	1.03	1.04	1.04	1.04	1.04	1.04	1.04	0.93	1.07	1.06	1.04	1.03	1.02	**1.01**	**1.00**	0.96
Average Basins	1.17	1.14	1.11	1.08	1.05	1.02	0.99	0.95	1.19	1.15	1.11	1.08	1.05	1.01	0.98	0.94	1.16	1.14	1.12	1.09	1.07	1.05	1.03	1.03	1.20	1.16	1.13	1.10	1.06	1.03	**1.00**	0.95
Average Frisian Inlet	*1.03*	*1.02*	**1.01**	**0.99**	*0.98*	*0.96*	*0.95*	*0.87*	**1.00**	*0.98*	*0.97*	*0.96*	*0.94*	*0.92*	*0.90*	*0.84*	*0.92*	*0.93*	*0.96*	*0.96*	*0.96*	*0.96*	*0.94*	*0.97*	*1.04*	*1.02*	*1.01*	**1.00**	*0.98*	*0.97*	*0.94*	*0.85*
Minimum	**1.01**	**1.00**	**1.00**	0.99	0.96	0.93	0.90	0.70	0.98	0.97	0.97	0.95	0.92	0.90	0.86	0.64	0.81	0.82	0.75	0.71	0.67	0.63	0.66	0.64	0.98	0.98	0.97	0.96	0.95	0.92	0.89	0.63
Maximum	1.37	1.32	1.27	1.23	1.19	1.15	1.11	1.08	1.43	1.38	1.33	1.29	1.24	1.20	1.16	1.13	1.89	1.75	1.63	1.52	1.42	1.33	1.30	1.29	1.44	1.38	1.33	1.29	1.24	1.20	1.16	1.12

(b) Amplitude ratios of the four main tidal constituents for different Manning friction coefficients

Station	$\Delta\varphi_{M2}$ 0.018	0.019	0.02	0.021	**0.022**	0.023	0.024	0.025	$\Delta\varphi_{S2}$ 0.018	0.019	0.02	0.021	**0.022**	0.023	0.024	0.025	$\Delta\varphi_{M4}$ 0.018	0.019	0.02	0.021	**0.022**	0.023	0.024	0.025	$\Delta\varphi_{N2}$ 0.018	0.019	0.02	0.021	**0.022**	0.023	0.024	0.025
Delfzijl	-1.79	-0.01	1.36	2.93	4.41	5.79	7.30	8.52	-0.82	1.14	2.65	4.33	5.89	7.33	8.87	10.11	9.29	14.17	9.10	13.17	17.06	20.72	35.24	38.71	-0.26	1.61	3.05	4.70	6.23	7.66	9.23	10.49
Den Helder	0.54	0.19	-0.15	-0.46	-0.76	-1.04	-1.29	-1.53	0.95	0.76	0.60	0.46	0.35	0.25	0.17	0.11	-3.98	-1.47	0.70	2.62	4.34	5.85	7.20	8.43	1.48	1.32	1.19	1.08	1.00	0.91	0.88	0.85
Den Oever buiten	-7.30	-6.49	-5.77	-5.08	-4.44	-3.83	-3.23	-2.70	-6.22	-5.23	-4.36	-3.50	-2.69	-1.93	-1.17	-0.48	-0.82	0.95	2.59	4.27	5.91	7.49	9.12	10.60	-9.77	-8.76	-7.85	-6.95	-6.11	-5.31	-4.51	-3.79
Eemshaven	-1.67	-0.76	0.99	1.78	2.51	3.21	3.01	-4.65	-0.72	0.21	2.07	2.85	3.57	4.25	3.95	-3.45	-9.25	-7.86	-5.72	-4.90	-4.31	-3.90	-4.54	6.01	-0.05	0.90	2.67	3.49	4.25	4.98	4.80	-3.46
Harlingen	-9.22	-7.34	-5.56	-3.89	-2.31	-0.81	0.62	0.19	-10.08	-8.21	-6.44	-4.76	-3.17	-1.65	-0.19	0.32	-5.08	-1.02	2.82	6.43	9.83	13.04	16.06	11.79	-9.47	-7.55	-5.72	-3.99	-2.34	-0.76	0.75	2.39
Huibertgat	0.22	0.14	0.06	-0.01	-0.07	-0.12	-0.16	1.98	0.85	0.77	0.70	0.64	0.60	0.56	0.55	1.21	-8.50	-8.41	-8.23	-7.94	-7.57	-7.13	-6.61	18.89	2.09	2.00	1.93	1.86	1.82	1.78	1.77	2.20
Kornwerderzand buiten	-8.79	-7.38	-6.06	-4.82	-3.64	-2.53	-1.46	-2.20	-8.28	-6.80	-5.42	-4.10	-2.84	-1.64	-0.48	-3.61	-9.06	-6.85	-4.86	-3.05	-1.42	0.05	1.37	-6.55	-10.55	-9.00	-7.52	-6.12	-4.78	-3.50	-2.28	-1.49
Lauwersoog	-2.36	-1.39	-0.53	0.38	1.26	2.12	3.03	-1.05	-2.50	-1.32	-0.27	0.83	1.89	2.91	3.99	-1.47	-12.93	-9.75	-6.70	-3.49	-0.32	2.80	6.05	12.69	0.96	2.01	2.94	3.93	4.90	5.83	6.83	-0.11
Nes	-3.06	-1.91	-0.82	0.21	1.18	2.09	2.96	1.36	-3.36	-2.08	-0.88	0.25	1.31	2.31	3.26	0.57	-10.02	-9.36	-8.12	-6.47	-4.53	-2.44	-0.25	0.01	-1.07	0.16	1.32	2.42	3.45	4.44	5.37	2.26
Oudeschild	-3.71	-3.80	-4.22	-4.34	-4.47	-4.61	-4.49	3.78	-3.63	-3.57	-3.83	-3.78	-3.75	-3.73	-3.45	4.15	-1.07	0.14	1.29	2.35	3.35	4.28	5.18	1.99	-4.01	-3.89	-4.10	-3.99	-3.91	-3.84	-3.50	6.25
Schiermonnikoog	0.38	1.61	1.10	2.21	3.28	4.33	7.30	13.73	1.34	2.81	2.08	3.41	4.70	5.95	9.54	12.29	-1.86	2.25	0.20	4.01	7.78	11.49	-337.59	118.00	3.01	4.34	3.45	4.64	5.81	6.95	10.44	19.54
Terschelling Noordzee	2.60	2.39	2.19	2.00	1.82	1.65	1.50	0.87	1.75	1.54	1.34	1.16	0.98	0.83	0.69	0.29	-1.83	-1.79	-1.67	-1.46	-1.18	-0.83	-0.43	-2.31	3.27	3.07	2.89	2.72	2.58	2.45	2.35	1.50
Texel Noordzee	1.00	0.83	0.67	0.54	0.42	0.32	0.24	3.83	0.25	0.20	0.17	0.16	0.17	0.20	0.25	4.94	9.97	10.24	10.51	10.78	11.04	11.29	11.54	9.04	2.23	2.17	2.14	2.15	2.18	2.23	2.30	7.71
Vlieland haven	-4.15	-3.78	-3.44	-3.14	-2.87	-2.62	-2.40	8.35	-5.43	-5.05	-4.72	-4.44	-4.19	-3.97	-3.78	10.76	-13.35	-13.02	-12.34	-11.39	-10.30	-9.11	-7.85	-333.78	-3.93	-3.48	-3.07	-2.70	-2.36	-2.05	-1.76	11.56
West-Terschelling	-4.48	-3.83	-3.24	-2.71	-2.22	-1.79	-1.40	-0.18	-4.79	-4.11	-3.51	-2.98	-2.52	-2.12	-1.77	0.55	-1.08	0.37	2.11	4.05	6.12	8.29	10.48	-6.04	-4.05	-3.31	-2.63	-2.02	-1.46	-0.96	-0.51	1.77
Wierumergronden	1.71	1.56	1.42	1.29	1.16	1.05	0.95	3.66	1.07	0.92	0.78	0.65	0.54	0.44	0.36	4.58	-4.41	-4.32	-4.14	-3.88	-3.55	-3.17	-2.76	-4.34	2.30	2.14	1.99	1.86	1.74	1.64	1.56	5.47
Average	2.51	1.87	1.38	0.82	0.30	0.20	0.78	2.12	2.48	1.75	1.19	0.55	0.05	0.62	1.30	2.55	4.00	2.23	1.40	0.32	2.02	3.67	16.11	7.30	1.74	1.02	0.46	0.19	0.81	1.40	2.11	3.95
Average Offshore	1.21	1.02	0.84	0.67	0.51	0.37	0.25	1.76	0.97	0.84	0.72	0.61	0.53	0.46	0.40	2.23	1.75	1.15	0.56	0.02	0.62	1.20	1.79	5.94	2.27	2.14	2.03	1.94	1.86	1.80	1.77	3.55
Average Basins	4.20	3.19	2.38	1.50	0.66	0.12	1.02	2.29	4.04	2.93	2.06	1.08	0.16	0.70	1.71	2.70	5.02	2.73	1.78	0.45	2.65	4.79	24.25	13.32	3.56	2.45	1.59	0.60	0.33	1.22	2.26	4.13
Average Frisian Inlet	*0.09*	*0.60*	*0.66*	*1.29*	*1.90*	*2.50*	*3.76*	*5.44*	*0.03*	*0.80*	*0.87*	*1.63*	*2.38*	*3.10*	*4.63*	*5.13*	*6.40*	*3.94*	*3.55*	*1.12*	*1.30*	*3.71*	*111.43*	*42.12*	*2.09*	*2.83*	*2.79*	*3.48*	*4.15*	*4.81*	*6.27*	*8.30*
Minimum	-9.22	-7.38	-6.06	-5.08	-4.47	-4.61	-4.49	-4.65	-10.08	-8.21	-6.44	-4.76	-4.19	-3.97	-3.78	-3.61	-13.35	-13.02	-12.34	-11.39	-10.30	-9.11	-337.59	-333.78	-10.55	-9.00	-7.85	-6.95	-6.11	-5.31	-4.51	-3.79
Maximum	2.60	2.39	2.19	2.93	4.41	5.79	7.30	13.73	1.75	2.81	2.65	4.33	5.89	7.33	9.54	12.29	9.97	14.17	10.51	13.17	17.06	20.72	35.24	118.00	3.27	4.34	3.45	4.70	6.23	7.66	10.44	19.54

(c) Phase lag differences of the four main tidal constituents for different Manning friction coefficients

Figure B.2: Hydrodynamic performance for different Manning friction coefficients, where the model results are compared to the observations

C

Wave modeling

In this appendix a further analysis has been conducted on the performance of the wave modeling with SWAN. This includes a comparison to other studies, an analysis of the effect of the root-mean-square error on the calculated sediment transports, and an analysis of the effect of the communication time step between the hydrodynamic and wave models on the calculated sediment transports.

C.1. Calibration

To correct the observed underestimation of the wave height by SWAN, the calculated wave heights from the ERA5 model have been increased. This is done by an overall increase of a certain percentage to better match the measured wave heights around the Friesche Zeegat. To preserve the wave steepness, the wave period has been scaled accordingly. The resulting performance is given in Figure C.1 and Table 4.3.

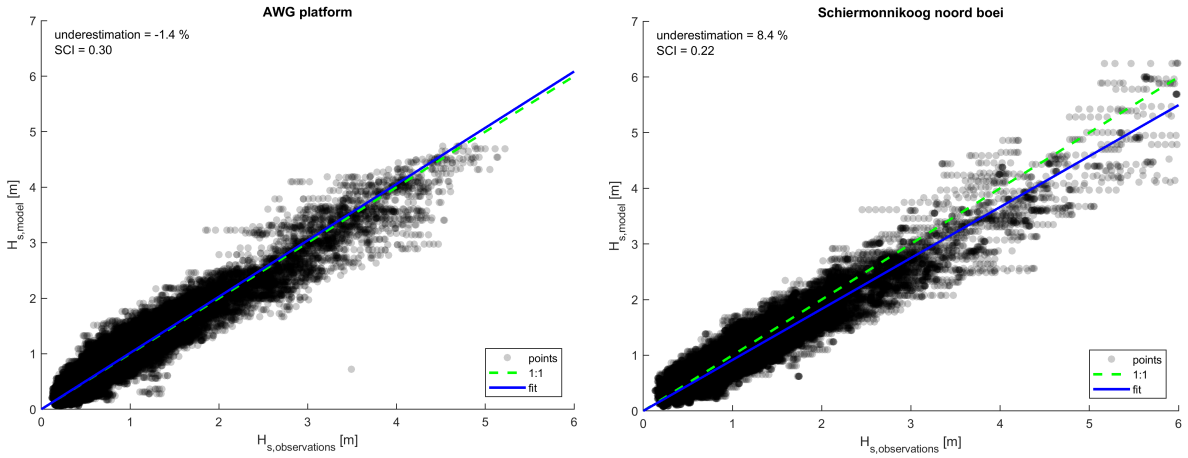

Figure C.1: Modeled wave heights plotted against observed wave heights with a fitted line showing the underestimation compared to a 1:1 fit

The remaining error in the modeled wave heights could be caused by differences in wave generation within the model domain. Overall, the result is deemed accurate enough to investigate sediment transports in the area of interest.

C.2. Comparison of the model results with other studies

The common approach to wave modeling is the implementation of observations from nearby wave buoys. These observations can be used as time series, or a derived energy spectrum can be used. These would have to be scaled to fit to the used boundaries of the model, which can be a tedious task.

Model	SCI_{Hm0}	Relative bias
AZG 1-1 in this thesis	0.2	0.04
AZG 1-2 in this thesis	0.2	0.03
AWG in this thesis	0.3	-0.07
SON in this thesis	0.2	0.06
AZG in Van der Westhuysen (2010)	0.2	0.18
AZG in Gautier et al. (2014)		0.04
Eastern Wadden Sea in Gautier et al. (2014)		0.14
AZG in Gautier and Van der Westhuysen (2010)		0.05
SWAN-ZuNo (Gautier and Caires, 2015)	0.19	0.09m (bias)
NCEP (Cavaleri et al., 2018)	0.20	-0.06

Table C.1: Overview of performance of developed model compared to other studies

In this model a less time-consuming approach has been used by implementing the model results of the larger ERA5 meteorological model. The set-up has been explained earlier, in Chapter 4.2.3.

This approach results in a slightly higher value for the root-mean-square errors. After normalizing the result with respect to the variance (or scatter index), it is visible that the representation corresponds rather well compared to similar studies. An overview is given in Table C.1.

C.3. Effect of the accuracy on sediment transport

The significant wave height in the model is generated by a wave related boundary condition from ERA5 on the larger wave grid and wind-driven wave generation in all wave grids, as mentioned before. The wave heights of the boundary condition have been altered to reduce the root-mean-square error with the measured signal around the Friesche Zeegat, namely at the stations *Amelander Zeegat 1-2*, *AWG platform* and *Schiermonnikoog Noord* (*SON*). The resulting RMSE is, with around 25 cm, still higher than typical values in other studies, where a more local and more refined wave grid has been applied. However, since a secondary purpose of this thesis is to investigate a new approach to modelling larger systems, the current set-up has been chosen. A further overview on the models wave representation performance compared to other studies is given in the next subsection.

To evaluate the influence of the RMSE, another run with a larger RMSE has been analyzed. The signal in this run follows from the exact same settings, but without wave generation by wind. This gives a visually similar result, but with a twice as large RMSE. An analysis has been conducted on the resulting sediment transport. This shows the same transport patterns in the area of interest. Also, the magnitudes of sediment transport differ with only 25%. Therefore, it is concluded that a further optimization of the wave representation will not result in a significantly more accurate sediment transport representation.

C.4. Effect of the communication time step on sediment transport

The communication time step between the hydrodynamic and the wave module is set at 60 minutes. The maximum difference in water level is 103 cm and the mean difference in water level is 33 cm for this time step at the wave buoy *Schiermonnikoog Noord*.

This time step is relatively large compared to other studies. However, a comparison with two identical runs with different time steps shows that a more common value of 20 minutes results in a virtually equal root-mean-square error, but a more than twice as high computation time. Therefore, the higher value for the time step is chosen for the model in this thesis.

The overall effect of a larger communication time step on the calculated sediment transports is rather small. However, locally, due to a large error in the suspended sediment transport this can be of importance. An overview of the local average difference in sediment transport between communication time steps of 20 minutes and 60 minutes is given in Figure C.2. It shows that mainly in the back barrier basin, at locations above +0m NAP, this time step is of importance to sediment transports. On the ebb-tidal delta this effect is minimal. However a up to 20% difference is visible in the eastern half of the channel Plaatgat in front of the island head coast. This has to be taken into account when interpreting the model results there.

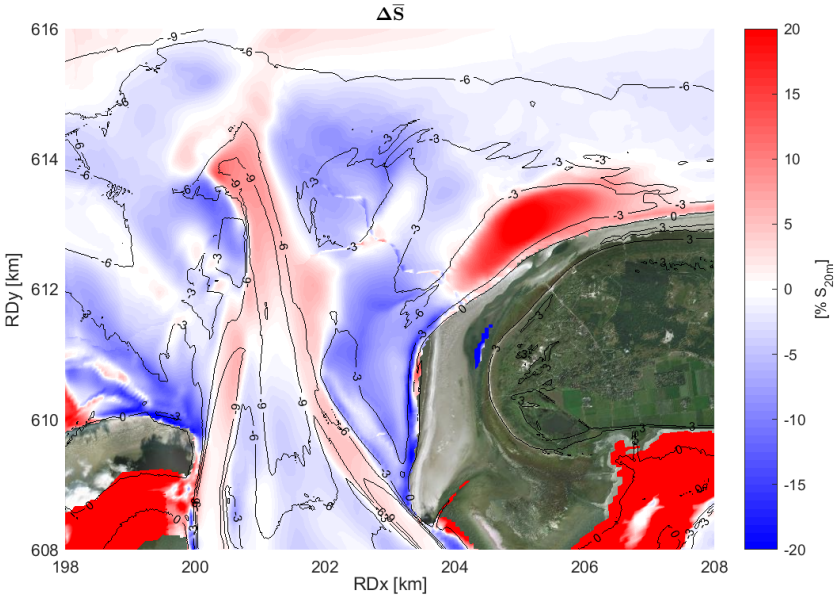

Figure C.2: Difference in total sediment transport per grid cell; colors indicate the difference in percentage of the total sediment transport of a model run with a communication time step of 20 minutes

D

Formulas for statistical analysis

In this thesis, several statistical parameters are presented to analyze the performance of the presented model. The used method is in agreement with Sutherland et al. (2004), focusing on calculating the bias and accuracy. This helps to objectively evaluate the skill of the model. Below, the used equations are presented.

D.1. Bias

The statistical bias determines the difference between computed values (X_i) and measured values (Y_i). Where the bias is positive, the computed dataset overestimates the observations and where the bias is negative the computed dataset underestimates the observations. The bias can be calculated with:

$$Bias = \frac{1}{N}\sum_{i=1}^{N}(Y_i - X_i)$$

N is the number of used data points.

To take the magnitude of the original values into account for a comparison between different locations, the relative bias can be calculated. For this parameter the bias is divided by the mean of the observations, as given with:

$$Relativebias = \frac{Bias}{\frac{1}{N}\sum_{i=1}^{N}(X_i)}$$

D.2. Accuracy

The accuracy (or *trueness*) is the description of systematic and random errors between the computed and measured values. To assess the accuracy, commonly the root-mean square error (*RMSE*) is calculated. This is done with:

$$RMSE = \sqrt{\frac{1}{N}\sum_{i=1}^{N}(Y_i - X_i)^2}$$

By dividing the root-mean-square error by the mean of the observations, the scatter index (*SCI*) can be found. This percentage of the difference of the root-mean-square error with the mean observations can be calculated with:

$$SCI = \frac{RMSE}{\frac{1}{N}\sum_{i=1}^{N}(X_i)}$$

E

Additional model results

In this appendix additional model results are presented. Section E.1 gives the annual average current and sediment transport over several cross-sections. In Section E.2 the variation in the wave height and resulting sediment transport pathways over the approaching shoal and through the channel Plaatgat during different stages in the tidal cycle and during a storm event are given. Section E.3 and E.4 give additional information on the sediment transport pathways and gradients over the ebb-tidal delta of the Zoutkamperlaag and over the offshore part of Schiermonnikoog NW.

E.1. Discharge and sediment transport per cross-section

Figure E.1 shows the variation in the annual average current and total sediment transport over the inlet at the height of RDy = 609 km. Three main channels can be distinguished, two ebb channels on the side (Zoutkamperlaag and Gat van Schiermonnikoog) and a flood shield with two minor flood channels on the sides. The direction of the current and transport correspond with the expected function, outward on the sides and inward in the middle.

Figures E.2, E.3, E.4 and E.5 show similar results for the *JarKus* transects along the island head coast of Schiermonnikoog. The annual average inward flow in the southwestern part, the divergence point near transect 303 and the annual average outward flow in the eastern part of the Plaatgat are clearly visible. Sediment transport directions over these transects are in line with the direction of the current.

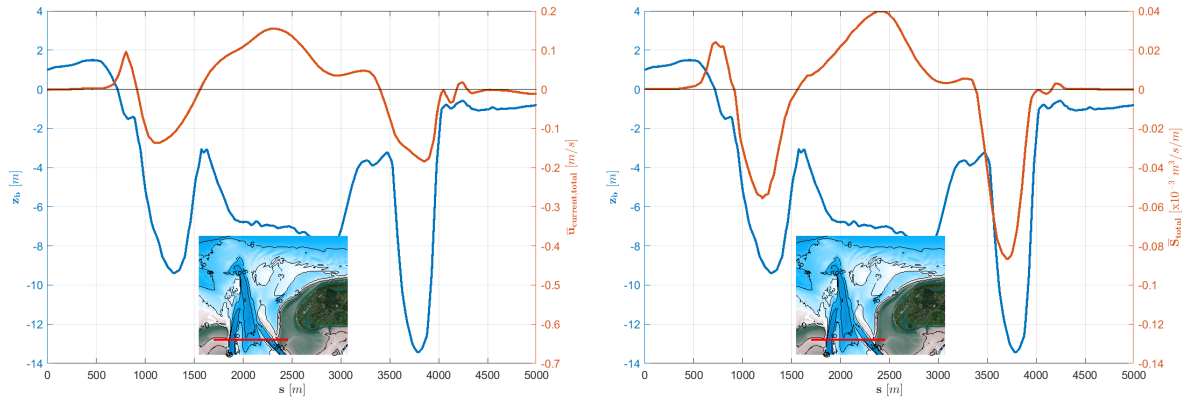

(a) Annual average current along the cross-section

(b) Annual average total sediment transport along the cross-section

Figure E.1: Current and sediment transport (red) through the inlet (RDy = 609 km, where positive and negative are inward (southward) and outward (northward) respectively, the distance s is measured from the island head, and the bed level z_b (blue) is given relative to NAP

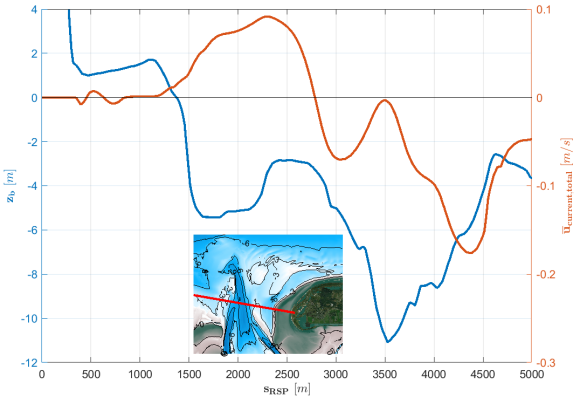

(a) Annual average current along the transect

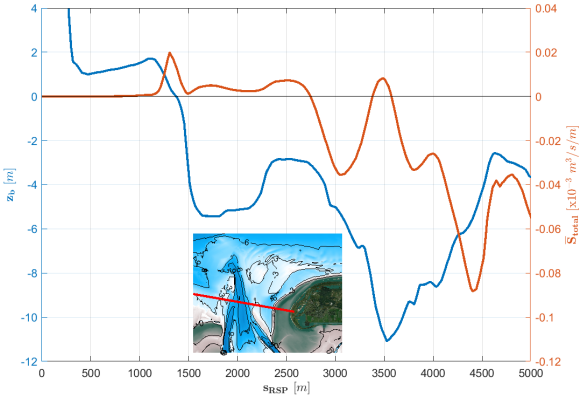

(b) Annual average total sediment transport along the transect

Figure E.2: Current and sediment transport (red) over the first 5 km of *JarKus* transect 220, where positive and negative are inward (southward) and outward (northward) respectively, the distance s_{RSP} is measured from the main beach pole, and the bed level z_b (blue) is given relative to NAP

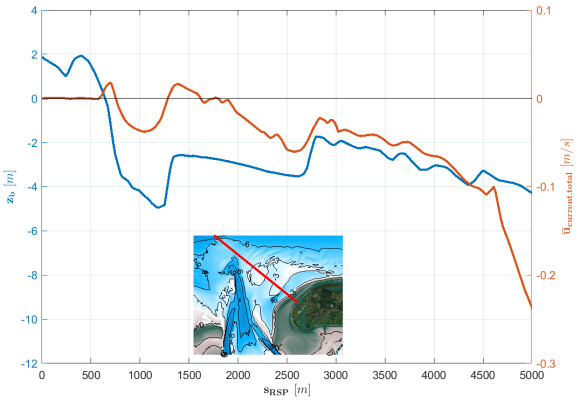

(a) Annual average current along the transect

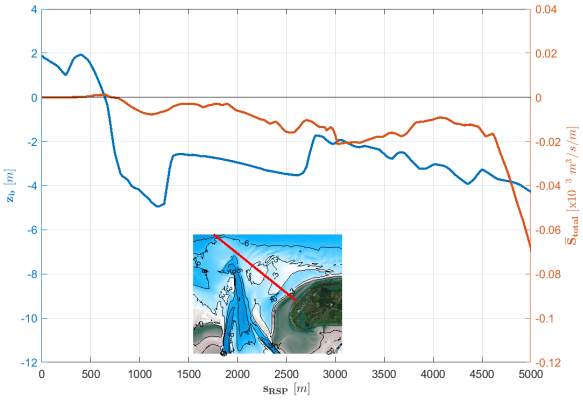

(b) Annual average total sediment transport along the transect

Figure E.3: Current and sediment transport (red) over the first 5 km of *JarKus* transect 303, where positive and negative are inward (southwestward) and outward (northeastward) respectively, the distance s_{RSP} is measured from the main beach pole, and the bed level z_b (blue) is given relative to NAP

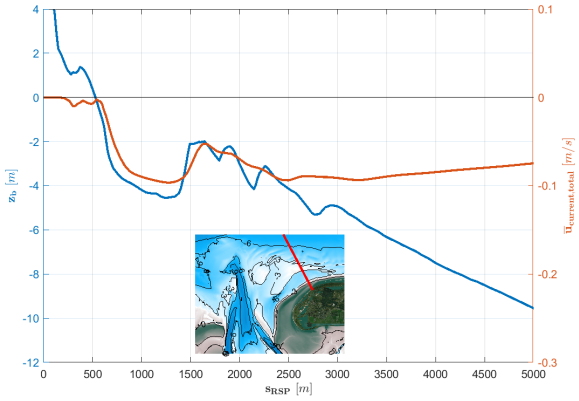

(a) Annual average current along the transect

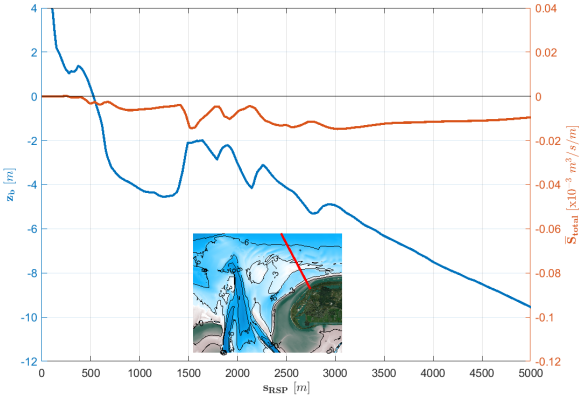

(b) Annual average total sediment transport along the transect

Figure E.4: Current and sediment transport (red) over the first 5 km of *JarKus* transect 420, where positive and negative are inward (westward) and outward (eastward) respectively, the distance s_{RSP} is measured from the main beach pole, and the bed level z_b (blue) is given relative to NAP

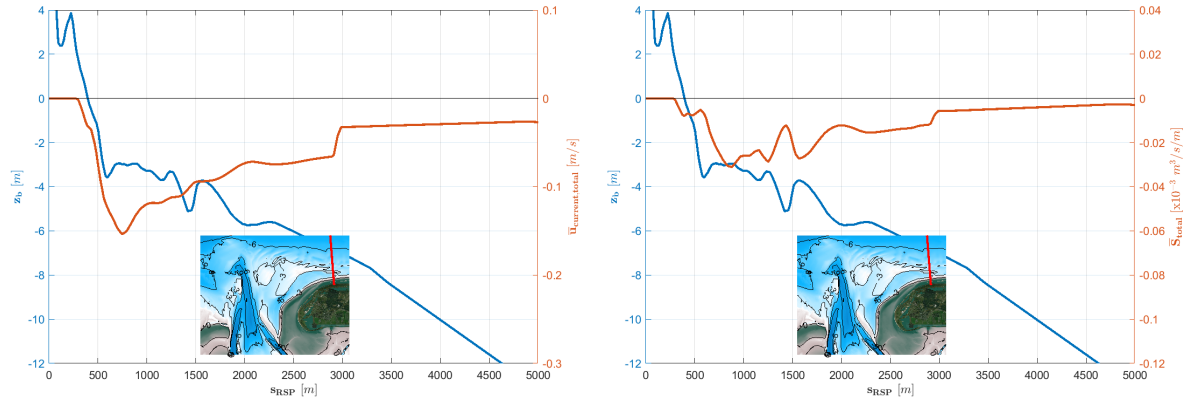

(a) Annual average current along the transect

(b) Annual average total sediment transport along the transect

Figure E.5: Current and sediment transport (red) over the first 5 km of *JarKus* transect 540, where positive and negative are inward (westward) and outward (eastward) respectively, the distance s_{RSP} is measured from the main beach pole, and the bed level z_b (blue) is given relative to NAP

E.2. Wave height and sediment transport at the Plaatgat

Figure E.6 shows the varying wave height and sediment transport pathway and intensity during several tidal cycles. The impact on the transport by the storm in the night of January 13 to 14, 2017 is clearly pronounced. Furthermore, the constantly present gradient in the wave height at the coast is visible.

In the morning of January 13, 2017, during low water slack, a medium high significant wave height of 2.5 m is observed farther offshore. Due to the low water level no large waves can propagate over the approaching shoal and the root-mean-square wave height in the Plaatgat is not higher than 0.4 m. These relatively low waves have their effect on the modeled sediment transport, which are only significant at the periphery of the shoal, where waves are larger. As water levels rise, larger waves can propagate over the shoal and the sediment transport in the shallower area increases. During the flood phase, the contribution of inflowing currents toward the southwest can be noted in the southwestern part of the Plaatgat. During the following ebb phase, currents are mainly directed toward the east. The resulting sediment transport is also directed toward the east and mainly present in the eastern part of the Plaatgat. Note how during the first tidal cycle the offshore wave height is rather constant and the local increase in wave height is purely related to the increasing water level.

The lower three panels show similar stages in the tidal cycle, but during the storm event. These show similar pathways, but significantly larger sediment transport intensities. Remarkable is the increased transport over the shoal into the eastern half of the Plaatgat during flood. Furthermore, the transport near the waterline is more pronounced due to the water level set-up.

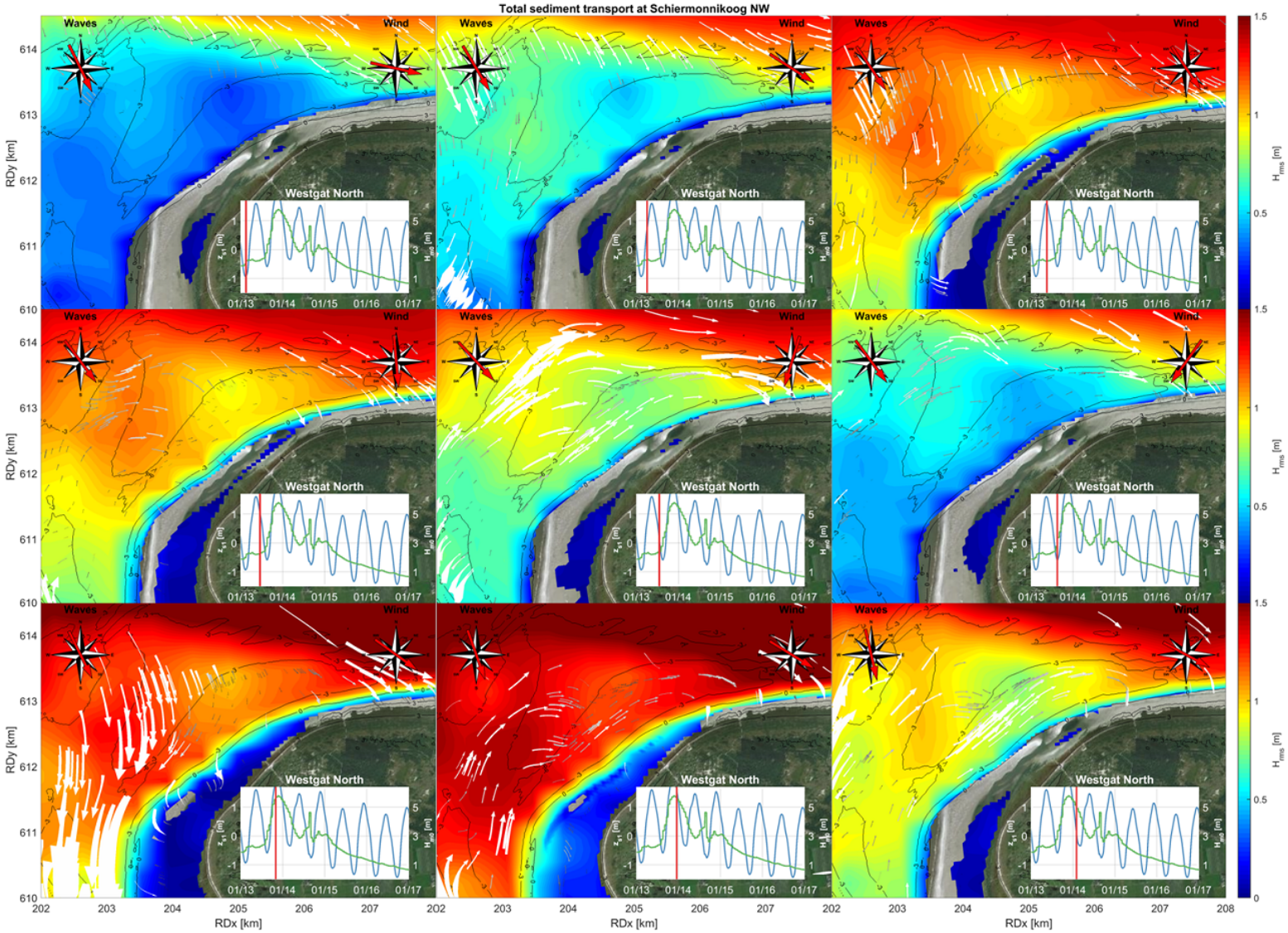

Figure E.6: Wave height and sediment transport pathway and intensity around the Plaatgat during several tidal cycles under varying wave conditions, where the significant wave height (green) and water level (blue) at the measurement buoy Schiermonnikoog Westgat are given in the subplots on top of the island

E.3. Sediment transport pathways

In addition to Figure 5.4 and the analysis in Section 5.2.3, Figure E.7 gives the sediment transport pathways for model runs with tidal forcing and wind and with tidal forcing and waves. By comparing the combined four subfigures from this section and Section 5.2.3, the effect of wind can be found. As concluded earlier, this is mainly an enhancement and deflection of transport toward the east and a dampening of transport to the west. This effect is in line with the prevailing wind direction from the west and southwest.

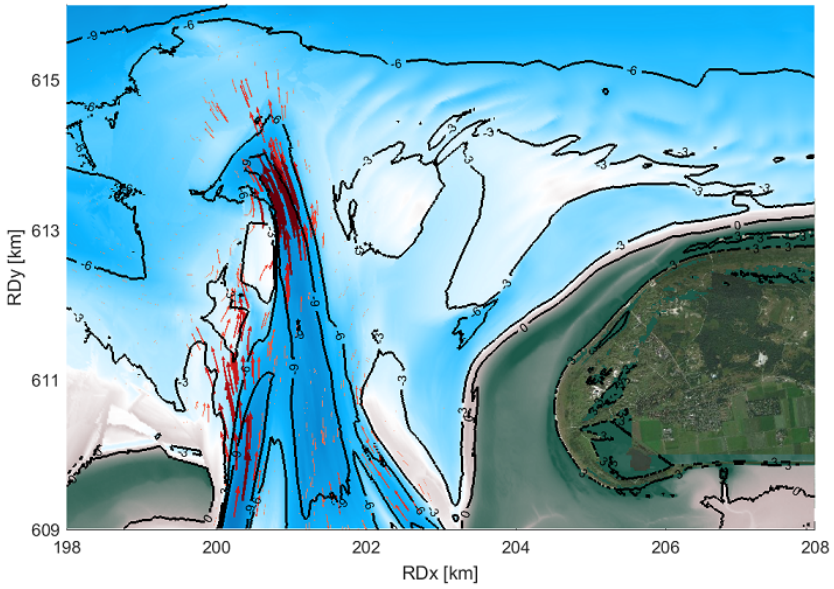

(a) For a model run with tidal forcing and wind (run 2)

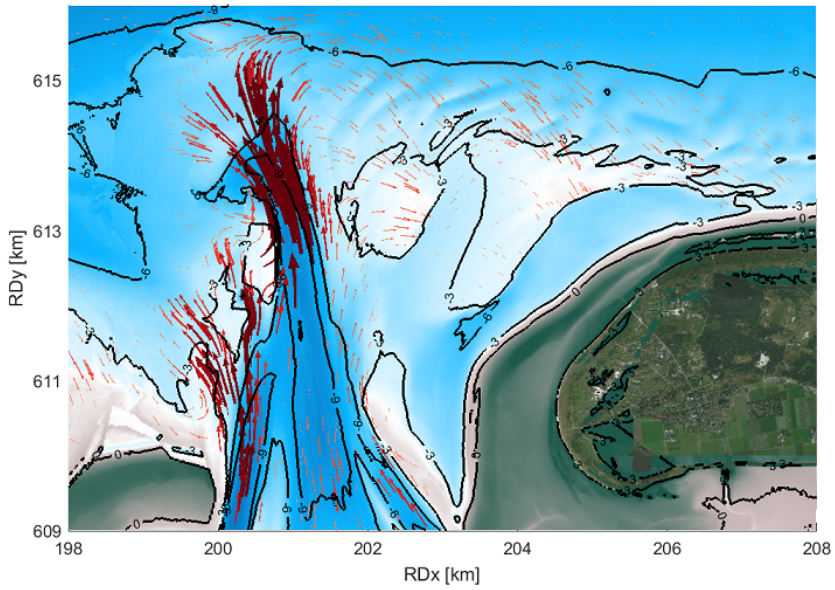

(b) For a model run with tidal forcing and waves (run 3)

Figure E.7: Annual average total sediment transport in 2017 at the Zoutkamperlaag inlet and ebb-tidal delta

E.4. Sediment transport at the Plaatgat on a grid

Similar to the pattern in Figure 5.8 in Section 5.4, the annual average total sediment transport in m^3/s for the modeled year 2017 is given in Figure E.8. The data is interpolated onto the presented grid from the map output of the model and helps to assess the sections with erosion and sedimentation in the offshore area near Schiermonnikoog NW. Additionally, this representation in m^3/s allows for a comparison with the results as presented in Nederhoff et al. (2016).

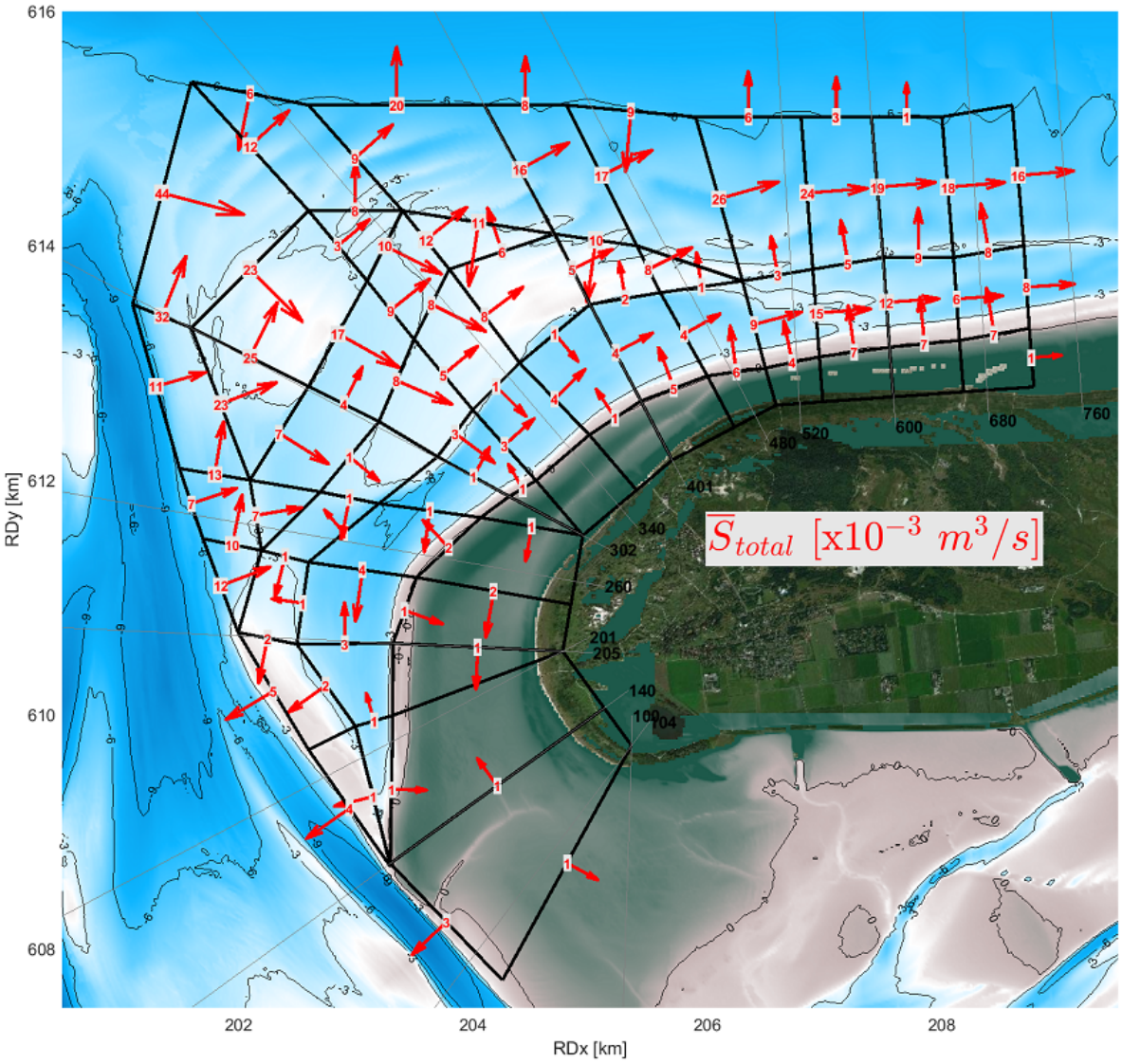

Figure E.8: Annual average total sediment transport along the Plaatgat and its surroundings on a structured grid

Glossary

accretion

the growth of land (toward the sea).

AHN

the Digital Elevation Model of the Netherlands (*Actueel Hoogtebestand Nederland*) by the Waterschapshuis.

avulsion

the loss of land (to the sea).

back barrier

a shallow basin at the landward side of a tidal inlet, formed by inflowing flood currents.

barrier island

an island parallel to the mainland coast with tidal inlets on the sides, formed by tidal and wave action (see Figure 2.1).

bathymetry

the measurement of water depth.

bias

the difference between computed and measured values (see Appendix D).

BKL

the basal coastline (*basiskustlijn*), as defined by Rijkswaterstaat, which defines the legally allowed most landward coastline position.

CFL-contition

the Courant-Friedrichs-Lewy condition determines the maximum time step based on the size of a grid cell and the occurring flow velocities.

DCSM-ZuNo

the Dutch Continental Shelf Model in combination with the Southern North Sea Model (*Zuidelijke Noordzee-model*) by Zijl et al. (2013), which is used for water level boundary conditions in this thesis.

Delft3D

a three-dimensional hydrodynamic and morphological model on a curvilinear grid by Deltares (Lesser et al., 2004).

Delft3D Flexible Mesh (FM)

a newly developed version of Delft3D, where all possible grid forms can be applied (Kernkamp et al., 2011).

DINO

Data en Informatie van de Nederlandse Ondergrond, a database by the Netherlands Organisation for Applied Scientific Research (*TNO*) with cores samples of the subsurface.

downdrift

with the direction of the tidal wave propagation (east in the Dutch Wadden Sea).

dune foot

the lowest point of dune, separating the dunes from the beach.

ebb-tidal delta

a dynamic shallow area at the seaward side of a tidal inlet system, formed by outflowing ebb currents.

ebb-channel

a channel in a tidal inlet system, where outflowing currents during the ebb phase are dominating.

embryo dunes

a most seaward, youngest dune.

EMODnet

the European Marine Observation and Data Network, providing the Greater North Sea bathymetry dataset.

Engelsmanplaat

the shoal in the middle of the Friesche Zeegat, separating the Pinkegat from the Zoutkamerplaag inlet (see Figure 1.1).

ERA5

the latest version of the ECMWF (*European Centre for Medium-Range Weather Forecasts*) Re-Analysis by Hersbach (2016), which is used for wave boundary conditions, wind speeds and atmospheric pressure in this thesis.

erosion

the loss of sediment, leading to a decrease of the bed level.

estuarine circulation

a circulating flow pattern in an arm of the sea with low-salinity outflow of water at the surface over high-salinity inflow of water at the bed.

flood-channel

a channel in a tidal inlet system, where inflowing currents during the flood phase are dominating.

flow bypassing and bar welding

a bypassing mechanism of sediment over a tidal inlet, following the offshore-directed ebb current through the ebb channel and the landward-directed bar (or shoal) migration over the ebb-tidal delta.

FM

Flexible Mesh, referring to the numerical modeling software Delft3D Flexible Mesh Suite by Deltares (2018), which allows for the use of unstructured hydrodynamic grids.

Friesche Zeegat

the tidal inlet system between the islands of Ameland and Schiermonnikoog, consisting of the Pinkegat and Zoutkamperlaag inlets (see Figure 1.1).

Gat van Schiermonnikoog

the eastern ebb channel in the Zoutkamperlaag inlet to the southwest of Schiermonnikoog (see Figure 1.1).

GEBCO

the General Bathymetric Chart of the Oceans by the International Hydrographic Organization and the Intergovernmental Oceanographic Commission of UNESCO.

gully

a channel.

Het Rif

the curve-shaped bar seaward of the Engelsmanplaat (see Figure 1.1).

hypsometry

the measurement of land elevation relative to sea level.

island tail

a downdrift (eastern) end of a barrier island (see Figure 2.1).

island head

an updrift (western) end of a barrier island (see Figure 2.1).

JarKus

the yearly bathymetric measurements by Rijkswaterstaat along cross-shore transects along the Dutch coast.

Lauwerszee

the former embayment connected to the North Sea by the Zoutkamperlaag, which has been closed off from the Wadden Sea by the Lauwersmeerdam in 1969, creating the present-day lake Lauwersmeer.

LiDAR

Laser Imaging Detection And Ranging, a technology to measure the surface elevation with laser pulses.

MKL

the momentary coastline (*momentane kustlijn*), as defined by Rijkswaterstaat, which defines the yearly calculated coastline position.

MLW

the Mean Low Water, the average low astronomical tide.

morphodynamics

with a changing morphology.

morphology

the form and structure (of an underwater surface).

morphostatic

with a fixed morphology.

MSL

the mean sea level, the average level of the water, varying per location.

NAP

the Amsterdam Ordnance Datum (*Normaal Amsterdams Peil*), a vertical datum in the European Vertical Reference System, used in Finland, Germany, the Netherlands, Norway and Sweden.

NCP

a grain size map of the Dutch Continental Shelf (*Nederlands Continentaal Plat*) by the Netherlands Organisation for Applied Scientific Research (*TNO*).

NTR

the non-tidal residual, also known as '*surge*', which includes the water level signal that cannot be related to tides.

paleogeography

the study of physical geography in the earth's history.

Pinkegat

the western main channel in the Friesche Zeegat with its ebb-tidal delta partially in front of Het Rif (see Figure 1.1).

Plaatgat

the former flood channel in front of the island head of Schiermonnikoog (see Figure 1.1).

RD

the coordinate reference system used in the Netherlands (*Rijksdriehoekscoördinaten*).

Rijkswaterstaat

the Directorate-General for Public Works and Water Management in the Netherlands, responsible for national waterways and roads, and for flood protection and prevention.

RMSE

the root-mean-square error, used to assess the accuracy of a representation (see Appendix D).

RSP

a main beach pole on a Dutch beach (*rijksstrandpaal*).

SCI

the scatter index, used to asses the accuracy of a representation (see Appendix D).

sedimentation

the deposition of sediment, leading to an increase of the bed level.

shoal

an underwater shallow area or bar.

SWAN

a wave model for nearshore, random, short-crested wind-generated waves (Booij et al., 1999; Holthuijsen et al., 1993; Ris et al., 1999).

tidal flat

a shallow area in coastal water, at a height between high and low water.

updrift

against the direction of the tidal wave propagation (west in the Dutch Wadden Sea).

Vaklodingen

the bathymetric measurements conducted every several years by Rijkswaterstaat for a larger area in the Dutch coastal system.

Westgat

the ebb-channel through the ebb-tidal delta of the Zoutkamperlaag (see Figure 1.1).

Wierumergronden

the part of the ebb-tidal delta of the Pinkegat at the island tail of Ameland (see Figure 1.1).

Zoutkamperlaag

the eastern main channel in the Friesche Zeegat with its ebb-tidal delta partially in front of the island head of Schiermonnikoog (see Figure 1.1).